



浮力秤量法による粒径分布測定法の研究開発

メタデータ	言語: eng
	出版者:
	公開日: 2012-07-11
	キーワード (Ja):
	キーワード (En): Particle size distribution, buoyancy, Allen region, stokes diameter, mean particle diameter
	作成者: ロンダン, タムブン
	メールアドレス:
URL	所属:
	https://doi.org/10.15118/00005092

**Research and Development of the Particle Size Distribution Analyzer
by the Buoyancy Weighing-Bar Method**

**Division of Chemical and Materials Engineering
Graduate School of Engineering
Muroran Institute of Technology**

Rondang Tambun

**Research and Development of the Particle Size Distribution Analyzer
by the Buoyancy Weighing-Bar Method**

**by
Rondang Tambun**

**A Dissertation
Submitted in Partial Fulfillment of the Requirements for Degree
of
Doctor of Engineering
in
Chemical Engineering**



**Division of Chemical and Materials Engineering
Graduate School of Engineering
Muroran Institute of Technology
Muroran, Japan**

February 2012

Certificate of Approval

Title : Research and Development of the Particle Size Distribution Analyzer
by the Buoyancy Weighing-Bar Method
Name of Student : Rondang Tambun

Approved and recommended for acceptance as a dissertation in partial fulfillment of the requirements for the degree of Doctor of Engineering in Chemical Engineering.

Date: February, 2012



Prof. Eiji Obata
Supervisor

Signed by the final examining committee:



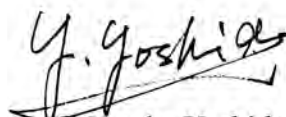
Asc. Prof. Yuichi Ohira
Chairman



Prof. Eiji Obata
Member



Asc. Prof. Mitsuhiro Ohta
Member



Prof. Yutaka Yoshida
Member

Abstract

The particle size distribution and mean particle size are the most important characteristics in particulate or powder technology. Various approaches have been used to measure particle size distributions. For solid–liquid systems, the particle size distributions have been measured by the Stokes diameter. The Andreasen pipette method, sedimentation balance method, centrifugal sedimentation method, etc. have been used to measure the particle size distribution in suspensions. These methods measure the migration velocities of particles in solution, and then particle size is calculated using Stokes formula. However, all these methods are time consuming and require special skills. On the other hand, a different principle can be used to analyze the particle size distribution through microscopy, laser diffraction/scattering method, and a Coulter counter method. These methods require numerous samples to accurately determine the particle size distribution. Although the laser diffraction/scattering and Coulter counter methods produce highly accurate results within a shorter time, they require extremely expensive equipment. Hence, a simple and cost effective method to determine the particle size distribution is highly demanded.

The investigation of particle size distributions by the buoyancy weighing-bar method which is a novel method in particle size distribution measurement have been done for several samples particles of Japan Industrial Standard (Test Powders 1 and Test Powders 2), Sumitomo 3M (glass beads K1, K37, S60HS), polystyrene beads (spherical), nylon beads (cylindrical), etc. The influence of solid concentration, influence of shape and size of weighing bar and influence of vessel size also had been investigated in particle size distribution measurement by the buoyancy weighing-bar method. The result data obtained by the buoyancy weighing-bar method were comparable with the others particle size analyzer, such as sedimentation balance method, Andreasen pipette method, Coulter counter method, microscopy and the laser diffraction/scattering method. The buoyancy weighing-bar method is suitable for measuring the settling particle size distribution and the floating particle size distribution. The buoyancy weighing-bar method could be used to measure the particle size distribution in Stokes region and in Allen region. The particle size distribution obtained by the buoyancy weighing-bar method could be used to estimate the smaller particle size by using the Rosin-Rammler distribution. Theory was rediscussed and the new mean particle size was defined. Beside, the buoyancy weighing-bar method could be used to determine the mean particle sizes for a ternary mixture and multi-component particles in a short time. This ability is very useful in the powder industry.

Similar to other methods to analyze particle size, the buoyancy weighing-bar method is accurate in an initially homogeneous suspension. Because the buoyancy weighing-bar method apparatus can be made by hand, it is also economical. Additionally, the buoyancy weighing-bar method is easier to be implemented compared to other sedimentation particle analysis methods.

Contents

	Page
Abstract	i
Contents	ii
List of Figures	v
List of Tables	vii
List of Papers	viii
Chapter 1 Introduction	1
1.1 Background	1
1.2. Principle of BWM	2
1.2.1 Settling particle	2
1.2.2 Floating particle	4
1.3 Calculation rules of PSDs by the BWM	6
1.3.1 Size interval	6
1.3.2 Time interval	6
1.3.3 Apparent mass interval	6
1.3.4 Size ratio	7
1.4 Previous research	7
1.5 Objective of the experiment	7
Chapter 2 Graphical analogy of particle size distribution among Andreasen pipette, sedimentation balance, fluidization curve and buoyancy weighing-bar methods	14
2.1 Introduction	14
2.2 Theory	14
2.2.1 Graphical analogy of PSD between the Andreasen pipette and fluidization curve methods	14
2.2.1.1 Andreasen pipette method	14
2.2.1.2 Fluidization curve method	15
2.2.2 Graphical analogy of PSD between the BWM and the sedimentation balance method	15
2.2.2.1 BWM	16
2.2.2.2 Sedimentation balance method	16
2.3 Material and Method	16
2.4 Results and Discussion	17
2.5 Conclusions	17
Chapter 3 Measurement and estimation of settling particle size distribution by the buoyancy weighing-bar method and the Rosin–Rammmler distribution	26
3.1 Introduction	26
3.2 Theory	26

3.3 Material and Method	27
3.4. Results and discussion	28
3.4.1 Combination validity of Rosin-Rammler distribution	29
3.4.2 Estimation accuracy	30
3.4.3. Suspended solid in spring water	30
3.5 Conclusions	31
Chapter 4 Graphical and numerical determinations of mean particle size of settling particles by the buoyancy weighing-bar method	42
4.1 Introduction	42
4.2 Theory	42
4.2.1 Schematic diagram of particle sedimentation	42
4.2.2 Definition of maximum particle size and velocity mean particle size of all the particles	44
4.2.3 Velocity mean particle sizes of all the particles and from a given particle size to a minimum size	45
4.2.4 Velocity mean particle size in the BWM	46
4.2.5 Particle size distributions and velocity mean particle sizes in multi-component mixtures	47
4.3 Material and Method	49
4.3.1 Sample particles	49
4.3.2 Experimental apparatus	49
4.3.3. Experimental conditions and methods	49
4.4 Results and discussion	50
4.5 Conclusions	51
Chapter 5 Measurement of the floating particle size distribution by the buoyancy weighing-bar method	61
5.1 Introduction	61
5.2 Theory	61
5.3 Materials and Methods	62
5.3.1 PSD measurement of glass beads GBL 100 (JIS Test Powders 2) and hollow glass beads K1 and S60HS (Sumitomo 3M) by the BWM	62
5.3.2 Influence of the weighing bar and vessel in the BWM on size distribution measurement of floating particle	63
5.4 Results and Discussion	64
5.4.1 PSD measurement of glass beads GBL 100 (JIS Test Powders 2) and hollow glass beads K1 and S60HS (Sumitomo 3M) by the BWM	64
5.4.1.1 PSD of glass beads GBL 100, JIS Test Powders 2 in heavy liquid	64
5.4.1.2 PSD of hollow glass beads K1, Sumitomo 3M	64
5.4.1.3 PSD of hollow glass beads S60HS, Sumitomo 3M	65
5.4.2 Influence of the weighing bar and vessel in the BWM on size distribution	

measurement of floating particle	65
5.4.2.1 Accuracy and repeatability of PSD measurements	65
5.4.2.2 Influence of weighing bar length	66
5.4.2.3 Influence of weighing bar diameter	66
5.4.2.4 Influence of vessel size	66
5.4.2.5 Influence of weighing bar shape	67
5.4.2.6 Influence of vessel shape and weighing bar position	67
5.4.2.7 Influence of the sectional area ratio	67
5.5 Conclusions	68
Chapter 6 Size distribution measurement of floating particles in the Allen region by the buoyancy weighing-bar method	79
6.1 Introduction	79
6.2 Theory	79
6.3 Materials and Methods	80
6.4. Results and Discussion	80
6.4.1. Spherical particles	80
6.4.2. Cylindrical particles	81
6.5 Conclusions	81
Chapter 7 Conclusions	87
7.1 Settling particles	87
7.2 Floating particles	88
References	90
Acknowledgements	95

List of Figures

- Figure 1.1 Determination of PSD by plot of pressure drop ΔP vs. superficial velocity u in fluidization
- Figure 1.2 Schematic diagram of particle settling
- Figure 1.3 Determination of settling PSD using the BWM
- Figure 1.4 Schematic diagram of particle floating
- Figure 1.5 Determination of the floating PSD using the BWM
- Figure 2.1 Graphical determination of PSD in Andreasen pipette method
- Figure 2.2 Graphical determination of PSD in settling balance method
- Figure 2.3 Schematic diagram of experiment apparatus
- Figure 2.4 Weighing bar (Slit-cylinder type)
- Figure 2.5 Apparent mass of weighing bar as a function of time (glass beads J-400)
- Figure 2.6 PSD of glass beads J-400
- Figure 2.7 PSD of white fused alumina no.2, JIS Test Powders 2
- Figure 2.8 PSD of white fused alumina no.3, JIS Test Powders 2
- Figure 2.9 PSD of particle mixture of white fused alumina no.2 and no.3 (40%:60%), JIS Test Powders no.2
- Figure 3.1 Apparent mass of weighing bar as a function of time
- Figure 3.2 PSDs of JIS Test Powders 2, No.4 (White fused alumina)
- Figure 3.3 PSDs of non-spherical silica sand Class 3 (JIS Test Powders 1)
- Figure 3.4 PSDs of the non-spherical calcium carbonate (heavy) Class 16, JIS Test Powders 1
- Figure 3.5 PSDs of the JIS Test Powders 1, class 4 (Talc)
- Figure 3.6 PSDs of magnesite (China)
- Figure 3.7 PSDs of soft-burned magnesia (China)
- Figure 3.8 PSDs of spherical glass beads GBL 30 (JIS Test Powders 2)
- Figure 3.9 PSDs of the JIS Test Powders 1, class 8 (KANTO (Japanese) loam)
- Figure 3.10 PSDs of the JIS Test Powders 1, class 5 (Fly ash)
- Figure 3.11 Rosin-Rammler plot (JIS Test Powders 1, class 3 (Silica sand))
- Figure 3.12 PSDs of JIS Test Powders 1, class 3 (Silica sand)
- Figure 3.13 PSDs of JIS Test Powders 1, class 10 (Fly ash) and class 11 (KANTO (Japanese) loam)
- Figure 3.14 PSDs of JIS Test Powders 1, class 17 (Calcium carbonate, heavy)
- Figure 3.15 PSDs of suspended solid in spring water
- Figure 4.1 Schematic diagram of the change in ideal particle settling over time.
- Figure 4.2 Mass ratio vs. settling time in ideal particle settling
- Figure 4.3 Determination of the particle size distribution and mean particle size of a ternary mixture using the buoyancy weighing bar method
- Figure 4.4 Determination of the particle size distribution and mean particle size of

	multi-component particles using the buoyancy weighing-bar method
Figure 4.5	Relationship between the mean particle size and mass frequency curve
Figure 4.6	Apparent mass of the weighing bar as a function of time with glass beads (GBL 30, JIS Test Powders 2)
Figure 4.7	Particle size distributions of glass beads (GBL 30, GBL 40, and GBL 60, JIS Test Powders 2)
Figure 4.8	Apparent mass of the weighing bar as a function of time with the ternary mixture (glass beads GBL 60, GBL 40 and GBL 30, JIS Test Powders 2)
Figure 4.9	Particle size distributions of a ternary mixture of glass beads (GBL 60, GBL 40 and GBL 30, JIS Test Powders 2)
Figure 5.1	Schematic diagram of the experimental apparatus, weighing bar and vessel
Figure 5.2	Schematic diagrams of the weighing bars
Figure 5.3	PSDs of glass beads GBL 100, JIS Test Powders 2 in heavy liquid
Figure 5.4	PSDs of hollow glass beads K1, Sumitomo 3M
Figure 5.5	PSDs of hollow glass beads S60HS, Sumitomo 3M
Figure 5.6	PSDs measured by microscopy, laser diffraction/scattering method and BWM
Figure 5.7	Time course change in the apparent mass of the weighing bar using the 1000 ml graduated cylinder
Figure 5.8	Influence of rod length on PSD (vessel diameter = 65 mm)
Figure 5.9	Influence of rod diameter on PSD (vessel diameter = 65 mm)
Figure 5.10	Influence of rod diameter on PSD (vessel diameter = 38 mm)
Figure 5.11	Influence of vessel size on PSD
Figure 5.12	Influence of weighing bar shape on PSD
Figure 5.13	PSDs measured in the square vessel
Figure 5.14	Particle sizes as a function of sectional area ratio
Figure 6.1	Apparent mass of the weighing bar as a function of time (spherical particle)
Figure 6.2	Particle size distributions of spherical particle
Figure 6.3	Apparent mass of the weighing bar as a function of time (cylindrical particle)
Figure 6.4	Particle size distributions of cylindrical particle

List of Tables

Table 1.1	History of several measurements methods in PSD
Table 2.1	Particle size of sample particles
Table 3.1	Properties of sample particles (granted by Japan Industrial Standard)
Table 4.1	Particle size of the sample particles
Table 4.2	Mean particle size of a ternary mixture of glass beads GBL 60, GBL 40, and GBL 30
Table 5.1	Sizes of weighing bar and vessel
Table 5.2	Particle size, standard deviation and variation coefficient
Table 6.1	Particle and liquid properties

List of Papers

<Papers>

- (1) Ohira, Y., K. Furukawa, **R. Tambun**, M. Shimadzu and E. Obata; Buoyancy Weighing-bar Method: - A Particle Size Distribution Measurement using New Settling Method -, *Journal of the Sedimentological Society of Japan*, **69**, 17-26 (2010.9)
- (2) **Tambun, R.**, T. Motoi, M. Shimadzu, Y. Ohira and E. Obata; Size Distribution Measurement of Floating Particles in the Allen Region by a Buoyancy Weighing-Bar Method, *Advanced Powder Technology*, **22**, 548-552 (2011.7)
- (3) Ohira, Y., K. Nakano, **R. Tambun**, M. Shimadzu, M. Ohta and E. Obata; Size Distribution Measurement of Floating Spherical Particles by the Buoyancy Weighing-Bar Method, *Kagaku Kogaku Ronbunshu*, **37**, 310-316 (2011.7)
- (4) **Tambun, R.**, M. Shimadzu, Y. Ohira and E. Obata; Definition of the New Mean Particle Size based on the Settling Velocity in Liquid, *Journal of Chemical Engineering of Japan*, in press
- (5) **Tambun, R.**, K. Nakano, M. Shimadzu, Y. Ohira and E. Obata; Sizes Influences of Weighing Bar and Vessel in the Buoyancy Weighing-Bar Method on Floating Particle Size Distribution Measurements, *Advanced Powder Technology*, in press
- (6) **Tambun, R.**, Y. Ohira, K. Furukawa, M. Hirayama, M. Shimadzu and E. Obata; Measurement and Estimation of Particle Size Distributions by the Buoyancy Weighing-Bar Method and the Rosin-Rammler Distribution at Construction Sites, *Particuology*, submitted

<Presentations>

- (1) **Tambun, R.**, Y. Ohira and E. Obata; Size Distribution Measurement of Settling Particles by a Buoyancy Weighing-Bar Method, JSED 2010, pp.90-91, Muroran, JAPAN (2010.3)
- (2) **Tambun, R.**, Y. Ohira and E. Obata; Graphical Analogy of Particle Size Distribution among Andreasen Pipette, Settling Balance, Fluidization-Curve and Buoyancy Weighing-Bar Method, 13th Asia Pacific Confederation of Chemical Engineering Congress (APCCChE 2010), CD-ROM, Chinese Taipei, TAIWAN-CHINA (2010.10)
- (3) **Tambun, R.**, M. Shimadzu, Y. Ohira and E. Obata; Influence of Solid Concentration on Particle Size Distribution Measurement by the Buoyancy Weighing-Bar Method, JSED 2011, pp.86-87, Muroran, JAPAN (2011.3)・・・JSED Poster Prize
- (4) Nakano, K., **R. Tambun**, M. Shimadzu, Y. Ohira, M. Ohta and E. Obata; Application of the Buoyancy Weighing-Bar Method to Floating Particle Size Measurement, JSED 2011, pp.88-89, Muroran, JAPAN (2011.3)
- (5) **Tambun, R.**, Y. Ohira and E. Obata; Graphical and Numerical Determinations of Mean Particle Diameter by Buoyancy Weighing Bar Method, 8th European Congress of Chemical Engineering (ECCE 2011), CD-ROM, Berlin, GERMANY (2011.9)

- (6) Kato, H., **R. Tambun**, M. Shimadzu, Y. Ohira and E. Obata; Measurement of Particle Density Distribution by the Buoyancy Weighing-bar Method, SCEJ 43th Autumn Meeting, Nagoya, JAPAN (2011.9)

Chapter 1

Introduction

1.1 Background

Various approaches have been used to measure particle size distributions [17]. The particle size distribution (PSD) is calculated based on several models, most often by number, by mass/volume and by surface. The modern sciences of PSDs have been published since the beginning of the 20th century. The short history of several modern sciences of PSDs measurements were shown in **Table 1.1**.

For solid–liquid systems, PSDs have been measured by the Stokes diameter. The Andreasen pipette method [16], sedimentation balance method [11], centrifugal sedimentation method [12], etc. have been used to measure the PSD in suspensions. These methods measure the migration velocities of particles in solution, and then particle size is calculated using Stokes formula. However, all these methods are time consuming and require special skills. On the other hand, a different principle can be used to analyze the PSD through microscopy [13], laser diffraction/scattering method [9], and Coulter counter method [19]. These methods require numerous samples to accurately determine the PSD. Although the laser diffraction/scattering and Coulter counter methods produce highly accurate results within a shorter time, they require extremely expensive equipment. Hence, a simple and cost effective method to determine the PSD is highly demanded.

Obata *et al.* have reported five measurements for PSD by fluidization in the laminar to turbulent flow region [1-7,14], and one of them can be obtained by a graphical measurement using a fluidization curve, *i.e.* the superficial velocity vs. pressure drop is plotted [4,5]. The fluidization curve is constructed using the same algorithm as the sedimentation (Odén) balance method [15].

The sedimentation method, which uses gravity, can simply and economically measure the PSD, but it is time consuming. Bardet and Young have reported that the buoyancy method can measure the PSD [10]. The buoyancy method determines the PSD by measuring the buoyancy of a weighing ball. We tried the buoyancy method, but we were unable to measure the PSD because the particles accumulated on the weighing ball. To prevent particle accumulation, we used a weighing bar.

Obata *et al.* have strived to develop a new method to measure the PSD using the buoyancy weighing bar method (BWM) [8]. In BWM, the change in suspension density due to particle migration is measured by weighing buoyancy against a weighing bar hung in a suspension. Although the buoyancy method uses incremental analysis, the BWM uses cumulative analysis. The principles of these two methods differ. In BWM the PSD is calculated using the length of the weighing bar and the change in the apparent mass of the weighing bar with time.

Although it is difficult to construct a handmade Odén balance, assembling a handmade weighing bar is easy. The proposed method is accurate just as the Andreasen pipette method and economical. Thus, the BWM is suitable to be used in developing countries.

1.2 Principle of BWM

1.2.1 Settling particle

PSD can be classified as either a cumulative or frequency function [17]. The distribution obtained in this method is the same cumulative function used in the Odén balance method [15] and manometric method. Although sedimentation curves are not really relevant to fluidization curves, they are analogous to plots of mass vs. settling time and plots of pressure drop vs. superficial velocity. **Figure 1** plots the pressure drop ΔP throughout the entire bed against the superficial velocity u [4-6]. If the superficial velocity u is u_3 , then:

$$\Delta P = \left[\frac{(\rho_p - \rho)M_0 g}{\rho_p A} \right] \left[\frac{D(x)}{100} \right] + u \frac{d\Delta P}{du} \equiv 0Y \quad (1.1)$$

$$\left[\frac{(\rho_p - \rho)M_0 g}{\rho_p A} \right] \left[\frac{D(x)}{100} \right] \equiv 0X, \quad u \frac{d\Delta P}{du} \equiv XY$$

where M_0 , A , and $D(x)$ are the total particle mass, cross-sectional area of the bed, and cumulative mass percentage undersize of particle size x , respectively. **Figure 1.1** graphically depicts the PSD using the fluidization curve.

The volume of the submerged weighing bar is $V_B = Ah$, where A is the cross-sectional area of the weighing bar and h is the length of the submerged weighing bar in the suspension. The densities of dispersion liquid containing the dispersant and particles are denoted as ρ_L , and ρ_p , respectively. The initial solid concentration of the suspension is C_0 [kg-solid/m³-suspension].

Figure 1.2 illustrates the schematic diagram of particle settling. **Figure 1.2(a)** shows that initial buoyant mass of the submerged weighing bar depended on the particles between the top of weighing bar and the bottom of that in the initial suspension.

At the settling time $t = 0$, the initial density of the suspension ρ_{S0} is:

$$\rho_{S0} = \rho_L + \frac{C_0}{\rho_p} (\rho_p - \rho_L) \quad (1.2)$$

Because the initial buoyant mass of the submerged weighing bar W_{B0} depends on the particles in the suspension from the suspension surface to depth h , W_{B0} can be defined as:

$$W_{B0} = V_B \rho_{S0} \quad (1.3)$$

Then the apparent mass of the weighing bar in the initial suspension is:

$$G_{B0} = V_B \rho_B - W_{B0} = V_B (\rho_B - \rho_{S0}) \quad (1.4)$$

where ρ_B is the density of the weighing bar.

Figure 1.2(b) shows that concentration of suspension C decreases with time, because large

particle have settled. The density of suspension ρ_{St} , the buoyant mass of weighing bar W_{Bt} and the apparent mass of the bar G_{Bt} in suspension at $t = t$ is given by the following equations:

$$\rho_{St} = \rho_L + \frac{(\rho_P - \rho_L)}{\rho_P} C \quad (1.5)$$

$$W_{Bt} = V_B \cdot \rho_{St} \quad (1.6)$$

$$G_{Bt} = V_B \cdot \rho_B - W_{Bt} = V_B \cdot \rho_B - V_B \cdot \rho_{St} = V_B (\rho_B - \rho_{St}) \quad (1.7)$$

Figure 1.2(c) shows that concentration of suspension C is finally zero, because small particles also have settled. The final density of suspension $\rho_{S\infty}$, the final buoyant mass of weighing bar $W_{B\infty}$ and the final apparent mass of the bar $G_{B\infty}$ in suspension at $t = t_{\min}$ is given by the following equations:

$$\rho_{S\infty} = \rho_L \quad (1.8)$$

$$W_{B\infty} = V_B \cdot \rho_L \quad (1.9)$$

$$G_{B\infty} = V_B \cdot \rho_B - W_{B\infty} = V_B (\rho_B - \rho_L) \quad (1.10)$$

Eq.(1.11) shows the mass balance of particles in suspension [17].

$$C_0 - C = C_0 \int_{x_i}^{x_{\max}} f(x) dx + C_0 \int_{x_{\min}}^{x_i} \frac{v(x)t}{h} f(x) dx \quad (1.11)$$

From Eqs.(1.3), (1.6), (1.9) and (1.11),

$$W_0 - W = (W_0 - W_{\infty}) \int_{x_i}^{x_{\max}} f(x) dx + (W_0 - W_{\infty}) \int_{x_{\min}}^{x_i} \frac{v(x)t}{h} f(x) dx \quad (1.12)$$

where $v(x)$ is the settling velocity of the particle, $f(x)$ is the mass frequency of the particle size x . Differentiate Eq.(1.12) with respect to the time t , we obtain:

$$-\frac{dW}{dt} = (W_0 - W_{\infty}) \int_{x_{\min}}^{x_i} \frac{v(x)}{h} f(x) dx \quad (1.13)$$

From Eqs.(1.12) and (1.13),

$$W_{Bt} = W_{Rt} + \left(\frac{dW_{Bt}}{dt} \right) t \quad (1.14)$$

where W_{Rt} is the mass of particles greater than particle size x , $W_0 - (W_0 - W_{\infty}) \int_{x_i}^{x_{\max}} f(x) dx$.

Combining Eqs. (1.7) and (1.14) produces:

$$G_{Bt} = V_B \cdot \rho_B - W_{Rt} + \left(\frac{dG_{Bt}}{dt} \right) t = G_{Rt} + \left(\frac{dG_{Bt}}{dt} \right) t \quad (1.15)$$

where $G_{Rt} = V_B \cdot \rho_B - W_{Rt}$, and $\frac{dG_{Bt}}{dt} = -\frac{dW_{Bt}}{dt}$, because, the decreasing mass of weighing bar is corresponding to the decreasing buoyant mass of the weighing bar. Value of G_{Rt} is calculated from tangent line based on Eq.(1.15). The cumulative mass oversize $R(x)$ is:

$$R(x) = \int_{x_i}^{x_{\max}} f(x) dx = \frac{G_{Rt} - G_{B0}}{G_{B\infty} - G_{B0}} = 1 - D(x) \quad (1.16)$$

Particle size x can be expressed by the following equation using Stokes formula:

$$x = \sqrt{\frac{18\mu_L v(x)}{g(\rho_P - \rho_L)}} \quad (1.17)$$

where g is the gravitational acceleration and μ_L is the viscosity of the dispersion liquid containing the dispersant. The sedimentation velocity of the particles $v(x)$ can be calculated by Eq. (1.18):

$$v(x) = \frac{h}{t} \quad (1.18)$$

where h is the submerged length of the weighing bar and t is the settling time. Particle size x given by Eq. (1.17) is the Stokes diameter. Thus, the theory of BWM is the similar to that for sedimentation balance analysis [15].

Figure 1.3 shows the calculation method of settling PSD. The upper right graph depicts the change in the apparent mass of weighing bar G_B with time, while the lower right graph shows the relationship between time and the reciprocal of the particle size. From Eqs. (1.17) and (1.18), time is proportional to the second power of the reciprocal of particle size. Hence, in this method, particle size x can be calculated at time t while G_{Rt} can simultaneously be calculated from tangent line based on Eq. (1.15). Mass percentage undersize $D(x)$ can be calculated by Eq. (1.16). Thus, the upper left graph illustrates the PSD from the calculated particle size x and $D(x)$.

1.2.2 Floating particle

Theoretically, the BWM can be applied not only to settling particles, but also to floating particles, including bubbles and liquid droplets [18]. However, the latter has not been verified. Let us assume the particles are uniformly dispersed in suspension. Schematic diagram of particle floating is shown in **Figure 1.4**. As shown in **Figure 1.4(a)**, the initial buoyant mass of the submerged weighing bar W_{B0} depended on the particles between the top of the weighing bar and the bottom of that in the suspension. The initial density of suspension ρ_{S0} , the initial buoyant mass of the weighing bar W_{B0} and the initial apparent mass of the bar G_{B0} in suspension at $t = 0$ is given by the following equations:

$$\rho_{S0} = \rho_L + \frac{C_0}{\rho_P}(\rho_P - \rho_L) \quad (1.19)$$

$$W_{B0} = V_B \rho_{S0} \quad (1.20)$$

$$G_{B0} = V_B \rho_B - W_{B0} = V_B(\rho_B - \rho_{S0}) \quad (1.21)$$

where the liquid density is ρ_L , the particle density is ρ_P , the initial concentration of suspension is C_0 [kg–solid/m³–suspension], the density of the weighing bar in suspension is ρ_B , the volume of the weighing bar is V_B . As shown in **Figure 1.4(b)**, concentration of suspension C decreases with the time, because large particles have floated. The density of suspension ρ_S , the buoyant mass of the weighing bar W_{Bt} and the apparent mass of the bar G_{Bt} in suspension at $t = t$ is given by the following equations:

$$\rho_S = \rho_L + \frac{C}{\rho_P}(\rho_P - \rho_L) \quad (1.22)$$

$$W_{Bt} = V_B \rho_S \quad (1.23)$$

$$G_{Bt} = V_B \rho_B - W_{Bt} = V_B(\rho_B - \rho_S) \quad (1.24)$$

As shown in **Figure 1.4(c)**, concentration of suspension C is finally zero, because small particles also have floated. The final density of suspension $\rho_{S\infty}$, the final buoyant mass of the weighing bar $W_{B\infty}$ and the final apparent mass of the weighing bar $G_{B\infty}$ in suspension at $t = \infty$ is given by the following equations:

$$\rho_{S\infty} = \rho_L \quad (1.25)$$

$$W_{B\infty} = V_B \rho_L \quad (1.26)$$

$$G_{B\infty} = V_B \rho_B - W_{B\infty} = V_B(\rho_B - \rho_L) \quad (1.27)$$

Eq.(1.28) shows the mass balance of particles in suspension [17].

$$C_0 - C = C_0 \int_{x_i}^{x_{\max}} f(x) dx + C_0 \int_{x_{\min}}^{x_i} \frac{v(x)t}{h} f(x) dx \quad (1.28)$$

From Eqs.(1.20), (1.23), (1.26) and (1.28),

$$W_0 - W = (W_0 - W_{\infty}) \int_{x_i}^{x_{\max}} f(x) dx + (W_0 - W_{\infty}) \int_{x_{\min}}^{x_i} \frac{v(x)t}{h} f(x) dx \quad (1.29)$$

where $v(x)$ is the floating velocity of the particle, $f(x)$ is the mass frequency of the particle size x . Differentiate Eq.(1.29) with respect to the time t , we obtain:

$$-\frac{dW}{dt} = (W_0 - W_{\infty}) \int_{x_{\min}}^{x_i} \frac{v(x)}{h} f(x) dx \quad (1.30)$$

From Eqs.(1.29) and (1.30),

$$W_{Bt} = W_{Rt} + \left(\frac{dW_{Bt}}{dt} \right) t \quad (1.31)$$

The apparent mass of the submerged weighing bar G_{Bt} is given by Eq.(1.24). It is gradually decreases from G_{B0} to $G_{B\infty}$. The volume and the density of the submerged weighing bar are constant value. Differentiate Eq.(1.24) with respect to the time t , we obtain:

$$\frac{dG_{Bt}}{dt} = -\frac{dW_{Bt}}{dt} \quad (1.32)$$

Therefore, from Eqs.(1.24), (1.31) and (1.32), we obtain:

$$G_{Bt} = V_B \rho_B - W_{Rt} + \left(\frac{dG_{Bt}}{dt} \right) t = G_{Rt} + \left(\frac{dG_{Bt}}{dt} \right) t \quad (1.33)$$

where $G_{Rt} = V_B \rho_B - W_{Rt}$. Value of G_{Rt} calculates from tangent line based on Eq.(1.33). The cumulative mass percentage oversize is:

$$R(x) = \int_{x_i}^{x_{\max}} f(x) dx = \frac{G_{Rt} - G_{B0}}{G_{B\infty} - G_{B0}} = 1 - D(x) \quad (1.34)$$

Particle size x is given by using Stokes formula. The floating velocity of the particles

$v(x)$ can be calculated by Eq. (1.34):

$$v(x) = \frac{h}{t} \quad (1.34)$$

where h is the submerged length of the weighing bar and t is the floating time.

Figure 1.5 shows the calculation method of floating PSD. The lower right graph depicts the change in the apparent mass of weighing bar G_B with time, while the upper right graph shows the relationship between time and the reciprocal of the particle size. This theory for the floating particles measured by the BWM is the similar to that for settling particles.

1.3 Calculation rules of PSDs by the BWM

There are some basics calculation rules for research data obtained. The calculation rules are necessary to obtain the more accuracy result. All these calculation rules give the close results, but have the different difficulty. The basic calculation rules are size interval, time interval, apparent mass interval and size ratio. Following is the procedure of those calculations.

1.3.1 Size interval

1. Calculate the size.
2. Set a size interval.
2. Cut the data based on size interval.
3. Calculate the PSD.
4. Check the undersize fraction from minimum size. If undersize fraction is smaller than previous data, then its data is cut. If undersize fraction is over 1, then size fraction is 1.
5. Data in Allen region have to be cut. (Sphere-shaped: $Re > 6$, Others: $Re > 2$)

1.3.2 Time interval

1. Set a time interval.
2. Cut the data based on time interval.
3. Calculate the PSD.
4. Check the undersize fraction from minimum size. If undersize fraction is smaller than previous data, then its data have to be cut. If undersize fraction is over 1, then size fraction is 1.
5. Data in Allen region have to be cut. (Sphere-shaped: $Re > 6$, Others: $Re > 2$)

1.3.3 Apparent mass interval

1. Set a apparent mass interval.

2. Cut the data based on apparent mass interval.
3. Calculate the PSD.
4. Check the undersize fraction from minimum size. If undersize fraction is smaller than previous data, then its data have to be cut. If undersize fraction is over 1, then size fraction is 1.
5. Data in Allen region have to be cut. (Sphere-shaped: $Re > 6$, Others: $Re > 2$)

1.3.4 Size ratio

1. Calculate the size.
2. Set a size ratio interval.
3. Cut the data based on size ratio.
4. Calculate the PSD.
5. Check the undersize fraction from minimum size. If undersize fraction is smaller than previous data, then its data is cut. If undersize fraction is over 1, then size fraction is 1.
6. Data in Allen region have to be cut. (Sphere-shaped: $Re > 6$, Others: $Re > 2$)

1.4 Previous research

There are two the important experiments had been done by using the BWM, they are:

1. New measurement of PSD by the BWM [8]. In this experiment, Obata *et al.* experimentally investigated the applicability of BWM to measure PSDs. They investigated that the BWM was a easy, useful and economical method in PSD measurement.
2. Measurement of the floating PSD by the BWM [18]. In this experiment, Motoi *et al.* concluded that the BWM could measure the floating PSDs.

1.5 Objective of the experiment

The purpose of this study is to develop the BWM as a novel method in PSD measurement. In this study, we investigated many factors affecting result of the PSD, such as:

1. Graphical analogy of PSD among Andreasen pipette method, settling balance method, fluidization curve and the BWM.
2. Measurement and estimation of PSD by the BWM and the Rosin-Rammler distribution.
3. Graphical and numerical determinations of mean particle size of settling particles by the BWM.
4. Influence of solid concentration on PSD measurement by the BWM.
5. Influence of the weighing bar and vessel in the BWM on floating PSD measurement.
6. Size distribution measurement of floating particles in the Allen region by the BWM.

Nomenclature

a	constant ($= \frac{18\mu_L}{h(\rho_P - \rho_L)g}$), $m^2 \cdot s$
A	cross-sectional area of weighing bar or fluidization bed, m^2
C	solid concentration of suspension, kg/m^3
$D(x)$	mass percentage undersize of particle size x , %
$f(x)$	mass frequency of the particle size x , m^{-1}
g	gravitational acceleration, m/s^2
G_{Bt}	mass of weighing bar at $t = t$, kg
G_{Rt}	$V_B \rho_B - W_{Rt}$, kg
h	submerged length of weighing bar, m
Re	Reynolds number ($= \frac{xv(x)\rho_L}{\mu_L}$), $-$
$R(x)$	mass percentage oversize of particle size x , %
t	time, s
u	superficial velocity, m/s
$v(x)$	settling velocity of particle size x , m/s
V_B	submerged volume of weighing bar, m^3
W_B	buoyant mass of the submerged weighing bar in the suspension, kg
W_{Rt}	$W_{B0} \int_x^{x_{max}} f(x)dx$, kg
x	particle size, m
μ_L	liquid viscosity, $Pa \cdot s$
ρ_L	liquid density, kg/m^3
ρ_B	density of weighing bar, kg/m^3
ρ_P	particle density, kg/m^3
ρ_S	density of suspension, kg/m^3
Subscripts	
max	maximum
min	minimum
0	initial $t=0$
∞	infinity $t = \infty$

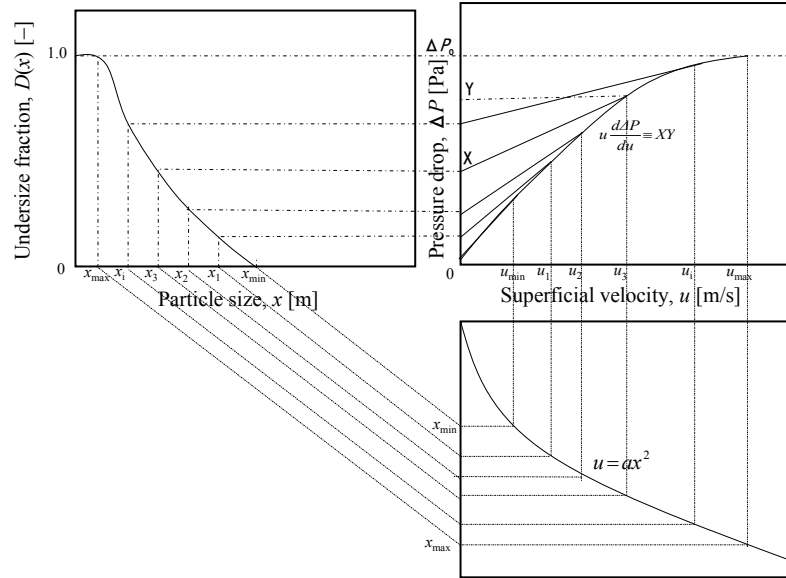


Figure 1.1 Determination of PSD by plot of pressure drop ΔP vs. superficial velocity u in fluidization.

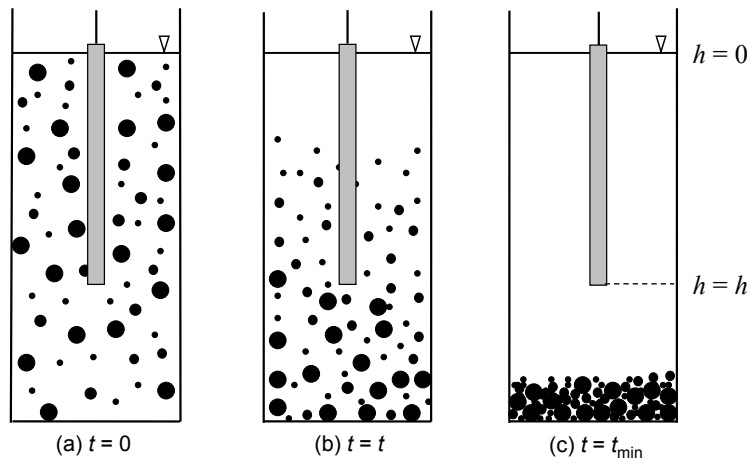


Figure 1.2 Schematic diagram of particle settling

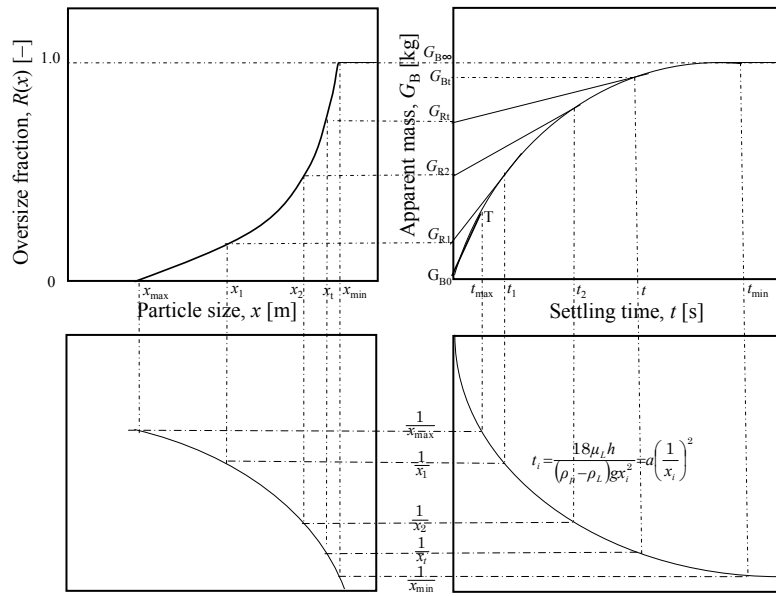


Figure 1.3 Determination of settling PSD using the BWM.

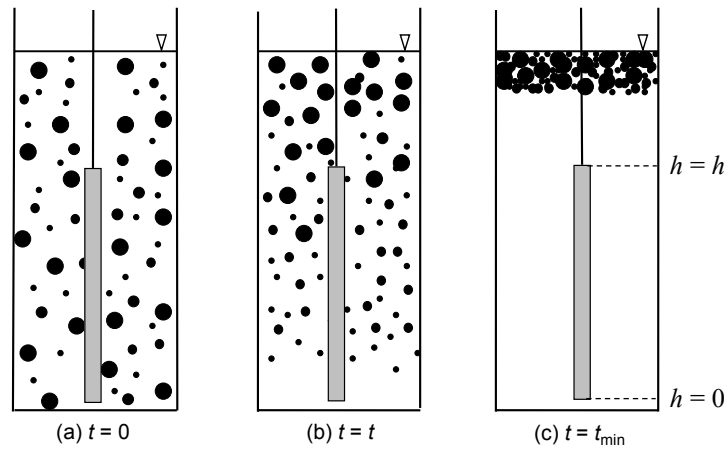


Figure 1.4 Schematic diagram of particle floating

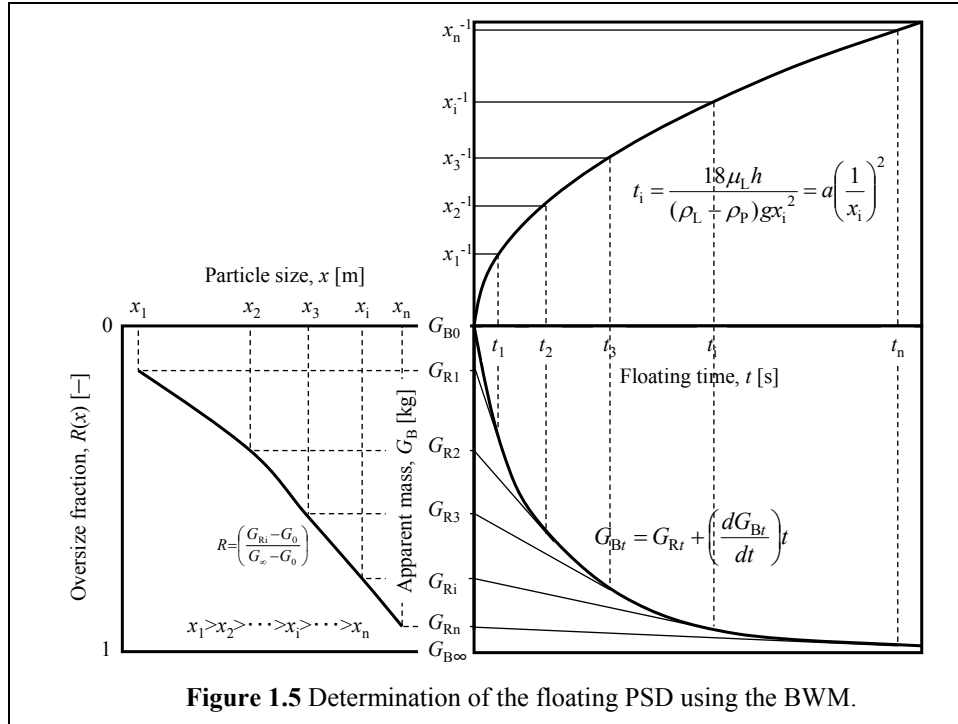


Figure 1.5 Determination of the floating PSD using the BWM.

Table 1.1 History of several measurements methods in PSD

Method	Author, title and journal	Year
Sedimentation	S. Odén; <i>Eine neue methode zur mechanischen Bodenanalyse</i> , Internationale Mitteilung fur Bodenkunde, 5, 575–311	1915
Sedimentation	S. Odén; <i>Eine neue methode zur bestimmung der körnerverteilung in suspensionen</i> , Kolloid Zeitschrift, 18, 33–47	1916
Manometric	G. Weigner; <i>Ist es der chemischen grogtechnik zur zeit schon msglich, ffir die</i> , Landw. Versuch. Stat, 91, 41	1918
Pipette	G. W. Robinson; A new method for the mechanical analysis of soils and other dispersions, Journal of Agricultural Science, 2, 306–321	1922
Microscopy	G. Martin, C. E. Blyth and H. Tongue; Trans. Ceram. Soc, 23, 61	1923
Sedimentation	S. Odén; The size distribution of particles in soils and the experimental methods of obtaining them, Soil Science, 19 (1), 1–35	1924
Hydrometer	W. J. Kelley; Determination of distribution of particle size, Industrial and Engi. Chemistry, 16, 928–930	1924
Hydrometer	G. J. Bouyoucos; The hydrometer as a new method for the mechanical analysis of soils, Soil Science, 23 (5), 343–354	1927
Pipette	H. M. Andreasen; The grinding of materials. theoretical and experimental researches on particle-size distribution incident to the disintegration process, Kolloid Beihefte, 27, 349–358	1928
X-ray	A. L. Patterson; The Scherrer formula for X-ray particle size determination, Physics Review, 56, 978–982	1939
Hydrometer “Divers”	S. Berg; <i>Ingenior videnskab</i> , Skrifter, 2, Danish Acad. Tech. Sci, Copenhagen	1940
Coulter counter	W. H. Coulter; Means for counting particles suspended in a fluid, US patent No. 2656508	Oct, 1953
Sedimentation and fluidization	J. F. Richardson and W. N. Zaki; Sedimentation and fluidisation. Part 1, Trans. Inst. Chem. Eng. 32, 35–53	1954
Centrifugal sedimentation	J. K. Donoghue and W. Bostock; Technique for particle-size analysis by centrifugal sedimentation, Transactions of the Institution of Chem. Engineers, 33 (1), 72–75	1955
Laser	W. M. Farmer; Measurement of particle size, number density, and velocity using a laser interferometer, Applied Optics, 11, 2603–2612	1972
Laser diffraction	J. Swithenbank, J. M. Beer, D. S. Taylor, D. Abbot and G.C. Mc Creath; A laser diagnostic for the measurement of droplet and particle size distribution, AIAA J, 76–79	1976

Fluidization	E. Obata, H. Watanabe and N. Endo; Measurement of size and size distribution of particles by fluidization, Journal of Chemical Engineering of Japan, 15, 23–28	1982
	E. Obata and H. Watanabe; Measurement of particle sizes by fluidization, Encyclopedia of Fluid Mechanics, Vol. 4, 221–236	1986
	E. Obata, H. Takahashi, M. Akiyoshi, K. Ando and H. Watanabe; Measurement of particle size distribution by superficial velocity and pressure drops across liquid–fluidized beds, Kagaku Kougaku Ronbunshu, 14, 103–106	1988
	E. Obata, H. Takahashi, M. Akiyoshi and K. Ando; The measurement of the size distribution of irregular particles by liquid–solid fluidization in a high Reynolds number, Journal of the Society of Powder Technology, 27, 301–307	1990
	E. Obata and K. Ando; Particle size measurements by fluidization: From laminar flow region to the turbulent flow region, Encyclopedia of Fluid Mechanics, Supplement 2, 169–189	1993
	E. Obata, M. Maruyama, Y. Ohira, M. Akiyoshi and K. Ando; The simultaneous measurement of crystal sizes and mass in a fluidized crystallizer, Journal of the Society of Powder Tech., 33, 456–461	1996
Buoyancy	J. P. Bardet and J. Young; Grain-size analysis by buoyancy method, Geotechnical Testing Journal, 20, 481–485	1997
Buoyancy weighing–bar	E. Obata, Y. Ohira and M. Ohta; New measurement of particle size distribution by a buoyancy weighing–bar method, Powder Technology, 196, 163–168	2009
	T. Motoi, Y. Ohira and E. Obata; Measurement of the floating particle size distribution by buoyancy weighing–bar method, Powder Technology, 201, 283–288	2010
	Y. Ohira, K. Furukawa, R. Tambun, M. Shimadzu and E. Obata; Buoyancy weighing–bar method: A particle size distribution measurement using new settling method, Journal of the Sedimentological Society of Japan, 69, 17–26	2010
	R. Tambun, T. Motoi, M. Shimadzu, Y. Ohira and E. Obata; Size distribution measurement of floating particles in the Allen region by a buoyancy weighing–bar method, Adv. Powder Tech., 22, 548–552	2011
	Y. Ohira, K. Nakano, R. Tambun, M. Shimadzu, M. Ohta and E. Obata; Size distribution measurement of floating spherical particles by the buoyancy weighing–bar method, Kagaku Kougaku Ronbunshu, 37, 310–316	2011

Chapter 2

Graphical Analogy of Particle Size Distribution among Andreasen Pipette, Sedimentation balance, Fluidization Curve and Buoyancy Weighing-bar Methods

2.1 Introduction

The particle size distribution (PSD) is absolutely essential to treating powders. The instruments for measuring the PSD are sieving screens, microscopes, sedimentation particle analyzers, and laser-scattering devices. In the sedimentation particle analyzers, there are several methods to measure the PSD, such as the Andreasen pipette method, fluidization method, sedimentation balance method, buoyancy weighing-bar method, etc [4]. All those methods can determine the PSD by graphical method and have graphical analogy with each other. One of analogy is cumulative undersize mass fraction obtained by Andreasen pipette and fluidization curve methods, and the other is the cumulative oversize mass fraction by the buoyancy weighing-bar and sedimentation balance methods. The Andreasen pipette method determines the undersize fraction of the PSD by plot of cumulative mass undersize vs. settling time. The fluidization curve method determines the undersize fraction of the PSD by plot of pressure drop vs. superficial velocity. On the other hand, the buoyancy weighing-bar and sedimentation balance methods determine the oversize fractions of the PSDs by plot of apparent mass of the weighing bar or cumulative mass oversize vs. settling time [1-6].

Theoretically, the buoyancy weighing-bar method (BWM) developed by us can be applied not only to measure the settling particles, but also the floating particles with different size [8]. In this paper, we focused to develop the BWM as a novel method in PSD measurement.

2.2 Theory

The PSD can be classified as either a cumulative ($R(x)$ or $D(x)$) or frequency ($f(x)$) function [7]. In this paper, all of the PSD signify the cumulative undersize $D(x)$ or oversize $R(x)$ mass fraction. The settling velocity of a particle in a fluid is naturally the terminal velocity in the laminar region.

2.2.1 Graphical analogy of PSD between the Andreasen pipette and fluidization curve methods

2.2.1.1 Andreasen pipette method

The maximum and minimum diameters of particles in a homogeneous suspension are symbolized as x_{\max} and x_{\min} , respectively. At a given time t from the beginning of sedimentation, a particle x having the terminal velocity $v(x) = h/t$ (which at the start were in

the top layer) have passed the point h . All of the particles having a velocity greater than h/t have passed below the point h and approached the bottom. The initial concentration of the powder is C_0 and the initial density of the suspension is ρ_{S0} . At $t = t$, the concentration C of the point h and the density ρ_{St} are given by the following equations (cf. **Figure 1.2** in Chapter 1):

$$\rho_{S0} = \rho_L + \frac{(\rho_P - \rho_L)}{\rho_P} C_0 \int_{x_{\min}}^{x_{\max}} f(x) dx \quad (2.1)$$

$$\rho_{St} = \rho_L + \frac{(\rho_P - \rho_L)}{\rho_P} C \int_{x_{\min}}^x f(x) dx \quad (2.2)$$

where ρ_L is the liquid density, ρ_P is the particle density, $f(x)$ is the mass frequency of particle size x , $\int_{x_{\min}}^{x_{\max}} f(x) dx = 1$, x is the particle size corresponding to: $v(x) = \frac{h}{t} = \frac{x^2(\rho_P - \rho_L)g}{18\mu}$,

where g is the gravitational acceleration, μ_L is the viscosity of the suspension liquid.

From Eqs. (2.1) and (2.2), the cumulative undersize mass fraction $D(x)$ is:

$$\frac{\rho_{St} - \rho_L}{\rho_{S0} - \rho_L} = \frac{C}{C_0} = \int_{x_{\min}}^x f(x) dx \equiv D(x) \quad (2.3)$$

The cumulative undersize mass fraction $D(x)$ and the particle diameter are constructed as **Figure 2.1**. Hence, the concentration of the point h have been the initial concentration C_0 from $t = 0$ to $t = t_{\max}$.

2.2.1.2 Fluidization curve method

Obata *et al.* have reported five measurements for the PSD by fluidization in the laminar to turbulent flow region, and one of them can be obtained by a graphical measurement using a fluidization curve, i.e. the superficial velocity vs. pressure drop [1-5]. There are partially fluidized and fixed beds in a fluidization system. The total pressure drop at a superficial velocity u becomes ΔP , which can be expressed as:

$$\Delta P = (\text{pressure drop in fluidized section}) + (\text{pressure drop on fixed bed}).$$

The relationship between pressure drop and mass frequency of particles present in terms of the fluidized particles of size x_{\min} to x and the particles in the fixed bed of size x to x_{\max} can be expressed as [2]:

$$\Delta P = \frac{(\rho_P - \rho_L)}{\rho_P A} M_0 \left\{ \int_{x_{\min}}^x f(x) dx + \frac{u}{u_{\max}} \int_x^{x_{\max}} \left(\frac{x_{\max}}{x} \right)^2 f(x) dx \right\} \quad (2.4)$$

where M_0 and A are the total mass of particles in a fluidization bed and cross-sectional area of the bed. **Figure 1.1** in Chapter 1 schematically illustrates the calculating method of the PSD used in fluidization curve. The PSD measurement graphics used in fluidization curve method (**Figure 1.1**) is analogous to that of PSD measurement graphics by Andreasen pipette method (**Figure 2.1**).

2.2.2 Graphical analogy of PSD between the BWM and the sedimentation balance method

2.2.2.1 BWM

Obata *et al.* have reported that the new measurement of the PSD by the BWM was analogous to the analysis of the sedimentation balance [4,6,8]. **Figures 1.2** and **1.3** in Chapter 1 illustrate the schematic diagram of particle settling and schematic illustrate the calculating method of the PSD used in the BWM, respectively. The line in $t = 0$ to t_{\max} is theoretically straight.

2.2.2.2 Sedimentation balance method

The theory of BWM is the similar to that of the sedimentation balance method. There is the pan for weighing the settling particles at the height h from a surface level. At the settling time t , the weight of the pan is as following equation [7].

$$w_t = M_0 \int_x^{x_{\max}} f(x) dx + M_0 \int_{x_{\min}}^x \frac{v(x)t}{h} f(x) dx \quad (2.5)$$

where M_0 is the total mass of the particles on the pan.

By differentiating with respect to time and multiplying by t ,

$$t \frac{dw}{dt} = M_0 \int_{x_{\min}}^x \frac{v(x)t}{h} f(x) dx \quad (2.6)$$

i.e.

$$w_t = M_0 \left\{ R(x_t) + \left(\frac{dw}{dt} \right) t \right\} \equiv w_0 w_{Rt} + w_{Rt} w_t \quad (2.7)$$

The PSD graphical measurement used in sedimentation balance method (**Figure 2.2**) is extremely analogous to that of PSD graphical measurement by the BWM (**Figure 1.3** in Chapter 1). Naturally the line in $t = 0$ to t_{\max} is straight.

2.3 Material and Method

Table 2.1 shows the particle size of the sample particles. The sample particles were glass beads J-400 (density: $2.40 \times 10^3 \text{ kg/m}^3$) and JIS Test Powder 2, white fused alumina no.2 (density: $3.91 \times 10^3 \text{ kg/m}^3$) and no.3 (density: $3.93 \times 10^3 \text{ kg/m}^3$). The particle densities were measured by the pycnometer.

Figure 2.3 schematically illustrates this experiment. The description of weighing bar is shown in **Figure 2.4**. The particle suspension was placed in a 1000 ml measuring cylinder (diameter: 65.0 mm, Sanplatec Co., Ltd). The weighing bar was hung from the analytical balance (GR-300: A&D Co., Ltd, minimum readout mass 0.1 mg) using a hanging wire. A personal computer was connected to the analytical balance with RS-232C to record data automatically. The weighing bar used in this experiment was aluminum slit cylinder (O.D.: 40 mm, I.D.: 30 mm, cylinder length: 210 mm, slit depth: 5.0 mm, slit length: 200 mm, submerged length: 200 mm, density: $2.70 \times 10^3 \text{ kg/m}^3$).

The experimental apparatus was placed in a box to avoid external effects such as airflow and temperature changes. A heater connected to the thermostat was placed in the box

to maintain the desired temperature of 298 K.

The suspensions had a solid concentration of 10 kg/m^3 (ca. 1 wt% in water). The suspensions were mixed in measuring cylinder. After thoroughly stirring the suspension using an agitator, the bar was set with the balance and was equipped with a personal computer. The measuring data, which consist of time t and the corresponding mass of the bar G_B , were recorded on a personal computer. The measuring time was 2 hours and the data were collected in 5-second intervals. After the measurements, the PSDs were calculated based on the above-described theory. Additionally, the PSDs were compared to the results from the sedimentation balance, Andreasen pipette and laser diffraction/ scattering method (Microtrac MT3000EX, Nikkiso Co., Ltd.).

2.4 Results and Discussion

Figure 2.5 shows the change with time in the apparent mass of the weighing bar G_B when the spherical glass beads J-400 was used. The apparent mass of the weighing bar increased over time until all the particles settled below the lower end of the weighing bar, and then the apparent mass of the weighing bar tended to become constant.

Figure 2.6 shows the PSD of spherical glass beads J-400. Based on the experimental result, the BWM gave the close result with the data obtained by sedimentation balance and laser diffraction/scattering methods, but not close to that measured by Andreasen pipette method. Hence, the BWM can measure the PSD of large particle up to $63 \mu\text{m}$ in water.

Figure 2.7 and **Figure 2.8** show the PSD of the white fused alumina no.2 and no.3, respectively. At those Figures, the PSDs measured by the BWM were close to those measured by Andreasen pipette and sedimentation balance methods. **Figure 2.9** shows the PSD of the particle mixture between no.2 and no.3 of white fused alumina by the BWM. The weight percentage of white fused alumina no.2 and white fused alumina no.3 were 40% and 60%, respectively. Based on the experimental result, the BWM can be used to measure the PSD of two-component particles with different size and gave the similar result with the data obtained by Andreasen pipette and sedimentation balance methods. As the particles of white fused alumina were needle-shaped not spherical, the PSDs measured by laser diffraction/scattering were slightly difficult from those measured by sedimentation particle analyzers.

As for the BWM, operability is easy, a personal error is small, and the price of the device is low.

2.5 Conclusions

We have investigated that there is the graphical analogy of PSD among Andreasen pipette, sedimentation balance, fluidization curve and buoyancy weighing-bar methods. Using the BWM, we measured the settling PSDs of glass beads J-400 and JIS Test Powders 2, white fused alumina no.2 and no.3. The following conclusions were determined:

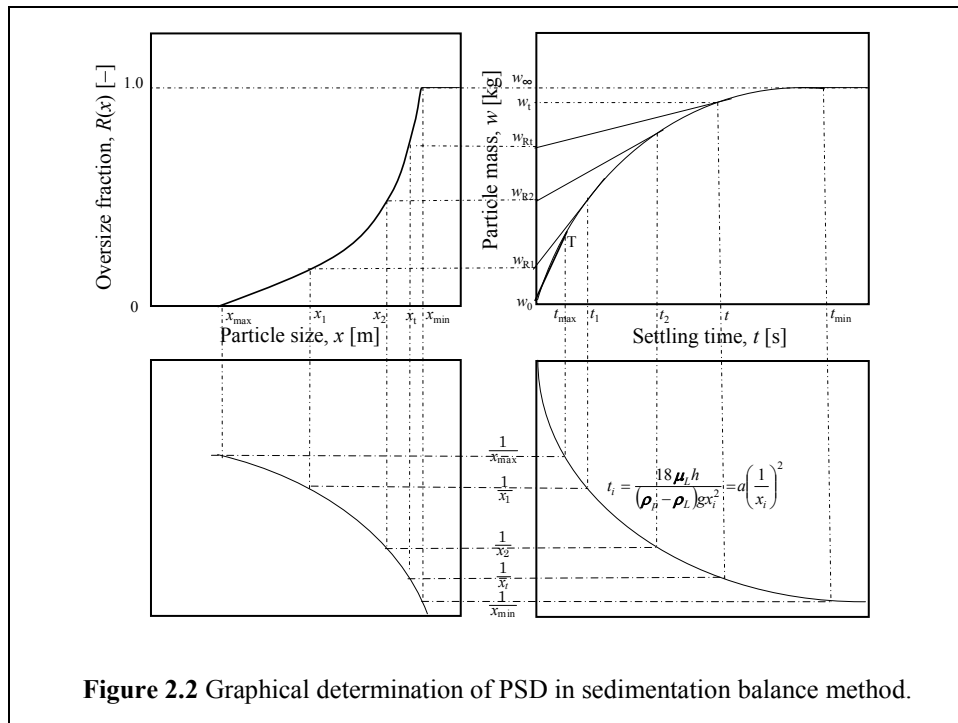
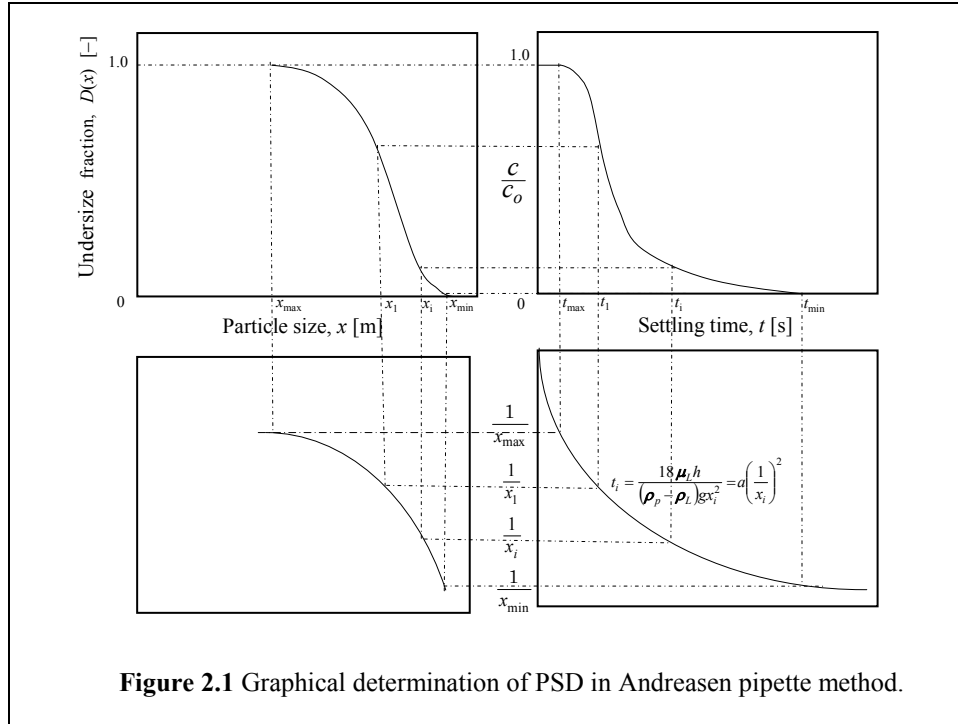
1. The PSD of large particle up to 63 μm can be measured in water using the BWM.
2. The BWM can measure the PSD of a needle-shaped particle for single and binary particles, and the result data obtained comparable to that measured by Andreasen pipette and sedimentation balance methods.

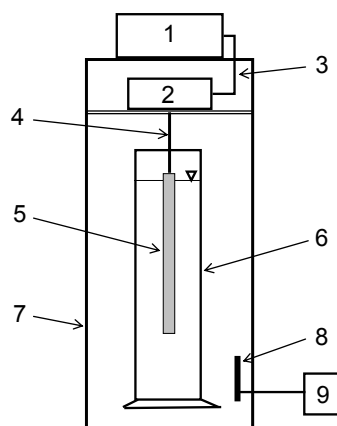
Nomenclature

A	cross-sectional area of the bed, m^2
C	solid concentration of suspension, kg/m^3
$D(x)$	undersize mass fraction of particle size x , –
$f(x)$	mass frequency of the particle size x , m^{-1}
g	gravitational acceleration, m/s^2
G_{Bt}	mass of weighing bar at $t = t$, kg
G_{Rt}	$V_B \rho_B - w_{\text{Rt}}$, kg
h	submerged length of weighing bar, m
M_0	total particle mass, kg
$R(x)$	oversize mass fraction of particle size x , –
t	time, s
u	superficial velocity, m/s
$v(x)$	sedimentation velocity of particle size x , m/s
V_B	submerged volume of weighing bar, m^3
w	mass of sediment, kg
w_B	buoyant mass of the submerged weighing bar in the suspension, kg
w_{Rt}	$w_{\text{B}0} \int_x^{x_{\text{max}}} f(x) dx$ or $M_0 \int_x^{x_{\text{max}}} f(x) dx$, kg
x	particle size, m
μ_L	liquid viscosity, $\text{Pa} \cdot \text{s}$
ρ_L	liquid density, kg/m^3
ρ_B	density of weighing bar, kg/m^3
ρ_P	particle density, kg/m^3
ρ_S	density of suspension, kg/m^3

Subscripts

max	maximum
min	minimum
0	initial $t = 0$
∞	infinity $t = \infty$





1. Personal computer 2. Analytical balance 3. RS-232C cable 4. Hanging wire
5. Weighing bar 6. Measuring glass cylinder 7. Thermal insulation vessel
8. Heating panel 9. Controller

Figure 2.3 Schematic diagram of experiment apparatus.

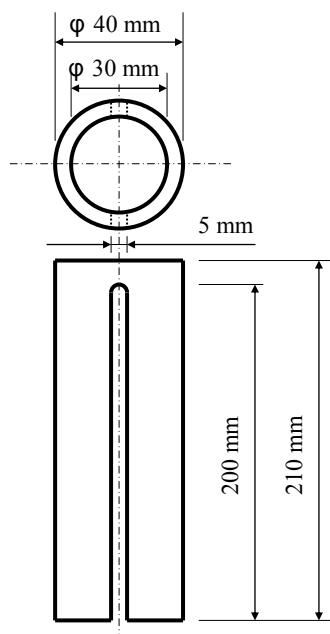


Figure 2.4 Weighing bar (Slit-cylinder type).

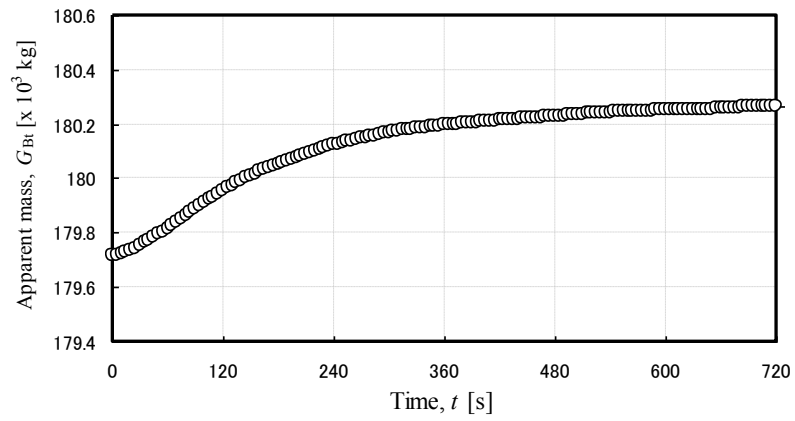


Figure 2.5 Apparent mass of weighing bar as a function of time (glass beads J-400).

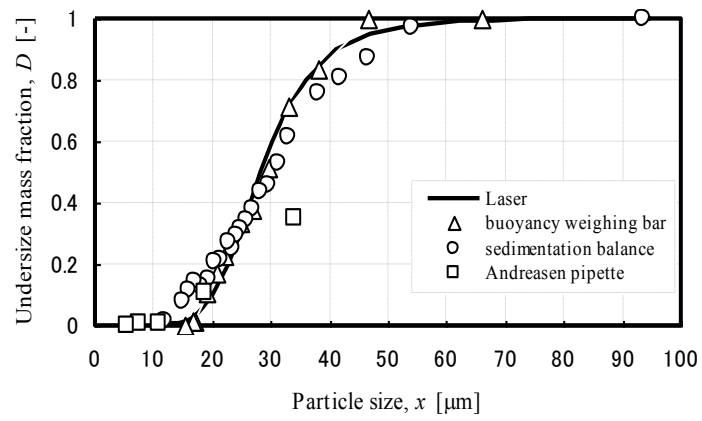


Figure 2.6 PSD of glass beads J-400.

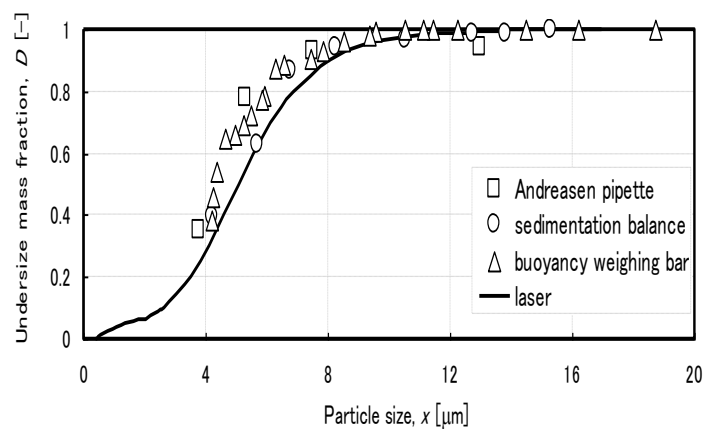


Figure 2.7 PSD of white fused alumina no.2, JIS Test Powders 2.

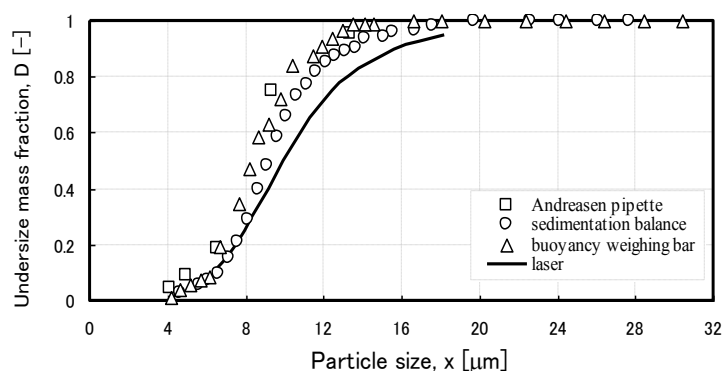


Figure 2.8 PSD of white fused alumina no.3, JIS Test Powders 2.

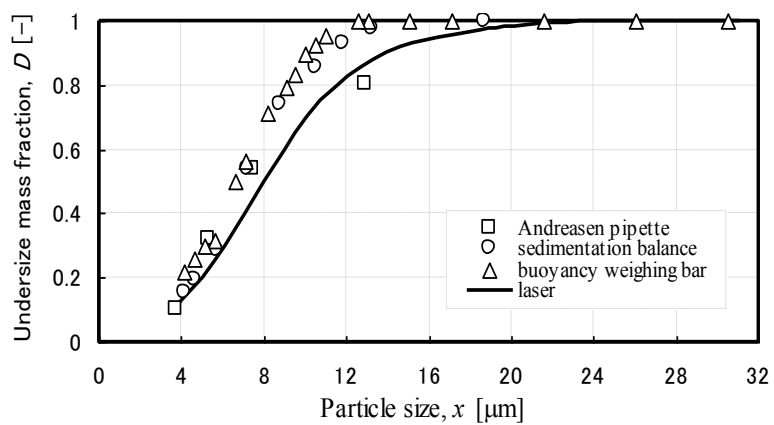


Figure 2.9 PSD of particle mixture of white fused alumina no.2 and no.3 (40%:60%), JIS Test Powders no.2.

Table 2.1

Particle size of sample particles.

Sample particles	Particle size (μm)				
	94% oversize	Median (80% or more)	50% oversize	3% oversize	Upper limit
White fused alumina no.2	2.0 min	—	4 ± 0.5	11 max	—
White fused alumina no.3	4.5 min	—	8 ± 0.6	20 max	—
J-400	—	< 45	—	—	63

Chapter 3

Measurement and Estimation of Settling Particle Size Distribution by the Buoyancy Weighing-Bar Method and the Rosin-Rammler Distribution

3.1 Introduction

Water might often spring when a soil near the river or lake dug up by an excavator. When spring water by digging contain soil particle, it is necessary to remove the suspended solid by flocculation and/or sedimentation for environmental preservation. For removing the suspended solid by flocculation and/or sedimentation, particle size distributions of soil and suspended solid in spring water are important information. Measurement of the particle size distribution (PSD) usually used the Andreasen pipette method [1], the hydrometer method [3], the centrifugal sedimentation method [5], the microscopy [16], the laser diffraction/scattering method [4], and the Coulter counter method [15]. The operation of the Andreasen pipette method, the microscopy and the hydrometer method is difficult though the equipment of those is cheap. On the other hands, although other methods produce highly accurate results within a shorter time, the equipments are extremely expensive. Each method is difficult to measure the PSD promptly on the construction field. It is necessary to develop the method of knowing the PSD at a low price and easily.

We have reported that the buoyancy weighing bar method (BWM) capable of measuring PSD of the settling particles [2,12,17]. The measurement result is almost equal to the sedimentation balance method [13]. However, the particle size measured within 2 hours was up to about 5 μm . To control the sedimentation process of suspended solid come from the construction field, it is necessary to determine the PSD of small particle which is less than about 5 μm . Particle size of less than about 5 μm has to measure for a long time or use the expensive equipments. These are not suitable for the measurement on the construction field. We thought that the PSD up to the small particle could be estimated by measuring data of the BWM and the Rosin-Rammler distribution [14].

In this paper, we discuss the estimation validity of the PSD which used the Rosin-Rammler distribution. For this estimation validity, we used the samples particles of suspended solids in spring water from a construction site near the Sorachi River at Furano, Hokkaido and JIS Test Powders 1 [silica sand (class 3), fly ash (class 10), KANTO (Japanese) loam (class 11), calcium carbonate, heavy (class 17)]. Besides, we experimentally investigated the PSD measurements of JIS Test Powders 1 (talc class 4, calcium carbonate (heavy) class 16, fly ash class 5), JIS Test Powders 2 (glass beads GBL 30, white fused alumina No.4), and magnesite and soft-burned magnesia (China). The influences of materials of weighing bar also were reported in this chapter.

3.2 Theory

In this section, the outline is briefly described because the theory of the settling PSD by the BWM has been explained in Chapter 1.2.1. The Rosin-Rammler distribution describes the relationship between particle size x and cumulative mass oversize R . Cumulative mass oversize R can be expressed as a function of particle size x by

$$R = \exp\left[-\left(\frac{x}{x_e}\right)^n\right], \quad (3.1)$$

where x_e is an absolute size constant and n is the distribution constant. To determine these parameters, Eq. (3.1) can be rewritten as

$$\ln \ln\left(\frac{1}{R}\right) = n \ln\left(\frac{x}{x_e}\right) = n \ln x - n \ln x_e. \quad (3.2)$$

Graphing $\ln \ln(1/R)$ versus $\ln x$ can determine distribution constant n from the slope. Absolute size constant x_e can be determined from the slope and intercept. The PSD can be calculated using Eq. (3.1), the distribution constant, and the absolute size constant.

3.3 Material and Method

The sample particles were silica sand class 3, talc class 4, calcium carbonate (heavy) class 16 and 17, fly ash class 5 and 10, KANTO (Japanese) loam class 11 (JIS Test Powders 1), spherical soda lime-silicate glass beads GBL 30, white fused alumina No.4 (JIS Test Powders 2), and magnesite (China, density: $3 \times 10^3 \text{ kg/m}^3$), soft-burned magnesia (China, density: $2.4 \times 10^3 \text{ kg/m}^3$).

Spring water was from a construction site near the Sorachi River at Furano, Hokkaido. Two liters of the suspension were separated into suspended solids and the dispersion liquid by a centrifugal separator (H-103N, Kokusan Co. Ltd.). The suspended solid concentration, ignition loss, and solid density analyzed according to JIS K0102 [8], JIS A1226 [7] and JIS A1202 [6] were 7.8 kg/m^3 , 0.041, and $2.71 \times 10^3 \text{ kg/m}^3$, respectively. NaHMP with a concentration of 0.078 kg/m^3 was used as a dispersant. The density and viscosity of the dispersion liquid added to NaHMP measured by the pycnometer [10] and Ubbelohde viscometer [9] were $1.00 \times 10^3 \text{ kg/m}^3$ and 0.89 mPa.s , respectively. **Table 3.1.** shows the properties of the sample particles [11].

Ion exchanged water and ethanol were used as liquid phase. The suspensions had a solid concentration of 10 kg/m^3 (ca. 1 wt.%). Sodium pyrophosphate (NaPP) and sodium hexametaphosphate (NaHMP), Kanto Chemical Co., Inc. were used as dispersant at using ion exchanged water as dispersion liquid.

The schematic diagram of the experiment apparatus and detail view of weighing bar are shown in **Figures 2.3** and **2.4**, respectively. The temperature during the experiment was maintained at 298 K. After thoroughly stirring the suspension using an agitator, the weighing bar was set with the balance and was equipped with a personal computer. The measuring data, which consist of time t and the corresponding apparent mass of the weighing bar G_B , were

recorded on a personal computer. The measuring time was one hour and the data were collected in 5-second intervals. After the measurement, the PSD was calculated based on theory and compared to the others method such as the laser diffraction/scattering (Microtrac MT3000EX, Nikkiso Co., Ltd.), Coulter counter, sedimentation balance, Andreasen pipette methods and the Rosin-Rammler distribution.

3.4. Results and discussion

Figure 3.1 shows the change with time in the apparent mass of the slit-cylinder when the initial concentration of the JIS Test Powders 2, No.4 (white fused alumina) was 5.0 kg/m^3 . The apparent mass of the slit-cylinder increased until all the particles settled below the lower end of the slit-cylinder, and then the apparent mass of the slit-cylinder became constant. The change in the apparent mass was due to the change in the buoyant mass against the slit-cylinder as well as particle settling.

Figure 3.2 shows the influence of solid concentration on PSDs measurement by the BWM when the JIS Test Powders 2, No.4 (white fused alumina) was used. The sodium hexametaphosphate (NaHMP) was used as dispersant. When the initial concentration of the JIS Test Powders 2, No.4 (white fused alumina) is 10 kg/m^3 or less, there is no effect of initial concentration on the PSD of the JIS Test Powders 2, No.4 (white fused alumina). When the initial concentration is 50 kg/m^3 , the PSD of the JIS Test Powders 2, No.4 (white fused alumina) could not be measured by the BWM. We found that the optimum solid concentration was 10 kg/m^3 or less. The PSD measured by the Andreasen pipette method is indicated by the filled triangle plots in **Figure 3.2**. The PSDs measured by the BWM were close to those measured by the Andreasen pipette method, but not close to those measured by the laser diffraction/scattering method, because the particle shape of the JIS Test Powders 2, No.4 (white fused alumina) is needle-shaped.

The effect of weighing bar density on PSD was investigated experimentally. **Figure 3.3** shows the PSDs of the non-spherical silica sand class 3, JIS Test Powders 1, when a bar composed of aluminum, copper, acryl resin and SUS 304 were used. The material of the weighing bar did not influence the PSD of non-spherical silica sand class 3, JIS Test Powders 1. The PSDs measured by the BWM was close to those measured by the sedimentation balance, Andreasen pipette and laser diffraction/scattering methods.

Figure 3.4 shows the PSDs of the non-spherical calcium carbonate (heavy) class 16, JIS Test Powders 1, when a bar composed of aluminum, copper and SUS 304 were used. The material of the weighing bar did not influence the PSD of non-spherical calcium carbonate (heavy) class 16, JIS Test Powders 1, and gave the similar result to those measured by sedimentation balance, Andreasen pipette, microscope and laser diffraction/scattering methods.

Figure 3.5 shows the PSDs of the JIS Test Powders 1, talc class 4. Ion exchanged water and ethanol were used as dispersion liquid. Sodium pyrophosphate (NaPP, Kanto Chemical

Co., Inc.) with the concentration of 3.0 kg/m^3 was used as dispersant at using ion exchanged water as dispersion liquid. As shown in Figure 3.5, there is no influence of dispersion liquid on the PSDs. The PSD of the talc class 4 measured by the BWM agreed well to those measured by sedimentation balance and Andreasen pipette methods, but not close to those measured by laser diffraction/scattering method, because the particle shape of the JIS Test Powders 1, talc class 4 is sheet-shaped. Hence, the BWM can measure the PSD of JIS Test Powders 1, talc class 4.

Figures 3.6 and 3.7 show the PSDs of magnesite (China) and soft-burned magnesia (China), respectively. The PSD of the magnesite (China) and soft-burned magnesia (China) measured by the BWM agreed well to those measured by laser diffraction/scattering method. Hence, the BWM can measure the PSD of magnesite and soft-burned magnesia (China).

Figure 3.8 shows the PSDs of the JIS Test Powders 2, glass beads GBL 30 (soda lime-silicate). The PSD of the glass beads GBL 30 measured by the BWM agreed well to those measured by Andreasen pipette, Coulter counter and laser diffraction/scattering methods. Hence, the BWM can measure the PSD of glass beads GBL 30 (JIS Test Powders 2).

Figure 3.9 shows the PSDs of the JIS Test Powders 1, class 8 (KANTO (Japanese) loam). The PSD of the class 8 (KANTO (Japanese) loam) measured by the BWM agreed well to those measured by sedimentation balance, Andreasen pipette and laser diffraction/scattering methods. Hence, the BWM can measure the PSD of JIS Test Powders 1, class 8 (KANTO (Japanese) loam).

Figure 3.10 shows the PSDs of the JIS Test Powders 1, fly ash class 5. The sodium pyrophosphate (NaPP) with the concentration of 3.0 kg/m^3 was used as dispersant. The PSD of the fly ash class 5 measured by the BWM agreed well to those measured by sedimentation balance and laser diffraction/scattering methods. Hence, the BWM can measure the PSD of JIS Test Powders 1, fly ash class 5.

3.4.1 Combination validity of Rosin-Rammler distribution

The PSDs of JIS Test Powders 1, class 3 (silica sand) measured by the BWM within 2 hours was shown in Figure 3.3. The minimum particle size that could be measured in the NaHMP solution is about $5 \text{ }\mu\text{m}$. To estimate particle sizes less than $5 \text{ }\mu\text{m}$, absolute size constant x_e and distribution constant n in Eq. (3.2) were calculated using that figure. **Figure 3.11** shows the Rosin-Rammler plot. Because the slope and intercept are 0.883 and -2.24 , absolute size constant x_e and distribution constant n are $12.6 \text{ }\mu\text{m}$ and 0.883, respectively. **Figure 3.12** shows the PSDs of JIS Test Powders 1, class 3 (silica sand). The open circles and dashed line denote previous data [2] and the PSD calculated by Eq. (3.2), respectively. The dashed line estimates cumulative mass oversize R at $1 \text{ }\mu\text{m}$ is about 0.9. The filled circles in Figure 3.12 show the standard data for the particle size by the sedimentation balance method from Japan Industrial Standard, and the squares denote the PSD measured within 24 hours. The PSD calculated by Eq. (3.2) is close to the standard data. Additionally, the PSD measured

within 24 hours agrees well with the dashed line. Hence, we conclude that the Rosin-Rammler distribution and data measured within two hours by the BWM can estimate the PSD.

3.4.2 Estimation accuracy

The PSD can be calculated theoretically by Eq. (3.2) and two data points. However, more data is necessary due to measurement errors. The cumulative mass oversize for JIS Test Powders 1, class 3 (silica sand) is up to about 0.6 within two hours. In this section, the lower limit of cumulative mass oversize measured by the BWM and the estimation accuracy are experimentally investigated.

Figure 3.13 shows the PSDs of JIS Test Powders 1, class 10 (fly ash) and class 11 (KANTO (Japanese) loam) with a measurement time of two hours as well as the JIS standard values and calculated values using Eq. (3.2). The values of the cumulative mass oversize are up to about 0.25 (class 10) and about 0.15 (class 11), but the PSD less than about 5 μm remain unknown within two hours. Using these data and Eq. (3.2), absolute size constant x_e and distribution constant n are calculated, respectively. The calculated line agrees well with the JIS standard values.

Figure 3.14 shows the PSD of JIS Test Powders 1, class 17 (calcium carbonate, heavy) as well as the calculation results from Eq. (3.2) and the JIS standard value. The value of cumulative mass oversize is up to about 0.10 within two hours. In this case, the calculated line does not agree with the JIS standard values. When the value of cumulative mass oversize exceeds 0.15, the PSDs can be estimated by Eq. (3.2). Therefore, the PSD was measured within six hours. The triangles and dashed line in Figure. 3.14 depict the PSD and the calculated result using Eq. (3.2), respectively. The value of the cumulative mass oversize is up to about 0.30 within six hours. The dashed line agrees well with the JIS standard values. Hence, the results indicate that Eq. (3.2) can estimate the PSD when the cumulative mass oversize exceeds 0.15.

3.4.3. Suspended solid in spring water

Figure 3.15 shows the PSD of suspended solids in spring water from a construction site near the Sorachi River at Furano, Hokkaido. The BWM measured the particle size of the suspended solid from 5 to 71 μm within two hours. The values of cumulative mass oversize are up to about 0.7. The dashed and solid lines in Figure 3.15 denote the calculated line by Eq. (3.2) and the data from the laser diffraction/scattering method, respectively. Although the principles of the laser diffraction/scattering method and the BWM differ, the PSD calculated by Eq. (3.2) provides results similar to those measured by the laser diffraction/scattering method. Hence, the PSD of suspended solids can be estimated by the BWM and the Rosin-Rammler distribution. Consequently, even without expensive laser diffraction/scattering equipment, the PSD of fine particles at a construction site can be determined.

3.5 Conclusions

1. For measuring the PSD of the JIS Test Powders 2, No.4 (White fused alumina), the suitable initial concentration is 10 kg/m^3 or less. The PSDs measured by the BWM was close to those measured by the Andreasen pipette method, but not close to those measured by the laser diffraction/scattering method.
2. When a bar composed of aluminum, copper, acryl resin and SUS 304 were used to measure the PSD of non-spherical silica sand class 3, JIS Test Powders 1, the material of the weighing bar did not influence the PSD. The PSDs measured by the BWM gave the similar result to those measured by the sedimentation balance, Andreasen pipette and laser diffraction/scattering methods.
3. When a bar composed of aluminum, copper and SUS 304 were used to measure the PSD of non-spherical calcium carbonate (heavy) class 16, JIS Test Powders 1, the material of the weighing bar did not influence the PSD. The PSDs measured by the BWM gave the similar result to those measured by sedimentation balance, Andreasen pipette, microscopy and laser diffraction/scattering methods.
4. BWM can measure the PSD of JIS Test Powders 1, talc class 4 used the ion exchanged water and ethanol as dispersion liquid. The PSD measured by the BWM agreed well to those measured by sedimentation balance and Andreasen pipette methods, but not close to those measured by laser diffraction/scattering method.
5. BWM can measure the PSD of magnesite (China) and soft-burned magnesia (China). The PSD measured by the BWM agreed well to those measured by laser diffraction/scattering method.
6. BWM can measure the PSD of glass beads GBL 30 (JIS Test Powders 2) and gave the close result to those measured by Andreasen pipette, Coulter counter and laser diffraction/scattering methods.
7. BWM can measure the PSD of JIS Test Powders 1, class 8 (KANTO (Japanese) loam). The PSD measured by the BWM agreed well to those measured by sedimentation balance, Andreasen pipette and laser diffraction/scattering methods.
8. BWM can measure the PSD of JIS Test Powders 1, fly ash class 5. The PSD measured by the BWM agreed well to those measured by sedimentation balance and laser diffraction/scattering methods.
9. The PSDs of JIS Test Powders 1, class 3, class 10 and class 11 could be measured by the BWM within two hours, and the Rosin-Rammler distribution can be estimated.
10. The PSD of JIS Test Powders 1, class 17 could not be estimated because the cumulative mass oversize is up to about 0.1 within two hours.
11. The PSD of suspended solids in spring water obtained at a construction site could be measured by the BWM and its Rosin-Rammler distribution.

Nomenclature

$D(x)$	mass percentage undersize of particle size x , %
G_{Bt}	mass of weighing bar at $t = t$, kg
G_{Rt}	$V_B \rho_B - W_{Rt}$, kg
n	distribution constant, -
R	cumulative mass oversize, -
t	time, s
x	particle size, m
x_e	absolute size constant, m

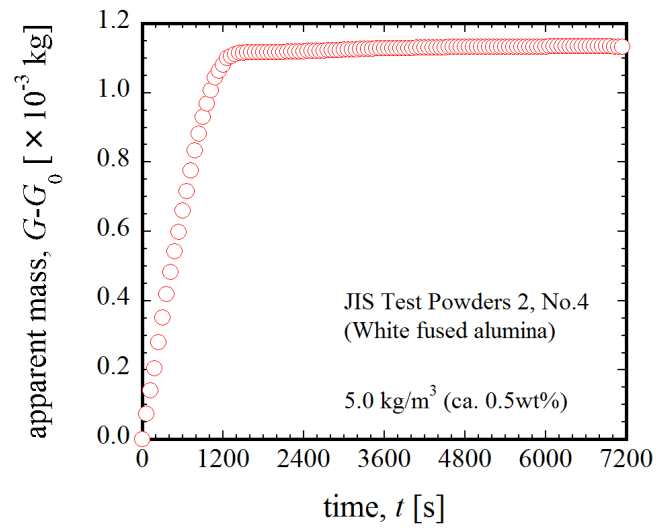


Figure 3.1 Apparent mass of weighing bar as a function of time.

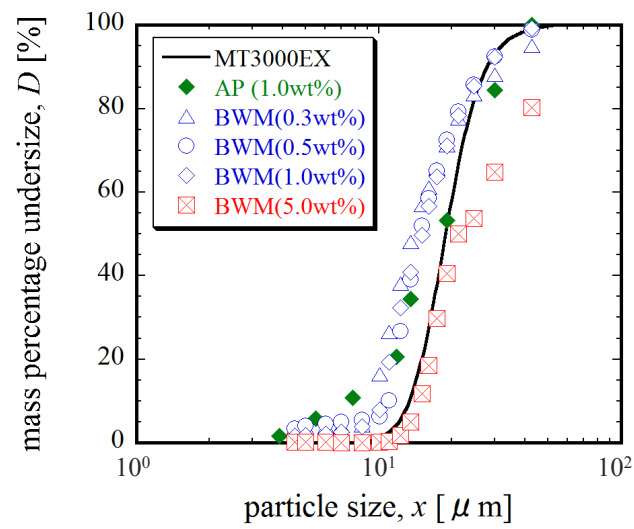


Figure 3.2 PSDs of JIS Test Powders 2, No.4 (white fused alumina).

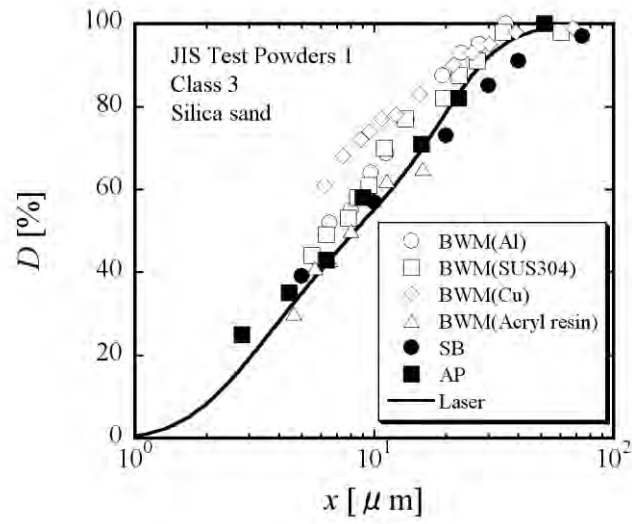


Figure 3.3 PSDs of non-spherical silica sand class 3 (JIS Test Powders 1).

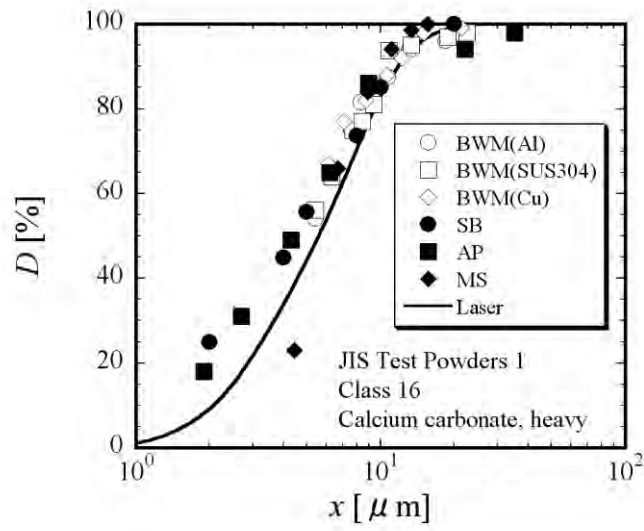


Figure 3.4 PSDs of the non-spherical calcium carbonate (heavy) class 16, JIS Test Powders 1.

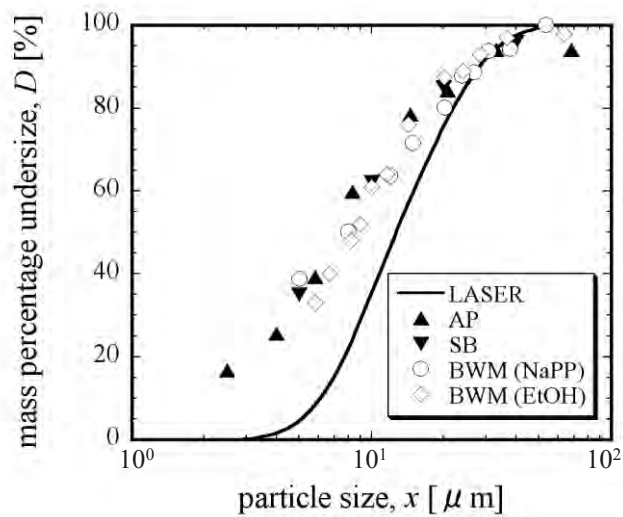


Figure 3.5 PSDs of the JIS Test Powders 1, class 4 (talca).

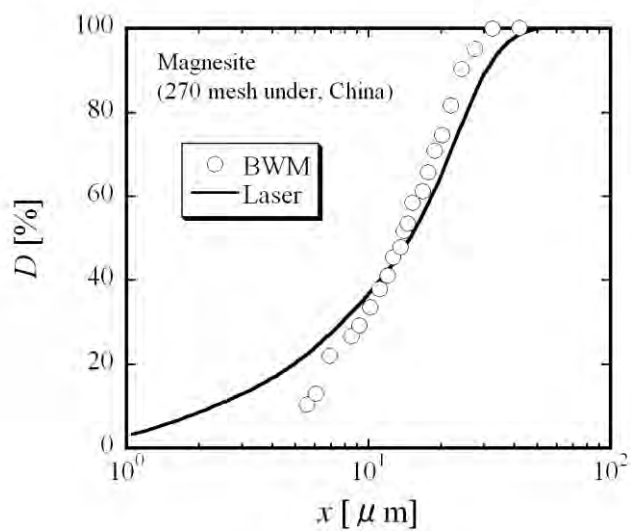


Figure 3.6 PSDs of magnesite (China).

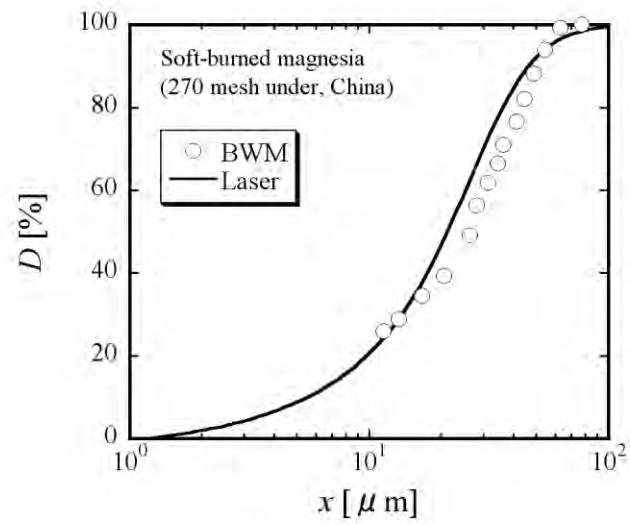


Figure 3.7 PSDs of soft-burned magnesia (China).

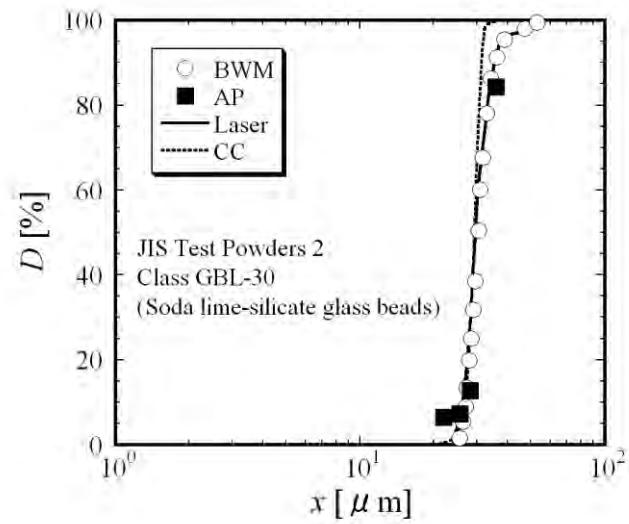


Figure 3.8 PSDs of spherical glass beads GBL 30 (JIS Test Powders 2).

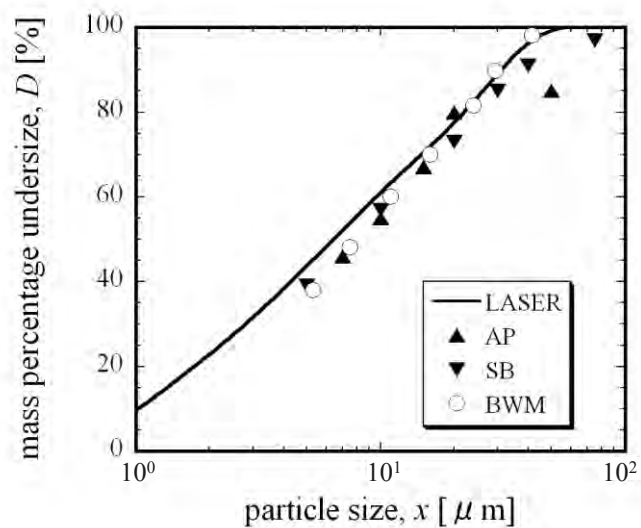


Figure 3.9 PSDs of the JIS Test Powders 1, class 8 (KANTO (Japanese) loam).

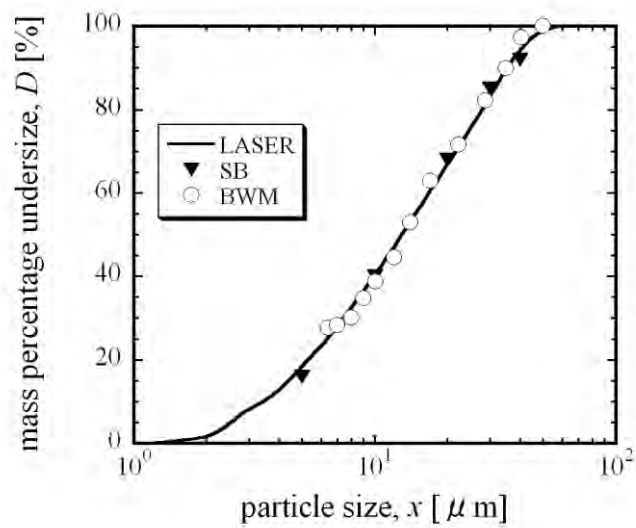


Figure 3.10 PSDs of the JIS Test Powders 1, class 5 (fly ash).

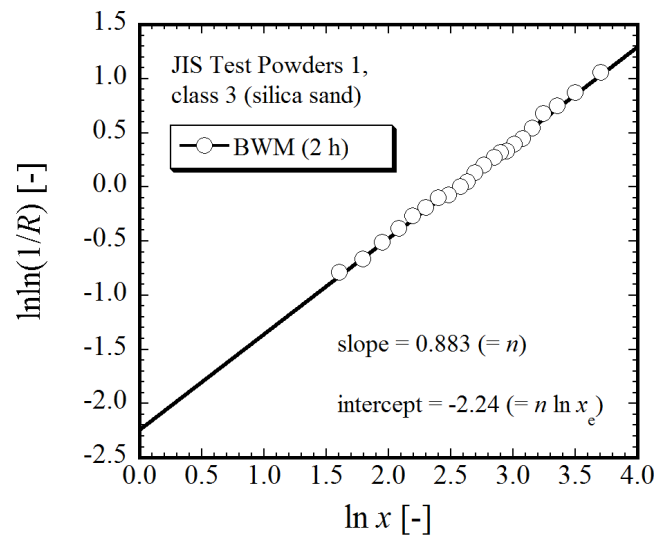


Figure 3.11 Rosin-Rammler plot (JIS Test Powders 1, class 3 (silica sand)).

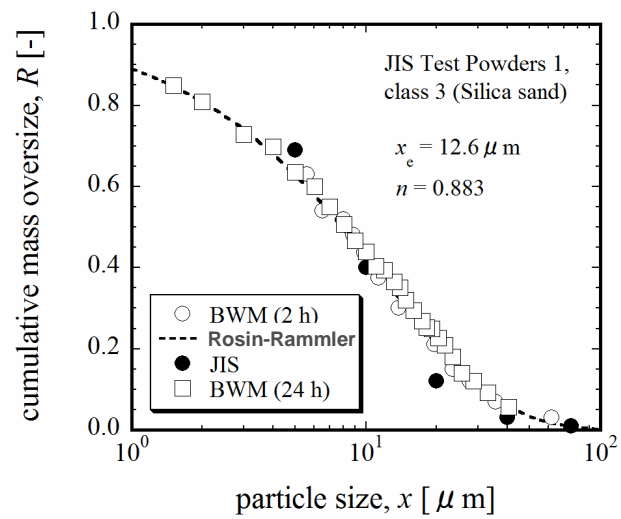


Figure 3.12 PSDs of JIS Test Powders 1, class 3 (silica sand).

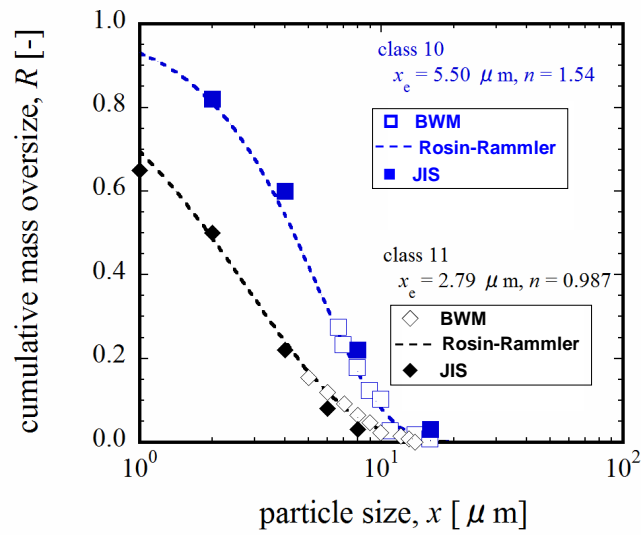


Figure 3.13 PSDs of JIS Test Powders 1, class 10 (fly ash) and class 11 (KANTO (Japanese) loam).

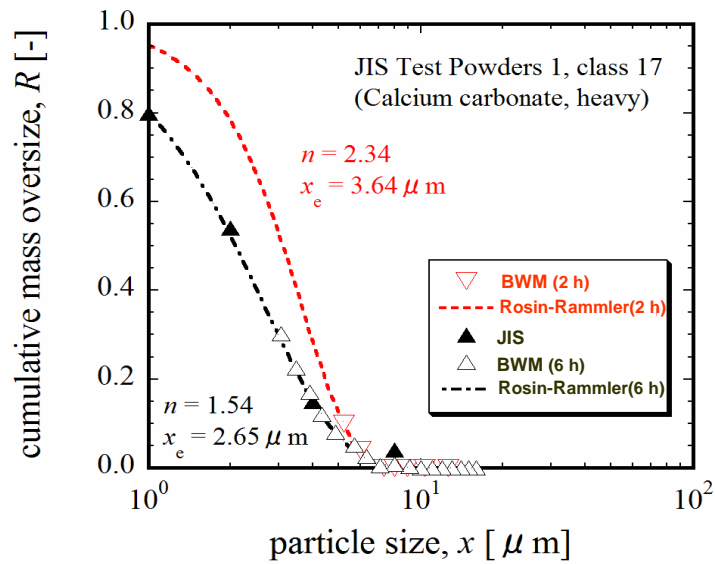


Figure 3.14 PSDs of JIS Test Powders 1, class 17 (calcium carbonate, heavy)

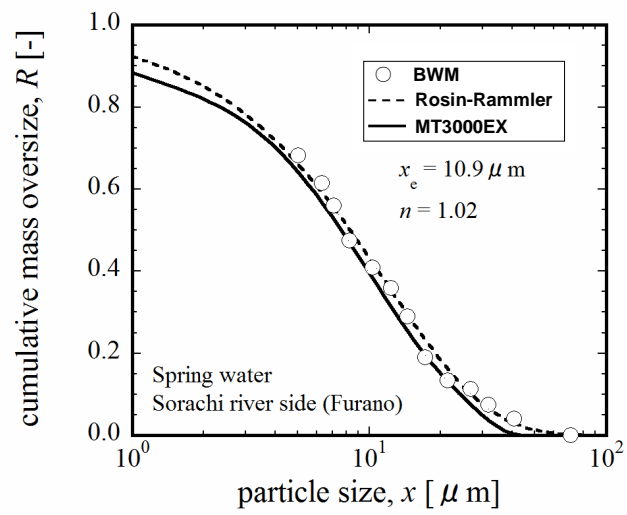


Figure 3.15 PSDs of suspended solid in spring water.

Table 3.1

Properties of sample particles (granted by Japan Industrial Standard).

Sample particle	Median size [m]	Particle density [kg/m ³]
JIS Test Powders 1, calcium carbonate (heavy) class 16	$3.6 - 4.6 \times 10^{-6}$	2700 – 2800
JIS Test Powders 1, silica sand class 3	$6.6 - 8.6 \times 10^{-6}$	2600 – 2700
JIS Test Powders 1, class 8 (KANTO (Japanese) loam)	$6.6 - 8.6 \times 10^{-6}$	2900 – 3100
JIS Test Powders 1, talc class 4	$7.2 - 9.2 \times 10^{-6}$	2700 – 2900
JIS Test Powders 1, fly ash class 5	$13 - 17 \times 10^{-6}$	2000 – 2300
JIS Test Powders 2, white fused alumina No. 4	$14 \pm 1 \times 10^{-6}$	3900 – 4000
JIS Test Powders 2, glass beads GBL 30	$30 \pm 1 \times 10^{-6}$	2100 – 2500

Chapter 4

Graphical and Numerical Determinations of Mean Particle Size of Settling Particles by the Buoyancy Weighing-Bar Method

4.1 Introduction

The particle size distribution (PSD) and mean particle size are the most important characteristics in particulate or powder technology. Sedimentation techniques to determine PSD consist of the Andreasen pipette, manometric pressure, sedimentation balance, buoyancy weighing-bar and fluidization curve methods. The buoyancy weighing-bar and fluidization curve methods were developed by Obata *et al* and Stanly–Wood *et al* [1-4,8]. Tambun *et al* have reported that the PSDs among Andreasen pipette, sedimentation balance, fluidization curve, and buoyancy weighing-bar methods have graphical similarities [10]. Because gravitation sedimentation methods use the settling velocity to determine particle size, the time-consuming measurement process is inconvenient when determining PSDs. Except for the Andreasen pipette method, sedimentation measurement methods determine the mean size of all the particles in a relatively short time.

Recall how the minimum fluidization velocity is determined in a fluidization system. Because the pressure drop of a fixed bed is proportional to the superficial velocity in a laminar flow region, the intersection point of the fluidization curve can determine the apparent minimum fluidization velocity of all the particles [1-3,6-9]. In the same manner, the increase in the apparent mass must be proportional to the settling time over a short period from the start until the maximum particles settle to the bottom of the sedimentation pan or below the submerged height of the weighing bar. However, the aforementioned phenomena have not been employed in particle size measurements.

This chapter proposes graphical and numerical determinations of the mean particle sizes employing the buoyancy weighing-bar method (BWM) as a novel method to measure PSD. The BWM with a slit-cylinder shaped weighing bar is used to determine the mean particle size for a ternary mixture and multi-component particles. Similar to other methods to analyze particle size, the BWM is accurate in an initially homogeneous suspension. Because the BWM apparatus can be made by hand, it is also economical. Additionally, the BWM is easier to be implemented compared to other settling particle analysis methods. The ability to determine the maximum particle size and mean particle size in a short time is useful in the powder industry.

4.2. Theory

4.2.1 Schematic diagram of particle settling

Sedimentation methods to determine the PSD depend on Stokes law and assume the particles in a suspension are spherical. For simplicity, the particles in this study are composed of three size and mass components x_L , M_L , x_M , M_M and x_S , M_S , respectively. **Figure 4.1** is a modified schematic diagram of particle settling with time, which was originally illustrated by Satone *et al* [5]. The volume of the submerged weighing bar is $V_B = Ah$ where A is the cross-sectional area of the weighing bar and h is the length of the submerged weighing bar in the suspension. The densities of the dispersion liquid and particles are denoted as ρ_L and ρ_P , respectively. The initial solid concentration of the suspension is C_0 [kg-solid/m³-suspension]. The Stokes velocity of a given particle size x_i is expressed as $v(x_i)$ [11]

$$v(x_i) = \frac{x_i^2 (\rho_P - \rho_L) g}{18 \mu_L} = \frac{h}{t_i} \quad (4.1)$$

From Eq. (4.1), $v(x_L)t_L = v(x_M)t_M = v(x_S)t_S = h$.

At a settling time $t = 0$ (Figure 4.1a), the initial density of the suspension (ρ_{S0}) is

$$\rho_{S0} = \rho_L + \frac{C_0}{\rho_P} (\rho_P - \rho_L) \quad (4.2)$$

Because the maximum buoyancy mass of the submerged weighing bar is $V_B \rho_{S0}$, the apparent mass of the weighing bar in the initial suspension is

$$G_{B0} = V_B (\rho_B - \rho_{S0}) \quad (4.3)$$

where ρ_B is the density of the weighing bar. The apparent mass of the weighing bar is transposed to $G_0 \equiv 0$ at $t = 0$.

At $0 < t < t_L$ (Figure 4.1b), the decreasing ratio of the buoyancy mass of the weighing bar is constant. The decreasing buoyancy mass for $t = t$ is

$$G_t = \frac{C_0 V_B t}{M_0 h} (v(x_L) M_L + v(x_M) M_M + v(x_S) M_S) \quad (4.4)$$

where $M_0 = M_L + M_M + M_S$.

At $t = t_L$ (Figure 4.1c), all the large particles have settled below the weighing bar, while the medium and small particles have settled to $v(x_M)t_L$ and $v(x_S)t_L$, respectively. The buoyancy mass at $t = t_L$ is

$$G_{tL} = \frac{C_0 V_B t_L}{M_0 h} (v(x_L) M_L + v(x_M) M_M + v(x_S) M_S) \quad (4.5)$$

At $t_L < t < t_M$ (Figure 4.1d), the decreasing ratio of the buoyancy mass of the weighing bar is constant again. The decreasing buoyancy mass for $t_L < t < t_M$ is smaller than that for $0 < t < t_L$. The decreasing buoyancy mass from $t = t_L$ to $t = t_M$ is

$$\frac{C_0 V_B (t - t_L)}{M_0 h} (v(x_M) M_M + v(x_S) M_S) \quad (4.6)$$

At $t = t_M$ (Figure 4.1e), all the medium particles have settled to the height h . Thus, the large and medium particles do not contribute between $h = 0$ and $h = h$. The buoyancy mass at $t = t_M$ is

$$G_{tM} = \frac{C_0 V_B}{M_0 h} (t_L v(x_L) M_L + t_M v(x_M) M_M + t_S v(x_S) M_S) \quad (4.7)$$

At $t = t_S$ (Figure 4.1f), the small particles have settled to height h . From time t_S , the buoyancy mass of the weighing bar is constant. Therefore, the transposed buoyancy mass is maximized.

$$G_{tS} = G_\infty = \frac{C_0 V_B}{M_0 h} (t_L v(x_L) M_L + t_M v(x_M) M_M + t_S v(x_S) M_S) \quad (4.8)$$

Using Eqs. (4.4)–(4.8) and Figure 4.1, **Figure 4.2** illustrates the decreasing buoyancy mass ratio of the weighing bar as a function of settling time, and yields the following relations

$$\frac{M_L}{M_0} = \frac{AB}{AO}, \quad \frac{M_M}{M_0} = \frac{BC'}{AO} \text{ and } \frac{M_S}{M_0} = \frac{C'O}{AO} \quad (4.9)$$

4.2.2 Definition of maximum particle size and velocity mean particle size of all the particles

The largest and the smallest particle sizes are $x_n = x_{\max}$ and $x_1 = x_{\min}$, respectively. A given particle size x_i corresponds to time t_i and the oversize fraction $R(x_i)$ is obtained by the intersection G_i . The mean size of all the particles and the apparent mean size of particles from x_1 to x_i are expressed as \bar{x}_0 and \bar{x}_i , respectively. The mean size of the particles from x_i to x_n is \bar{x}_i , and is above the line. In contrast, the mean size of the particles from x_1 to x_i is \underline{x}_i , and is below the line. The apparent minimum fluidization velocity (\bar{u}_{mf}) of multi-component particles has been determined by measuring the pressure drop through the particles in the fixed bed state. The procedure for determining the minimum fluidization velocity of multi-component particles was proposed by Obata *et al.* (1982) and Rincon *et al.* (1994). It was the following equation:

$$\bar{u}_{mf} = \left(\sum_{i=1}^n \frac{M_i}{M_0 u_{mfi}} \right)^{-1} \quad \left(\sum_{i=1}^n M_i = M_0 \right) \quad (4.10)$$

As the minimum fluidization velocity (u_{mfi}) of single particle is expressed by the Kozeny-Carman equation, Eq. (4.10) is rewritten by

$$\bar{x}_0 = \left(\sum_{i=1}^n \frac{M_i}{M_0 x_i^2} \right)^{-\frac{1}{2}} \quad (4.11)$$

where \bar{x}_0 refers to the apparent mean particle size of all the particles. Naturally, \bar{x}_0 corresponds to the apparent minimum fluidization velocity of multi-component particles. As described above, the curve of measuring mass vs. settling time by the buoyancy weighing-bar method is same as the weighing characteristics in ideal particle settling.

In Figure 4.2, the largest particles (x_L) settle to the bottom height (h) of the weighing bar at t_L . As the large, medium and small particles have settled to $v(x_L)t_L$, $v(x_M)t_L$ and $v(x_S)t_L$, respectively, the decreasing buoyancy mass is constant. Therefore, the line $A\delta$ must

be a straight line and the maximum particle size must be

$$x_L = \sqrt{\frac{18\mu_L h}{g(\rho_P - \rho_L)t_L}} \quad (4.12)$$

As the angle of the straight line $A\delta$ corresponds to the mass ratio of M_L , M_M and M_S , the intersection $\bar{t}_0 = t_L$ of the extrapolated straight line $A\delta$ and the total mass $M_L + M_M + M_S = M_0$ must be compatible with the mean particle size of all the particles ($\bar{x}_0 = \underline{x}_L$). This mean particle size defines the velocity mean particle size in terms of the Stokes velocity.

$$\frac{h}{t_L} = v(\bar{x}_0) = v(\underline{x}_L) = \frac{\bar{x}_0^2 (\rho_P - \rho_L)g}{18\mu_L} \quad (4.13)$$

Hence, the velocity mean particle size is not the median particle size based on mass but that is extremely useful in the powder industry, because the velocity mean particle size which is supplied by the sedimentation techniques can be measurable in a few minutes.

The intersection t_M of the extrapolated straight line $\delta\delta'$ and the total mass corresponds to the velocity mean particle size of M_M and M_S . Therefore,

$$\frac{h}{t_M} = v(\underline{x}_M) = \frac{\underline{x}_M^2 (\rho_P - \rho_L)g}{18\mu_L} \quad (4.14)$$

4.2.3 Velocity mean particle sizes of all the particles and from a given particle size to a minimum size

In the BWM, the initial concentration of the suspension, the volume, and the height of the weighing bar do not have principled relations when determining the PSD. However, as the largest particles settle to the bottom height of the weighing bar, the decreasing buoyancy mass ratio is constant at a maximum value. Figure 4.2 depicts the relationship between the buoyancy mass ratio and settling time.

At $0 < t < t_L$, the maximal decreasing buoyancy mass ratio is 1.0. Because the large particles have settled to the bottom height of the weighing bar at $t = t_L$, the decreasing buoyancy mass ratio depends on M_M and M_S from this point. From Eq. (4.5), the decreasing buoyancy mass ratio at $t = t_L$ corresponds to $G_{tL} = \delta$. The intersection $\bar{t}_0 = t_L > t_L$ of the extrapolated straight line $A\delta$ corresponds to the velocity mean size of all the particles \bar{x}_0 .

$$\text{From Eq. (4.1), } \bar{x}_0 = \underline{x}_L = \sqrt{\frac{18\mu_L h}{g(\rho_P - \rho_L)t_L}} \quad (4.15)$$

Hence, the velocity mean size of all the particles \bar{x}_0 is same as the velocity mean particle size from the maximum size to the minimum size \underline{x}_L . Further details are discussed later.

At $t = t_M$, the medium particles have settled to the bottom height of the weighing bar, and the decreasing buoyancy mass ratio corresponds to $G_{tM} = \delta'$. The intersection $D(x_M) = (M_M + M_S)/M_0$ of the intercept at the point δ' refers to the mass fraction undersize $D(x_M)$. In

contrast, the intersection $\underline{t}_M > t_M$ of the extrapolated straight line $\delta\delta'$ corresponds to the velocity mean particle size of M_M and M_S . Therefore,

$$\underline{x}_M = \sqrt{\frac{18\mu_L h}{g(\rho_P - \rho_L)\underline{t}_M}} \quad (4.16)$$

At $t = t_S = \underline{t}_S$, all the particles have settled to the bottom height of the weighing bar. The small particle size is same as the velocity mean particle size from the small particle size to the minimum size,

$$x_S = \underline{x}_S = \sqrt{\frac{18\mu_L h}{g(\rho_P - \rho_L)\underline{t}_S}} \quad (4.17)$$

The mass ratio of all the small particles corresponds to line segment $C'0$, and the point C' refers to M_S/M_0 and undersize mass fraction $D(x_S)$.

At $t = t_L$, the mass ratio of the small particles, which have settled to $v(x_S)t_L$ at t_L , corresponds to line segment $C'D'$. Similarly the mass ratio of the medium and small particles corresponds to segment BD . Therefore, the mass ratios of large, medium, and small particles at t_L correspond to AB , BC , and $CD = C'D'$, respectively. Because triangle $AD\delta$ is similar to $A0\underline{t}_L$, the Stokes velocity of the velocity mean size of all particles is expressed by $v(\bar{x}_0) = \frac{h}{\underline{t}_L} = \frac{\bar{x}_0(\rho_P - \rho_L)g}{18\mu_L}$. The particle sizes of large and medium particles are naturally

obtained by $\underline{x}_L = \sqrt{\frac{18\mu_L h}{g(\rho_P - \rho_L)\underline{t}_L}}$ and $\underline{x}_M = \sqrt{\frac{18\mu_L h}{g(\rho_P - \rho_L)\underline{t}_M}}$, respectively.

4.2.4 Velocity mean particle size in the BWM

Obata *et al* and Stanly–Wood *et al* have developed PSD measurements of dispersed particles in a fluid using a fluidization curve and the buoyancy of a weighing bar [1-4,8]. Tambun *et al* have reported that the Andreasen pipette, sedimentation balance, fluidization curve, and buoyancy weighing-bar methods produce graphically analogous PSDs [10].

Figure 4.1 schematically depicts particle settling of a ternary mixture. If the raw particles are comprised of three components with particle sizes x_L , x_M and x_S , the apparent mass of each type of particle in the volume of the submerged weighing bar is G_L , G_M , and G_S , respectively. **Figure 4.3** shows the relationships between the buoyancy mass of each component or all the particles and settling time. At incipient time, $t = 0$, it is assumed that the apparent buoyancy mass of the weighing bar is zero. At $t = t_L$, all large particles x_L settle at height h . When all small particles x_S settle at $t = t_S$, the apparent buoyancy mass of the weighing bar is $G_{tS} = G_\infty = G_L + G_M + G_S$. Thus, the following equations hold.

$$\delta = \alpha + \beta + \gamma = G_{tL} \quad (4.18)$$

$$\delta' = \alpha' + \beta' + \gamma = G_{tM} \quad (4.19)$$

$$\delta'' = \alpha'' + \beta' + \gamma = G_S + G_M + G_L = G_{tS} = G_{\infty} \quad (4.20)$$

The velocity mean particle size \bar{x}_0 of the ternary mixture refers to the intersection of the extrapolated straight line 0δ because all the particles are settling within settling time t_L . Similarly, the velocity mean particle size \underline{x}_M of a binary mixture refers to the intersection of the extrapolated straight line $\delta\delta'$ because large particles settle below the weighing bar. According to Figure 4.3,

$$\tan \angle \delta' G_L \gamma = \tan \angle \beta' 0 t_M + \tan \angle \alpha' 0 t_M \quad (4.21)$$

The velocity mean particle size of small particles (\underline{x}_S) is the intersection of the extrapolated straight line $\delta''\delta'$ because small particles are only present at the level of the weighing bar after time t_M . The oversize mass fraction $R(x) = 1 - D(x)$ of particle sizes x_L , x_M , and x_S is determined in Figure 4.3. The relationship between settling time t and particle size x is expressed by Stokes equation as Eq. (4.1). The velocity mean size of all particles (\bar{x}_0) and the velocity mean particle size from the medium particle size x_M to small particle size x_S (\underline{x}_M) are derived by the following equations. From Eq.(4.21),

$$\begin{aligned} \alpha &= M_S \left(\frac{t_L}{t_S} \right), \quad \beta = M_M \left(\frac{t_L}{t_M} \right), \quad \gamma = M_L \left(\frac{t_L}{t_L} \right), \text{ and } C_0 V_B \frac{M_i}{M_0} \equiv \Delta G_i, \\ G_{\infty} \left(\frac{h}{t_0} \right) &= G_{tL} \left(\frac{h}{t_L} \right) = \left(\Delta G_S \left(\frac{t_L}{t_S} \right) + \Delta G_M \left(\frac{t_L}{t_M} \right) + \Delta G_S \left(\frac{t_L}{t_L} \right) \right) \left(\frac{h}{t_L} \right) \\ &= \Delta G_S v(x_S) + \Delta G_M v(x_M) + \Delta G_L v(x_L) \end{aligned} \quad (4.22)$$

where $G_{\infty} = \Delta G_S + \Delta G_M + \Delta G_L$. Therefore,

$$\bar{x}_0 = \left(\frac{M_S x_S^2}{M_0} + \frac{M_M x_M^2}{M_0} + \frac{M_L x_L^2}{M_0} \right)^{\frac{1}{2}} = \left(\frac{\Delta G_S x_S^2}{G_{\infty}} + \frac{\Delta G_M x_M^2}{G_{\infty}} + \frac{\Delta G_L x_L^2}{G_{\infty}} \right)^{\frac{1}{2}} \quad (4.23)$$

The velocity mean particle size from the medium particle size x_M to small particle size x_S is derived by Eq. (4.24).

$$\underline{x}_M = \left(\frac{\Delta G_S x_S^2}{G_{\infty}} + \frac{\Delta G_M x_M^2}{G_{\infty}} \right)^{\frac{1}{2}} \quad (4.24)$$

4.2.5 Particle size distributions and velocity mean particle sizes in multi-component mixtures

Figure 4.4 depicts the relationship between the buoyancy mass and settling time in multi-component mixtures. The largest and the smallest particle sizes, $x_{\max} = x_n$ and $x_{\min} = x_1$, are described at time t_{\max} and t_{\min} , respectively. A given particle size x_i corresponds to time t_i and the oversize fraction $R(x_i)$ is obtained by the intersection G_i . The velocity mean size of all the particles and the apparent mean size of particles from x_{\min} to x_i are expressed as \bar{x}_0 and \underline{x}_i , respectively. The velocity mean size of the particles from x_i to $x_{\max} = x_n$ is \bar{x}_i , and is above the line. In contrast, the velocity mean size of the particles from x_{\min} to x_i is \underline{x}_i , and is below the line. From sedimentation balance theory,

$$G_{ti} = G_{\infty} \int_{x_i}^{x_{\max}} f(x) dx + \left(\frac{dG_B}{dt} \right)_{ti} t_i = 0G_i + G_i G_{ti} \quad (4.25)$$

where $f(x)$ is a function that defines the frequency distribution of the particles. The cumulative oversize mass fractions $R(x_i)$ is

$$R(x_i) = \int_{x_i}^{x_{\max}} f(x) dx = \frac{G_i}{G_{\infty}} = 1 - D(x_i) \quad (4.26)$$

The PSD of all the particles is shown in Figure 4.4. The maximum size of the particles is defined by t_{\max} .

Velocity mean particle sizes \bar{x}_0 and \bar{x}_i of all the particles as well as particles from a given size x_i to a maximum size x_{\max} have been defined by the fluidization curve method for the PSD [8]. Meanwhile, velocity mean particle sizes \bar{x}_0 and \bar{x}_i can be obtained by the BWM. Figures 4.3 and 4.4 clearly show that

$$\frac{G_{\infty}}{\bar{t}_0} = \frac{G_{t_{\max}}}{t_{\max}} = \sum_{i=1}^n \frac{\Delta G_i \frac{t_{\max}}{t_i}}{t_{\max}} = \sum_{i=1}^n \frac{\Delta G_i}{t_i} \quad (4.27)$$

where

$$\sum_{i=1}^n \Delta G_i = G_{\infty}$$

Hence, ΔG_i is the buoyancy difference mass of particles x_i . Multiplying all the terms by the height of the weighing bar h yields

$$G_{\infty} v(\bar{x}_0) = G_{t_{\max}} v(x_{\max}) = \sum_{i=1}^n \Delta G_i v(x_i) \quad (4.28)$$

where

$$v(\bar{x}_0) = \frac{h}{\bar{t}_0}, v(x_{\max}) = \frac{h}{t_{\max}} \text{ and } v(x_i) = \frac{h}{t_i}$$

At $t = t_i$,

$$\frac{G_{\infty} - G_i}{t_i} = \sum_{i=1}^i \frac{\Delta G_i}{t_i} \quad (4.29)$$

where

$$G_{\infty} - G_i = \sum_{i=1}^i \Delta G_i$$

Therefore,

$$\bar{x}_0 = \left(\sum_{i=1}^n \frac{\Delta G_i x_i^2}{G_{\infty}} \right)^{\frac{1}{2}} \quad \left(\sum_{i=1}^n \Delta G_i = G_{\infty} \right) \quad (4.30)$$

$$\bar{x}_i = \left(\sum_{i=1}^i \frac{\Delta G_i x_i^2}{G_{\infty} - G_i} \right)^{\frac{1}{2}} \quad \left(\sum_{i=1}^i \Delta G_i = G_{\infty} - G_i \right) \quad (4.31)$$

Additionally, the velocity mean particle size of all particles \bar{x}_0 must be the summation, which

is large mean size \bar{x}_i determined by adding small mean size \underline{x}_i

$$\bar{x}_0 = \left(1 - \frac{G_i}{G_\infty}\right) \underline{x}_i + \left(\frac{G_i}{G_\infty}\right) \bar{x}_i \quad (4.32)$$

Figure 4.5 shows all the mean sizes. It is obvious that all the equations in the BWM are realized in the sedimentation balance and manometric pressure methods.

4.3 Materials and experiment

4.3.1 Sample particles

The sample particles were spherical glass beads [GBL 60, GBL 40 and GBL 30, JIS Test Powders 2 (soda lime-silicate glass)]. According to pycnometer measurements, the particle densities of the sample materials were $2.30 - 2.37 \times 10^3 \text{ kg/m}^3$. **Table 4.1** shows the particle size of 10%, 50% and 90% oversize measured by a Coulter counter (Japan Industrial Standard). The particle sizes with 50% oversize of glass beads of GBL 30, GBL 40 and GBL 60 were 30 μm , 41 μm and 59 μm , respectively.

4.3.2 Experimental apparatus

The full details of experiment apparatus and weighing bar can be seen in **Figures 2.3** and **2.4**, respectively. Briefly, the particle suspension was placed in a 1000 ml graduated cylinder (diameter: 65.0 mm). The weighing bar was hung from an analytical balance (GR-300: A&D Co., Ltd., minimum readout mass 0.1 mg) using a hanging wire. A personal computer was connected to the analytical balance with RS-232C recorded data automatically. The weighing bar was an aluminum slit cylinder (O.D.: 40 mm, I.D.: 30 mm, cylinder length: 210 mm, slit depth: 5.0 mm, slit length: 200 mm, submerged length: 200 mm, density: $2.70 \times 10^3 \text{ kg/m}^3$).

The experimental apparatus was placed in a box to avoid external effects such as airflow and temperature changes. A heater connected to the thermostat was placed in the box to maintain the desired temperature of 298 K.

4.3.3. Experimental conditions and methods

Glycerol (Kanto Chemical Co., Ltd.) was used as an improver. The liquid phase was a glycerol solution (concentration: 40 wt%). The density and viscosity measured by the pycnometer and the Ubbelohde viscometer were $1.064 - 1.086 \times 10^3 \text{ kg/m}^3$ and $2.32 - 2.91 \times 10^{-3} \text{ Pa}\cdot\text{s}$, respectively. The suspensions had a solid concentration of 10 kg/m^3 (ca. 1 wt.% in glycerol solution). There is no effect of a solid concentration on the PSD when the concentrations are 10 kg/m^3 or less [12]. When a ternary mixture was used, the mass percentage of GBL 60, GBL 40 and GBL 30 were 30wt%, 40wt% and 30wt%, respectively.

After thoroughly stirring the suspension using an agitator, the weighing bar was set with a balance, which was hooked to a personal computer. The measured data, which consisted of time t and the corresponding apparent mass of the weighing bar G_B , were recorded on a personal computer in 5-s intervals for 1 h. Afterwards, the velocity mean particle size were analyzed based on theory. Additionally, the velocity mean particle sizes were compared to the calculated results. The calculation mode means that each type of glass bead (GBL 60, GBL 40 and GBL 30) was measured separately by the laser diffraction/scattering method (Microtrac MT3000EX, Nikkiso Co., Ltd.), and then determined based on the aforementioned theory.

4.4. Results and discussion

Figure 4.6 shows the change with time in the apparent mass of the weighing bar (G_B) when spherical glass GBL 30 beads were used. The apparent mass of the weighing bar increased over time until all the particles settled below the weighing bar. Because the tendency of the apparent mass to increase changed at 620 s, the maximum particle size of tested sample was

$$x_{\max} = \left(\frac{(18)(0.003)(0.2)}{(9.81)(237 - 1064)(620)} \right)^{\frac{1}{2}} = 35.2 \text{ } \mu\text{m}.$$

The apparent mass of the weighing bar became constant at 1300 s. The minimum particle size of tested sample was

$$x_{\min} = \left(\frac{(18)(0.003)(0.2)}{(9.81)(237 - 1064)(1300)} \right)^{\frac{1}{2}} = 24.3 \text{ } \mu\text{m}.$$

As shown in Table 4.1, particle sizes with 10% and 90% oversize were 34 μm and 26 μm , respectively, which are very similar. Thus, the change in the apparent mass of the weighing bar over time can be used to calculate the particle size range. In Figure 4.6, the mean size of glass beads GBL 30 corresponded to Stokes equation. For example, from $\bar{t}_0 = 840$ s,

$$\bar{x}_0 = \left(\frac{(18)(0.003)(0.2)}{(9.81)(237 - 1064)(840)} \right)^{\frac{1}{2}} = 30.2 \text{ } \mu\text{m},$$

whereas the particle size with 50% oversize by the laser diffraction/scattering method was 30.1 μm . Similar analyses were performed for GBL 40 and GBL 60. In these cases, the range of Reynolds number is 0.0015-0.047.

Figure 4.7 shows the PSDs of spherical glass beads of GBL 30, GBL 40 and GBL 60 measured by the BWM. The lines indicate data from the laser diffraction/scattering method. Table 4.1 lists the 50% oversize for particles measured by the BWM and the laser diffraction/scattering method. The BWM, laser diffraction/scattering method, and Coulter counter (Japan Industrial Standard) produced similar particle sizes with 50% oversize

measured. Thus, the BWM and laser diffraction/scattering method provide similar PSDs.

Figure 4.8 shows the change in the apparent mass of the weighing bar (G_B) over time when a ternary spherical particle mixture of glass beads (GBL 60, GBL 40 and GBL 30) was used. The apparent mass of the weighing bar increased over time until all the particles settled below the weighing bar, and the apparent mass of the weighing bar became constant. Because the tendency of the apparent mass of the weighing bar to increase changed at 200 s, the maximum particle size of sample mixture was 65.0 μm . The apparent mass of the weighing bar became constant at 1300 s. The minimum particle size of sample mixture was 25.5 μm . As shown in Table 4.1, the particle size with 10% oversize for GBL 60 was 63 μm , while the particle size with 90% oversize for GBL 30 was 26 μm . Because these oversize values are similar, it is concluded that the change in the apparent mass of the weighing bar with time can be used to calculate the particle size range of the sample mixture.

Figure 4.9 shows the PSD of a ternary spherical particle mixture of glass beads (GBL 60, GBL 40 and GBL 30). The dashed and solid lines are the calculated results by multiplying each mass percentage by the single GBLs and that from the laser diffraction/scattering method, respectively. The data from the BWM is close to the dashed line, confirming that the BWM can measure the PSD of a ternary mixture. Although the reason is currently unclear, the PSD measured by the laser diffraction/scattering method is inconsistent with the calculated result for a ternary particle mixture.

In Figure 4.9, the velocity mean particle size \bar{x}_0 of the ternary mixture was 44.9 μm because $\bar{t}_0 = 420$ s. Once GBL 60 settled, the velocity mean particle size of GBL 40 and GBL 30 can be calculated. Likewise, the velocity mean particle size of GBL 30 can be calculated after GBL 40 has settled. **Table 4.2** shows the velocity mean particle sizes measured by the BWM and those calculated by results of single particles. Equation (4.30) was used to calculate the results from both the BWM and laser diffraction/scattering data. As described in Table 4.1, the results were calculated by multiplying each particle size with 50% oversize by the single GBLs. Based on the experimental results, the BWM can measure the velocity mean particle size of a ternary spherical particle mixture and provides results similar to the calculated results. Hence, it is concluded that the BWM can determine the velocity mean particle size of all the particles in a ternary mixture within 200 s.

4.5 Conclusions

The PSD and velocity mean particle size can be determined graphically by the BWM. The following conclusions are determined:

1. The velocity mean size of all particles (\bar{x}_0) and the velocity mean size of particles from x_1 to x_i (\bar{x}_i) by the BWM are determined by

$$\bar{x}_0 = \left(\sum_{i=1}^n \frac{\Delta G_i x_i^2}{G_\infty} \right)^{\frac{1}{2}} \quad \left(\sum_{i=1}^n \Delta G_i = G_\infty \right)$$

$$\underline{x}_i = \left(\sum_{i=1}^i \frac{\Delta G_i x_i^2}{G_\infty} \right)^{\frac{1}{2}} \quad \left(\sum_{i=1}^i \Delta G_i = G_\infty - G_i \right)$$

where ΔG_i is the buoyancy difference mass of particles x_i .

2. The maximum particle size can be defined by t_{\max} .
3. The velocity mean sizes of particles (\underline{x}_i) can be recognized graphically by the BWM.
4. The PSD and mean particle size for a ternary spherical particle mixture of glass beads (GBL 60, GBL 40 and GBL 30) can be measured by the BWM because the BWM measured and calculated results are similar.

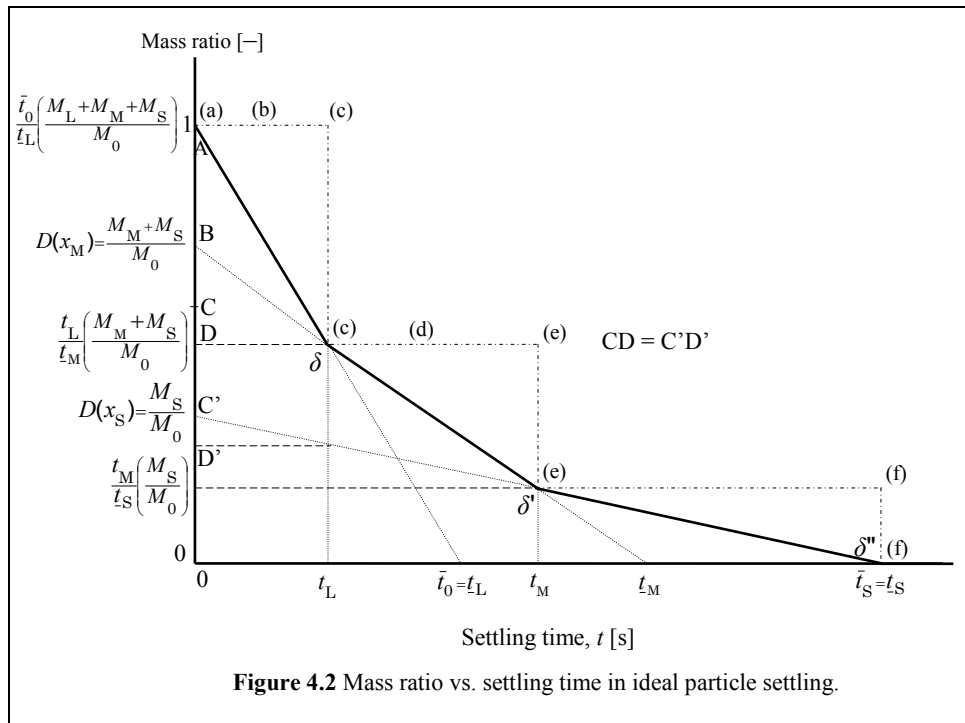
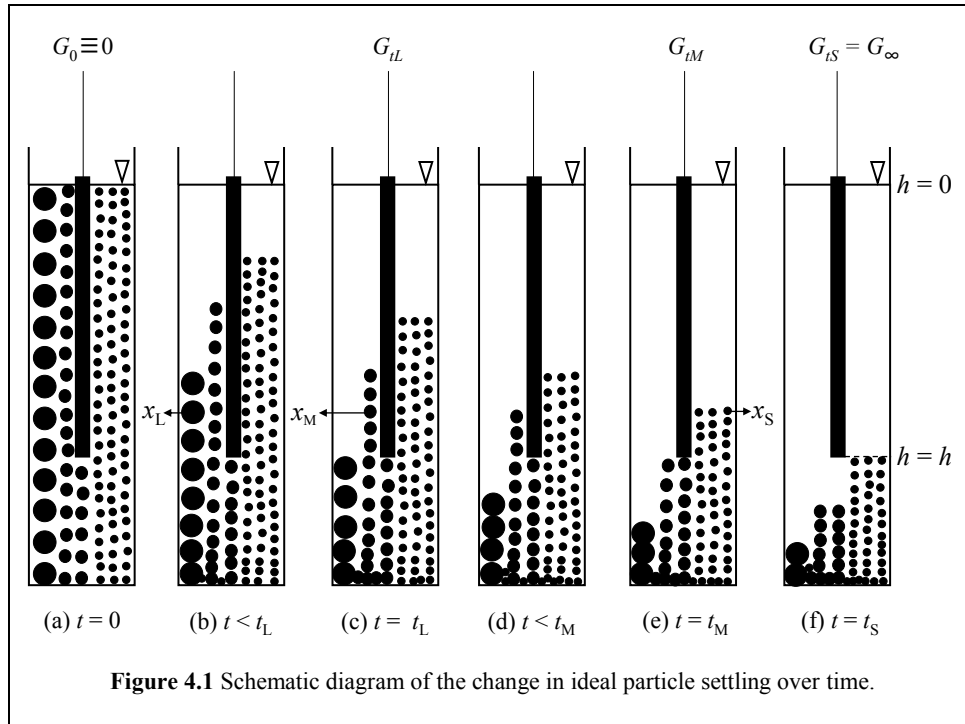
Nomenclature

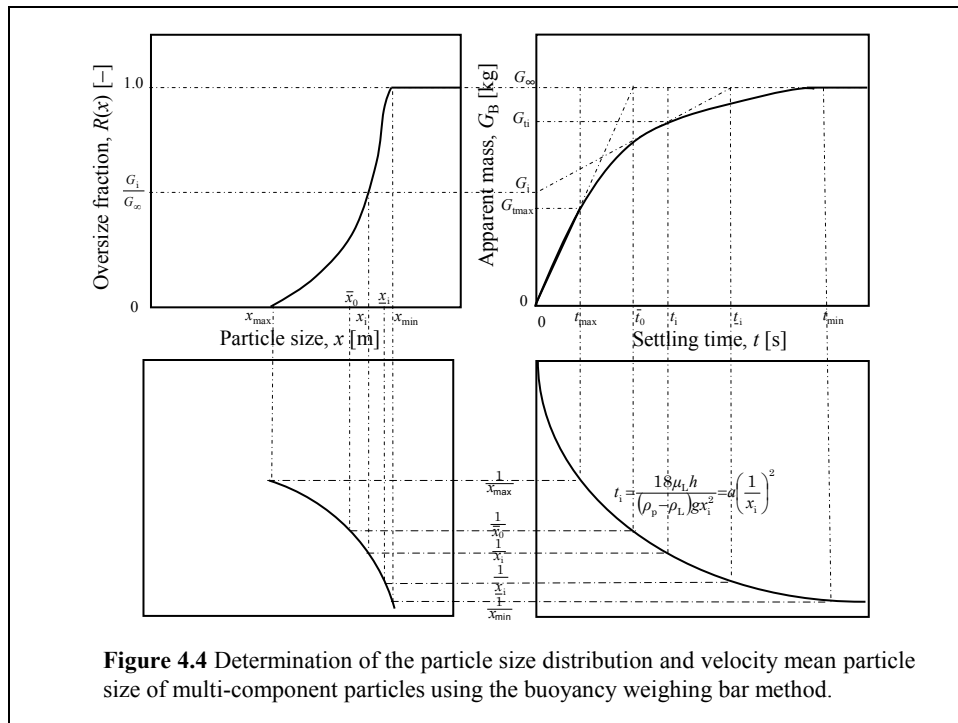
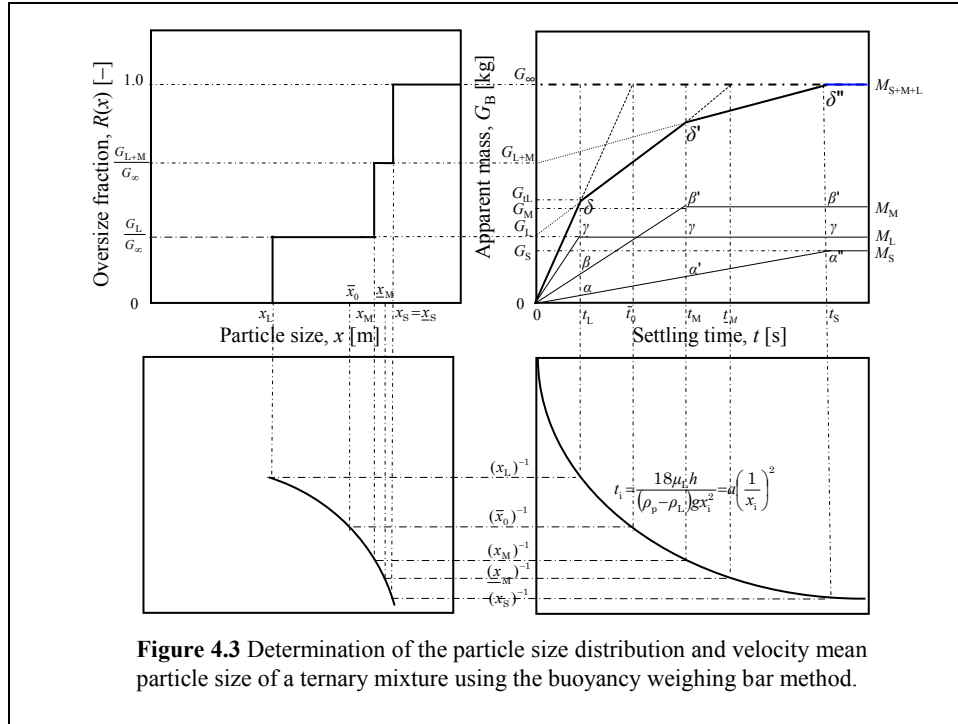
A	cross-sectional area of the weighing bar, m^2
C_0	initial solid concentration of the suspension, kg/m^3
$D(x)$	undersize mass fraction of particle size x , –
$f(x)$	mass frequency of particle size x , m^{-1}
g	gravitational acceleration, m/s^2
G	apparent buoyant mass of the weighing bar, kg
G_{ti}	apparent mass of the weighing bar at $t = t_i$, kg
G_∞	$G_L + G_M + G_S$, kg
h	submerged length of the weighing bar, m
M	particle mass, kg
M_0	$M_L + M_M + M_S$, kg
Re	Reynolds number ($= \frac{xv(x)\rho_L}{\mu_L}$), –
$R(x)$	oversize mass fraction of particle size x , –
t	time, s
u	superficial velocity, m/s
$v(x)$	settling velocity of particle size x , m/s
V_B	submerged volume of the weighing bar, m^3
x	particle size, m
\bar{x}_0	velocity mean particle size of all particles, m
\bar{x}_i	velocity mean particle size from x_i to x_{max} , m
\underline{x}_i	velocity mean particle size from x_{min} to x_i , m
ΔG	buoyancy difference mass of the particles, kg
μ_L	liquid viscosity, $\text{Pa}\cdot\text{s}$
ρ_B	density of the weighing bar, kg/m^3
ρ_L	liquid density, kg/m^3
ρ_P	particle density, kg/m^3
ρ_{S0}	initial density of the suspension, kg/m^3

Subscripts

1	first, minimum
i	i-th
L	large
M	medium
max	maximum
mf	minimum fluidization
min	minimum
n	n-th, maximum

S	small
∞	total





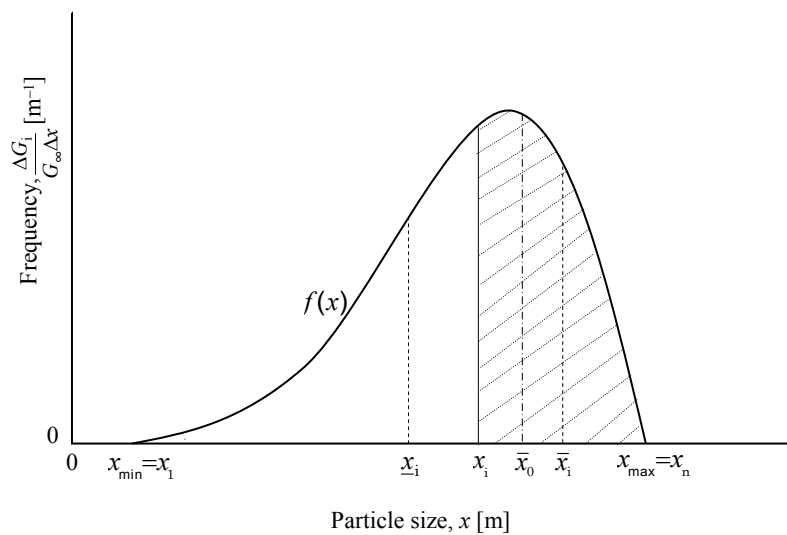


Figure 4.5 Relationship between the mean particle size and mass frequency curve.

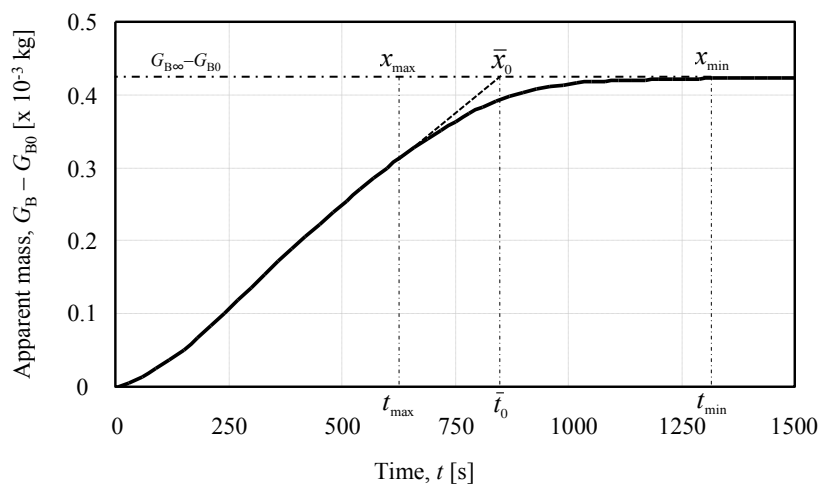


Figure 4.6 Apparent mass of the weighing bar as a function of time with glass beads (GBL 30, JIS Test Powders 2).

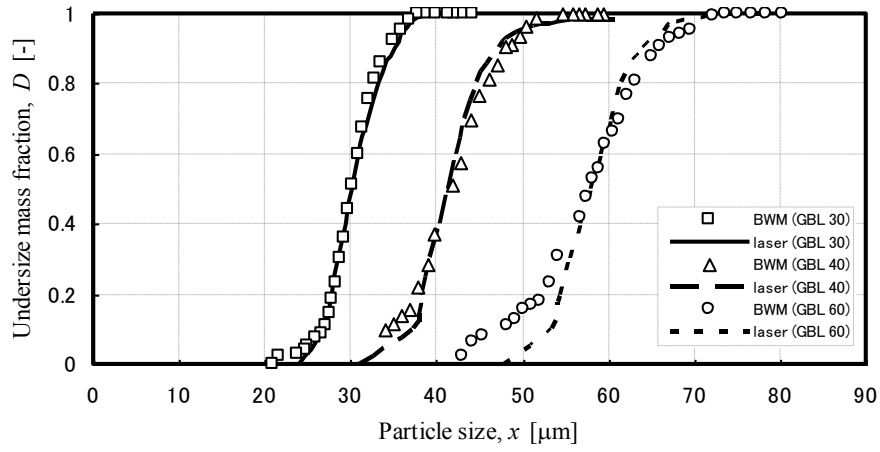


Figure 4.7 Particle size distributions of glass beads (GBL 30, GBL 40 and GBL 60, JIS Test Powders 2).

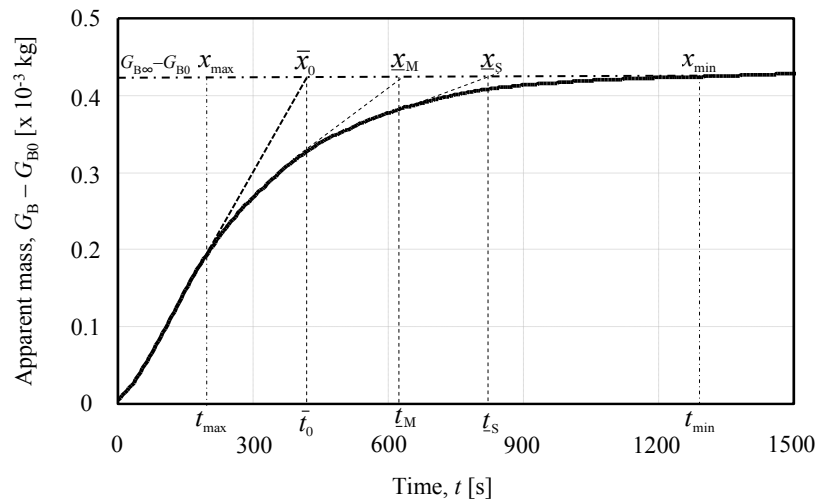


Figure 4.8 Apparent mass of the weighing bar as a function of time with the ternary mixture (glass beads GBL 60, GBL 40 and GBL 30, JIS Test Powders 2).

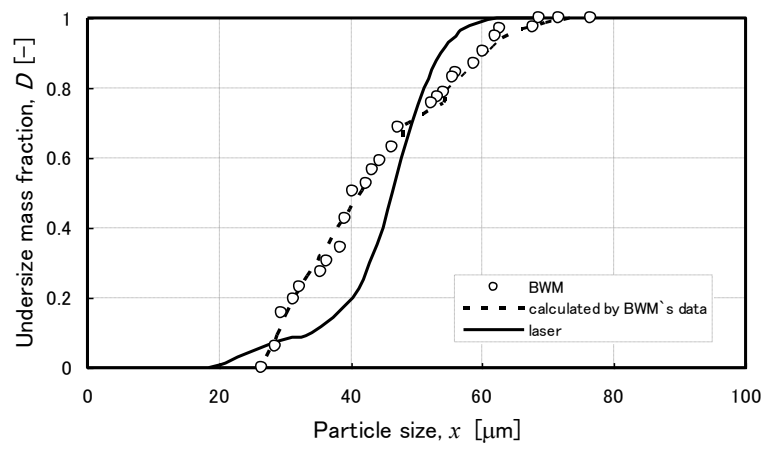


Figure 4.9 Particle size distributions of a ternary mixture of glass beads (GBL 60, GBL 40 and GBL 30, JIS Test Powders 2).

Table 4.1 Particle size of the sample particles.

Sample particles	PSD by Coulter counter (Japan Industrial Standard) [μm]			50% oversize by BWM [μm]	50% oversize by laser [μm]
	90% oversize	50% oversize	10% oversize		
GBL 30	26 min	30 ± 1.0	34 max	30.2	30.1
GBL 40	37 min	41 ± 1.0	45 max	41.6	41.3
GBL 60	55 min	59 ± 1.0	63 max	57.8	58.0

Table 4.2 Mean particle size of a ternary mixture of glass beads GBL 60, GBL 40, and GBL 30

Composition	Mean particle size			
	graphically by the BWM		calculated by BWM's data	calculated by laser's data
GBL 60, GBL 40, GBL 30	$\bar{t}_0 = 420 \text{ s}$	$\bar{x}_0 = 44.9 \mu\text{m}$	$\bar{x}_0 = 44.3 \mu\text{m}$	$\bar{x}_0 = 44.3 \mu\text{m}$
GBL 40, GBL 30	$\bar{t}_M = 610 \text{ s}$	$\bar{x}_M = 37.2 \mu\text{m}$	$\bar{x}_M = 37.1 \mu\text{m}$	$\bar{x}_M = 36.9 \mu\text{m}$
GBL 30	$\bar{t}_S = 840 \text{ s}$	$\bar{x}_S = 31.7 \mu\text{m}$	$\bar{x}_S = 30.2 \mu\text{m}$	$\bar{x}_S = 30.1 \mu\text{m}$

Chapter 5

Measurement of the Floating Particle Size Distribution by the Buoyancy Weighing–Bar Method

5.1 Introduction

Buoyancy weighing-bar method (BWM) is a settling method capable of measuring particle size distribution (PSD) [1]. The accuracy of this method is similar to that of the sedimentation balance method or the Andreasen pipette method. Additionally, the material of the weighing bar does not affect the results, and a particle size of 5 μm in water can be measured in two hours. Furthermore, the PSD of large particles in a viscous liquid can be measured using the BWM. We have reported PSD measurements of the floating particles by the BWM [6,8,9]. The ability to measure the PSDs of floating solid particles suggests that the theory for the size distribution measurement of the settling particle can be applied to floating particles. The precision of the PSD is comparable to that of the laser diffraction/ scattering method, which is a representative high precision method.

Becker *et al.* have reported sedimentation length and pan size affect the PSD using the sedimentation balance and settling particles [2]. Thus, we need to evaluate the influence of particle migration lengths as well as the size of the weighing bar and vessel on the BWM. In this chapter, we reported the influences of the sizes and shapes of weighing bar and vessel on the size distribution measurements of floating particles by the BWM. Also we experimentally investigate the PSD measurement of hollow glass beads K1 (Sumitomo 3M), hollow glass beads S60HS (Sumitomo 3M) and the glass beads GBL 100 (JIS Test Powders 2) by the BWM.

5.2 Theory

In this section, the outline is briefly described because the theory of floating PSD measured by the BWM has been explained in Chapter 1.2.2. Equation (5.1) shows the buoyant mass balance for weighing bar in the suspension.

$$W_0 - W = (W_0 - W_\infty) \int_{x_i}^{x_{\max}} f(x) dx + (W_0 - W_\infty) \int_{x_{\min}}^{x_i} \frac{v(x)t}{h} f(x) dx, \quad (5.1)$$

where W is buoyant mass, h is length of the weighing bar, $v(x)$ is the floating velocity of the particle and $f(x)$ is the mass frequency of the particle size x . The density of the suspension ρ_S and the apparent mass of the weighing bar G in the suspension are given by the following equations:

$$G = V_B \rho_B - W = V_B (\rho_B - \rho_S), \quad (5.2)$$

where ρ_S is the suspension density, ρ_B is the weighing bar density in suspension and V_B is the

weighing bar volume. Differentiate Eqs. (5.1) and (5.2) with respect to the time t , we obtain:

$$G = G_R + \left(\frac{dG}{dt} \right) t. \quad (5.3)$$

Value of G_R calculates from tangent line based on Eq. (5.3). The cumulative mass oversize is

$$R(x) = \int_x^{x_{\max}} f(x) dx = \frac{G_{Rt} - G_{B0}}{G_{B\infty} - G_{B0}} = 1 - D(x) \quad (5.4)$$

where D is cumulative mass undersize.

At $Re < 6$, particle size x is given by the following equation using Stokes formula modified the voidage function:

$$x = \frac{1}{\phi} \sqrt{\frac{18\mu_L v(x) F(\varepsilon)}{g(\rho_L - \rho_P)}} \quad (5.5)$$

where, ϕ is Wadell's shape factor, g is the gravitational acceleration, μ_L is the viscosity of the dispersion liquid contained the dispersant, ε is voidage, and $F(\varepsilon)$ is the voidage function. Wadell's shape factor for a cylindrical particle ϕ is calculated using Eq. (5.6) [7] as

$$\phi = \frac{\text{surface area of a sphere with the same volume as the particle}}{\text{surface area of the particle}} \quad (5.6)$$

The voidage function is calculated by the Richardson and Zaki correlation [3].

$$F(\varepsilon) = \varepsilon^{-4.65} \quad (5.7)$$

The floating velocity of the particles $v(x)$ can be calculated by Eq. (5.8):

$$v(x) = \frac{h}{t} \quad (5.8)$$

where h is the submerged length of the weighing bar and t is the floating time.

5.3 Materials and Methods

5.3.1 PSD measurement of glass beads GBL 100 (JIS Test Powders 2) and hollow glass beads K1 and S60HS (Sumitomo 3M) by the BWM

The details of the experimental apparatus are shown in **Figure 5.1**. The samples particles are glass beads GBL 100 JIS Test Powders 2 (density: $2.30 \times 10^3 \text{ kg/m}^3$), hollow glass beads K1 Sumitomo 3M (density: $0.125 \times 10^3 \text{ kg/m}^3$) and hollow glass beads S60HS Sumitomo 3M (density: $0.600 \times 10^3 \text{ kg/m}^3$). The particles suspensions were placed in the 1000 ml graduated cylinder (diameter: 65 mm).

Figure 5.2 schematically depicts the weighing bars. For sample particle glass beads GBL 100 JIS Test Powders 2, the titanium weighing bar (diameter: 10 mm, length: 250 mm, density: $4.20 \times 10^3 \text{ kg/m}^3$) was hung from an analytical balance with a hook for underfloor weighing (GR-300, A & D Co., Ltd.) using a hanging wire. Sodium polytungstate solution (density: $2.71 \times 10^3 \text{ kg/m}^3$, viscosity: 15.6 mPa.s) was used as the liquid. The sodium

polytungstate solution was Newtonian fluid. Viscosity of sodium polytungstate solution was measured by the viscometer (DV-II+, Brookfield). The particle concentration was set at 10 kg/m³. The laser diffraction/scattering method (MT3000EX, Nikkiso Co., Ltd.), the microscope method (MIC-D, Olympus) and Coulter counter method were used to validate the PSD obtained from the experiments.

For sample particle hollow glass beads K1 (Sumitomo 3M), the aluminum weighing bar (diameter: 10 mm, length: 250 mm, density: 2.70×10^3 kg/m³) was hung from an analytical balance with a hook for underfloor weighing (GR-300, A & D Co., Ltd.) using a hanging wire. The laser diffraction/scattering method (Microtrac MT3000EX, Nikkiso Co., Ltd.) and the microscope method (MIC-D, Olympus) were used to validate the PSD obtained from the experiments. Ion exchanged water (density: 1.00×10^3 kg/m³, viscosity: 0.89×10^{-3} Pa.s) and sodium hexametaphosphate were used as the liquid phase and dispersant, respectively. The initial volume concentrations of the hollow glass bead were set at 0.01.

For sample particle hollow glass beads S60HS (Sumitomo 3M), an aluminum weighing bar (diameter: 10 mm, density: 2.70×10^3 kg/m³) was hung from an analytical balance with a hook for underfloor weighing (GR-300, A & D Co., Ltd.) using a hanging wire. The weighing bars lengths are 100 mm and 250 mm. The laser diffraction/scattering method (Microtrac MT3000EX, Nikkiso Co., Ltd.) and the microscope method (MIC-D, Olympus) were used to validate the PSD obtained from the experiments. Ion exchanged water (density: 1.00×10^3 kg/m³, viscosity: 0.89 mPa.s) and sodium hexametaphosphate were used as the liquid and dispersant, respectively. The initial volume concentrations of the hollow glass beads were set at 0.01.

The bottoms of the weighing bars were set from the bottom of the graduated cylinder to the position at 10 mm. A personal computer was connected to the analytical balance, and the apparent masses of weighing bars were collected in one second interval. To avoid external effects such as airflow and temperature changes, the experimental apparatus was placed in a box and the temperature during the experiment was maintained at 298 K.

To prepare a suspension, 1000 ml liquid and the particles to be tested were mixed in graduated cylinder. Using a hanging wire, which did not extend due to the weight of the bar, a bar was hung from the electronic precision weighing balance. After thoroughly stirring the suspension using an agitator, the bar was set with the balance, and this was recorded as $t = 0$ s. The apparent mass of weighing bar was recorded on a personal computer. After the measurements, we calculated the PSD of the hollow glass beads.

5.3.2 Influence of the weighing bar and vessel in the BWM on size distribution measurement of floating particle

Figures 5.1 and 5.2 depict the experimental apparatus, which consists of a suspension vessel, weighing bar, analytical balance, and defines the sizes of the weighing bars and vessels. The aluminum weighing bars included various sized rods (diameter: 5-35 mm, length:

109-250 mm, density: $2.70 \times 10^3 \text{ kg/m}^3$), a square rod ($12 \times 12 \times 210 \text{ mm}$, density: $2.70 \times 10^3 \text{ kg/m}^3$) and a sheet ($1.5 \times 25 \times 210 \text{ mm}$, density: $2.70 \times 10^3 \text{ kg/m}^3$). A floating particle suspension was placed in a graduated cylinder (50-1000 ml, diameter: 21-65 mm, SIBATA Scientific Technology Ltd.) or a square vessel ($100 \times 100 \times 170 \text{ mm}$). The weighing bars were suspended from the analytical balance with a hook for underfloor weighing (GR-300, maximum mass: 310 g, minimum readout mass: 0.1 mg, A & D Co., Ltd.) using a hanging wire. Data were collected in 3 s intervals using a personal computer connected to the analytical balance. **Table 5.1** shows the sizes and shapes of the weighing bars and vessels. The sample particles were hollow glass beads K37 (Glass beads K37; density: $0.370 \times 10^3 \text{ kg/m}^3$; Sumitomo 3M). The shape factor of the sample particles ϕ was 1, because particles were spherical. Ion exchanged water (density: $1.00 \times 10^3 \text{ kg/m}^3$; viscosity: $0.89 \text{ mPa} \cdot \text{s}$) was used as the dispersion liquid. The concentration of the suspension was set to 3.7 kg/m^3 , and the temperature during the experiments was maintained at 298 K. Additionally, the PSDs were compared to the results from the laser diffraction/scattering method (Microtrac MT3000EX, Nikkiso Co., Ltd.) and microscopy (MIC-D, OLYMPUS Co.).

To prepare a suspension, ion exchanged water and hollow glass beads K37 were mixed in a vessel. After thoroughly stirring with a hand-type agitator, the weighing bar was suspended from the analytical balance via a hanging wire, and this was recorded as $t = 0 \text{ s}$. Collected data consisted of time and the apparent mass of the weighing bar. After the measurements, we calculated the PSD of the sample particles based on the aforementioned theory.

5.4 Results and Discussion

5.4.1 PSD measurement of glass beads GBL 100 (JIS Test Powders 2) and hollow glass beads K1 and S60HS (Sumitomo 3M) by the BWM

5.4.1.1 PSD of glass beads GBL 100, JIS Test Powders 2 in heavy liquid

Figure 5.3 shows the PSDs obtained from the floating experiments using the glass beads GBL 100 (JIS Test Powders 2) in sodium polytungstate solution. Reynolds number of the particles was smaller than 0.005 in the present study. Range of the glass beads was 75–125 μm . In this figure, the PSDs measured by the laser diffraction/scattering, microscope and the Coulter counter methods are indicated by the solid line, circle keys and dotted line, respectively. The PSDs measured by the BWM were close to those measured by the laser diffraction/scattering and microscope methods. We concluded that the PSD of the glass beads GBL 100 (JIS Test Powders 2) could be measured in sodium polytungstate solution by the BWM.

5.4.1.2 PSD of hollow glass beads K1, Sumitomo 3M

Figure 5.4 shows the PSDs obtained from the floating experiments using the hollow

glass beads K1. The range of particle size is 16–105 μm . In this figure, the PSDs measured by the laser diffraction/scattering and microscope methods are indicated by the solid line and circle keys, respectively. The PSDs measured by the BWM were close to those measured by the laser diffraction/scattering and microscope methods.

5.4.1.3 PSD of hollow glass beads S60HS, Sumitomo 3M

Figure 5.5 shows the PSDs of the hollow glass beads S60HS measured using the weighing bar of 100 mm in length. The PSDs measured by the laser diffraction/scattering method and the microscope method are indicated by the line and diamond key in this figure. The PSD measured by the BWM was close to those measured by the laser diffraction/scattering method and the microscope method. We concluded that the PSD of the hollow glass beads S60HS (Glass beads S60HS) could be measured by the BWM.

The PSD of the hollow glass beads S60HS measured using the weighing bar of 250 mm in length is also shown in **Figure 5.5**. In this case, the time course change in the apparent mass of the weighing bar did not become constant. The particle size calculated at 7200 s is about 12 μm , because the calculated floating velocity is 3.5×10^{-3} m/s. However, the PSD using the weighing bar of 250 mm in length was close to those measured using the weighing bar of 100 mm in length.

5.4.2 Influence of the weighing bar and vessel in the BWM on size distribution measurement of floating particle

5.4.2.1 Accuracy and repeatability of PSD measurements

As shown in a previous paper [8], hollow glass beads K37 are spherical. Feret's diameter as a particle size was determined using 200 particles and microscopy. **Figure 5.6** shows the PSDs of hollow glass beads K37 measured by microscopy and the laser diffraction/scattering method. Particle sizes ranged was 14–90 μm . The relative refractive index of the hollow glass beads K37 was set to 1.51, which is same as that of soda-lime glass. The PSDs were measured five times where each trial was conducted independently by a different person. Although each trial did not produce identical results, the measured PSDs were similar. Moreover, the PSD measured by microscopy was similar to that measured by the laser diffraction/scattering method. The data measured by the laser diffraction/scattering method was statistically analyzed, and **Table 5.2** shows the calculated values of the average, standard deviation and variation coefficient. The range of the variation coefficient was 0.051 to 0.095. The PSD was determined using the average values.

Figure 5.6 shows that the PSDs of hollow glass beads K37 measured by the BWM were similar to those measured by the microscopy and the laser diffraction/scattering method. The data measured by the BWM was statistically analyzed. **Table 5.2** also shows the calculated values of average, standard deviation and variation coefficient by the BWM. The variation coefficient ranged between 0.016 and 0.087. The variation coefficients of the buoyancy

weighing-bar and laser diffraction/scattering methods were similar. Hence, the accuracy of BWM is equivalent to that of the laser diffraction/scattering method.

Figure 5.7 shows the changes in the apparent mass with time measured using a 1000 ml graduated cylinder (diameter: 65 mm) and a weighing bar (diameter: 10 mm; length: 250 mm). The apparent mass of the weighing bar decreased until all the particles floated above the upper end of the weighing bar, and then the apparent mass of the weighing bar became constant. The variation in the apparent mass was due to the change in the buoyant mass against the weighing bar along with the particles floating.

5.4.2.2 Influence of weighing bar length

Becker *et al.* have reported the effects of sedimentation length [2]. In this work, the floating length and weighing bar length are the same. Previously, we have reported that small particles of hollow glass beads S60HS cannot be measured using a long weighing bar [9]. **Figure 5.8** shows the PSDs of hollow glass beads K37 measured using the BWM by rods with varying lengths as well as the laser diffraction/scattering method. Regardless of the weighing bar length, the PSD could be measured. The solid line denotes the PSD from the averaged data using the laser diffraction/scattering method (Table 5.2). The red dashed and blue dashed lines denote the average particle size plus or minus one standard deviation, respectively. The PSDs measured by the BWM are within plus or minus one standard deviation. Hence, we conclude that the BWM can correctly determine the PSD using a weighing bar length of 109 to 250 mm.

5.4.2.3 Influence of weighing bar diameter

Figure 5.9 shows the PSDs measured using a 1000 ml graduated cylinder (diameter: 65 mm) and rods with different diameters. The solid, red dashed, and blue dashed lines represent the average particle size, average particle size plus one standard deviation, and average particle size minus one standard deviation from the laser diffraction/scattering method, respectively. All trials using the BWM produced similar size distributions. Moreover, the results confirm that rods with diameters between 10 and 25 mm successfully measured the PSDs of hollow glass beads K37.

Figure 5.10 shows the PSDs measured using a 250 ml graduated cylinder (diameter: 38 mm) and varying diameter rods. Rods with diameters between 20 and 35 mm gave PSDs that were outside the standard deviation range of the laser diffraction/scattering method. These observations indicate that the PSD cannot be measured using a large rod and small vessel.

5.4.2.4 Influence of vessel size

Figure 5.11 shows the PSDs measured using a rod with a 10 mm diameter and different graduated cylinders. Regardless of the volume of the graduated cylinder, the PSDs measured using a 210 mm long rod were almost identical. Additionally, employing a 109 mm long rod gave the same results. The PSDs measured by the BWM are within one standard deviation of

the average using the laser diffraction/scattering method. Thus, using graduate cylinders between 50 and 1000 ml and 10 mm diameter rods with lengths between 109 and 210 mm can measure the PSD of hollow glass beads K37.

5.4.2.5 Influence of weighing bar shape

Figure 5.12 shows the PSDs measured by using the aluminum square rods and the aluminum sheet as weighing bars. The continuous line represents that distribution measured by the laser diffraction/scattering method. The square rods and the sheet gave almost the same PSDs when the volumes of the graduated cylinders were 500 ml and 1000 ml. In these cases, both the aluminum square rods and aluminum sheet can be used as the weighing bar to measure the PSD of hollow glass beads. On the other hand, the square rod did not give the similar PSDs when the volume of the graduated cylinder was 100 ml. We considered that the Boycott effect influences the measurement results of PSD [5].

5.4.2.6 Influence of vessel shape and weighing bar position

To investigate the influence of vessel shape, the PSD of hollow glass beads were measured by using the square vessel and the aluminum rod with the 10 mm diameter. The suspension height and the rod length were 140 mm and 109 mm, respectively. The weighing bar positions were center (50 mm-50 mm) and off-center (20 mm-20 mm) in the square vessel. **Figure 5.13** shows the PSDs using the square vessel. The continuous line indicates the distribution measured by the laser diffraction/scattering method. The PSDs measured at the center were same as those measured at off-center, and agreed well with the laser diffraction/scattering method. Hence, the location of the weighing bar does not influence the PSDs, and the square vessel can effectively measure the distribution of hollow glass beads.

5.4.2.7 Influence of the sectional area ratio

The sectional area ratio a/a_C is defined by the following formula

$$\text{sectional area ratio, } a/a_C = \frac{\text{sectional area of weighing bar, } a}{\text{sectional area of vessel, } a_C}. \quad (5.9)$$

Figure 5.14 shows the particle sizes with 10%, 50% and 90% undersize as a function of the sectional area ratio. The solid, red dashed and blue dashed lines denote the average particle size using the laser diffraction/scattering method, average particle size plus standard deviation, and average particle size minus standard deviation, respectively. The error bars are the variation coefficient of the BWM in Table 5.2. A PSD measurement is deemed feasible when the data or the error bar is within one standard deviation of the average using the laser diffraction/scattering method. However, the BWM is not applicable when the data and error bars extend beyond this range.

The particle sizes increased when the sectional area ratio exceeded 0.2. This increase has been attributed to the wall effect [10] and Boycott effect [4]. Although the wall effect has been reported to influence the migration velocity when the size ratio of the particle to the

vessel is large, the wall effect slows the migration velocity of the particles. Because the impact of the wall effect is the opposite of the observed trend, the influence of the wall effect on the velocity of floating particles is negligible. The Boycott effect occurs when the sectional area ratio of pan/vessel is large. Due to a concentration difference, liquid flow accelerates the migration velocity. Hence, the Boycott effect cannot be ignored if the sectional area ratio of the pan and vessel exceeds 0.3 [5]. Because the migration velocity of the particles accelerates according to the Boycott effect, the measured PSD is larger than the actual distribution. Herein the Boycott effect cannot be ignored when the sectional area ratio of the rod and vessel is greater than about 0.2.

On the other hand, the particle sizes of 10% undersize increased when the sectional area ratio was less than about 0.02. In addition to the wall and Boycott effects, there may be another factor in this case. Although this factor is currently unclear, particle size measurements may be difficult due to the small volume of the weighing bar. Additionally, the variation coefficient of the particle size of 10% undersize measured by the BWM is about one-sixth of that measured the laser diffraction/scattering method. If the variation coefficient of the BWM is the same as that of the laser diffraction/scattering method, then the PSD may be measured. Consequently, we conclude that the BWM can measure PSDs when the range of the sectional area ratio is 0.02-0.2.

5.5 Conclusions

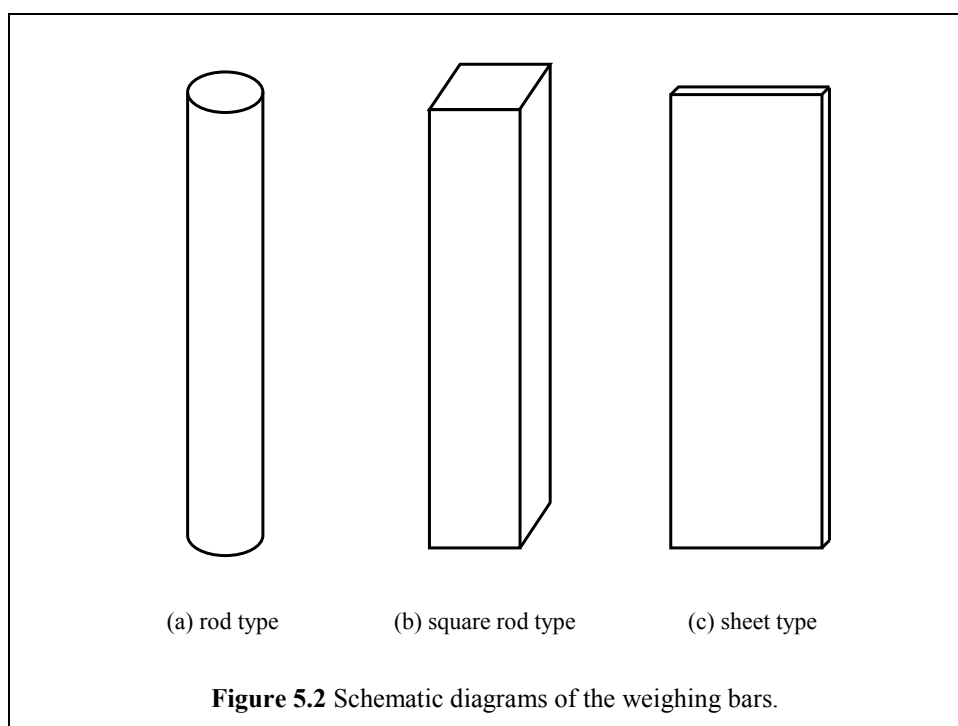
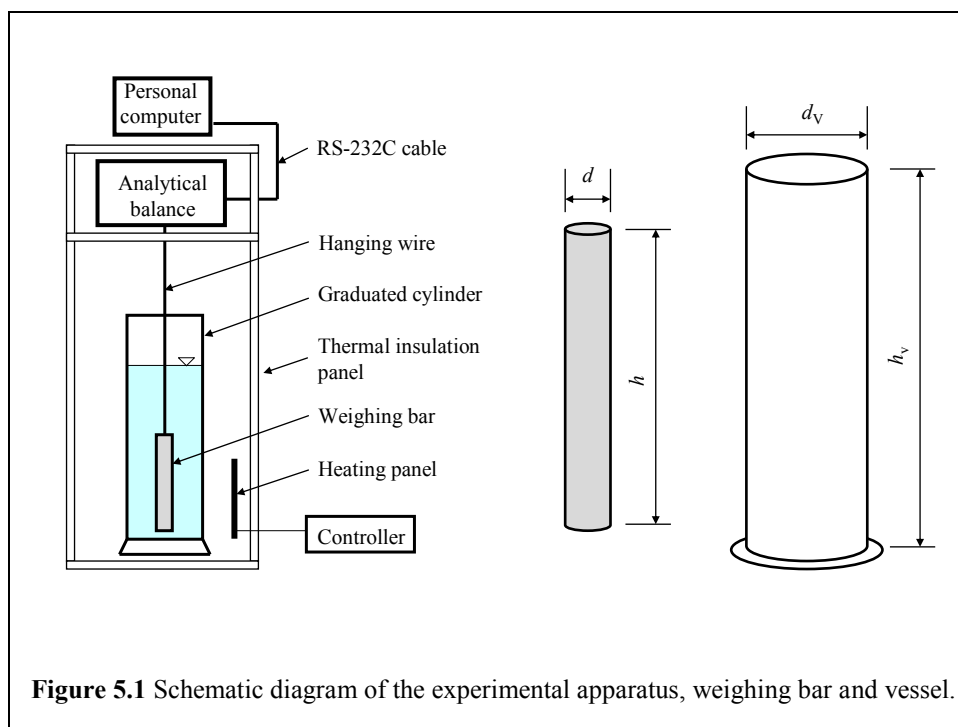
Using the BWM, we measured the floating PSD and discuss the influence of particle migration lengths as well as the sizes and shapes of the weighing bar and vessel. The following results were determined:

1. The PSDs of hollow glass beads GBL 100 (JIS Test Powders 2) can be measured in sodium polytungstate solution and close to those measured by the laser diffraction/scattering and microscope methods.
2. The PSDs of the hollow glass beads K1 (Sumitomo 3M) can be measured using the BWM and the precision of the PSD is comparable to that obtained by the laser diffraction/scattering and microscope methods.
3. The PSDs of the hollow glass beads S60HS (Sumitomo 3M) can be measured using the BWM and the precision of the PSD is comparable to those obtained by the laser diffraction/scattering method and the microscope method, but when the long type weighing bar (250 mm) was used, small particle of the hollow glass beads S60HS could not measure in 2 h.
4. The PSDs of hollow glass beads K37 (Sumitomo 3M) can be measured by the BWM and the result obtained is comparable to those determined by microscopy and laser diffraction/scattering methods.
5. The influence of the weighing bar length on the PSD could not be confirmed for the hollow glass beads K37.

6. When the graduated cylinder was used as the vessel, the PSDs of hollow glass beads K37 could be measured by using the square rod or sheet as the weighing bar.
7. When the rod with the 10 mm diameter was used as the weighing bar, the PSDs of hollow glass beads K37 could be measured by using the square vessel. The location of the weighing bar does not influence the PSDs.
8. The PSDs can be measured by the BWM when the sectional area ratio is 0.02-0.2.

Nomenclature

a	sectional area of the weighing bar, m^2
a_C	sectional area of the vessel, m^2
d	rod diameter, m
d_V	vessel diameter, m
D	cumulative mass undersize, %
$f(x)$	mass frequency of particle size x , m^{-1}
$F(\varepsilon)$	voidage function, –
g	gravitational acceleration, m/s^2
G	apparent mass of the weighing bar, kg
G_R	$V_B \rho_B - W_R$, kg
h	length of the weighing bar, m
h_V	height of the vessel, m
R	cumulative mass oversize, %
Re	Reynolds number ($= \frac{xv(x)\rho_L}{\mu_L}$), –
t	time, s
$v(x)$	floating velocity of particle size x , m/s
V_B	volume of the weighing bar, m^3
W	buoyant mass of the weighing bar in a suspension, kg
W_R	$W_0 - (W_0 - W_\infty) \int_{x_i}^{x_{\max}} f(x) dx$, kg
x	particle size, m
ε	voidage, –
ϕ	Wadell's shape factor, –
μ_L	liquid viscosity, $\text{Pa} \cdot \text{s}$
ρ_L	liquid density, kg/m^3
ρ_B	density of the weighing bar, kg/m^3
ρ_P	particle density, kg/m^3
ρ_S	density of the suspension, kg/m^3
ζ	standard deviation, m
Subscript	
i	i th
max	maximum
min	minimum
0	initial $t = 0$
10	10%
50	50%
90	90%



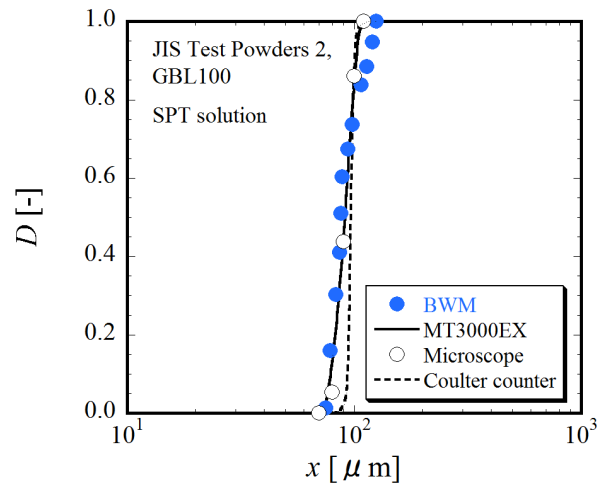


Figure 5.3 PSDs of glass beads GBL 100, JIS Test Powders 2 in heavy liquid.

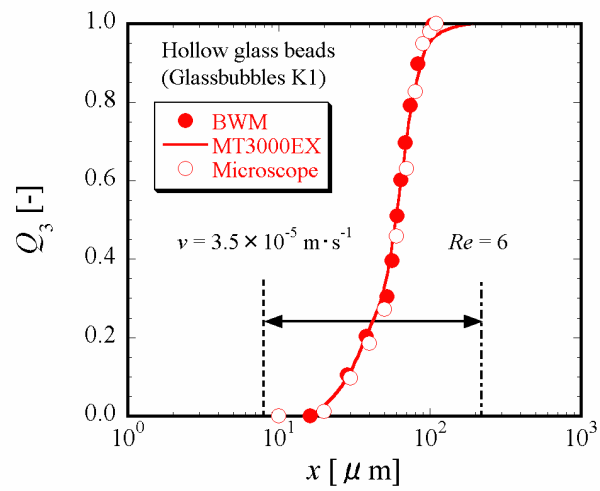


Figure 5.4 PSDs of hollow glass bubbles K1, Sumitomo 3M.

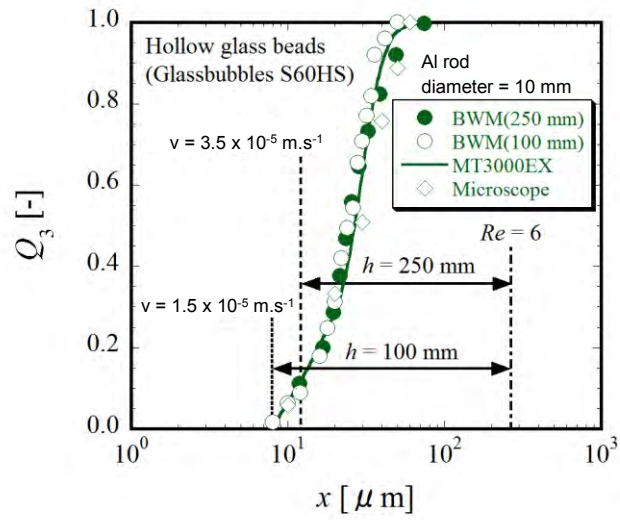


Figure 5.5 PSDs of hollow glass bubbles S60HS, Sumitomo 3M.

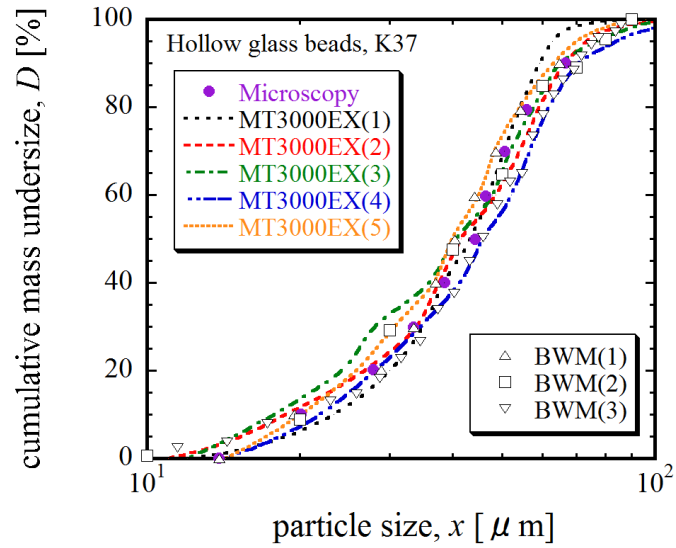


Figure 5.6 PSDs measured by microscopy, laser diffraction/scattering method and BWM.

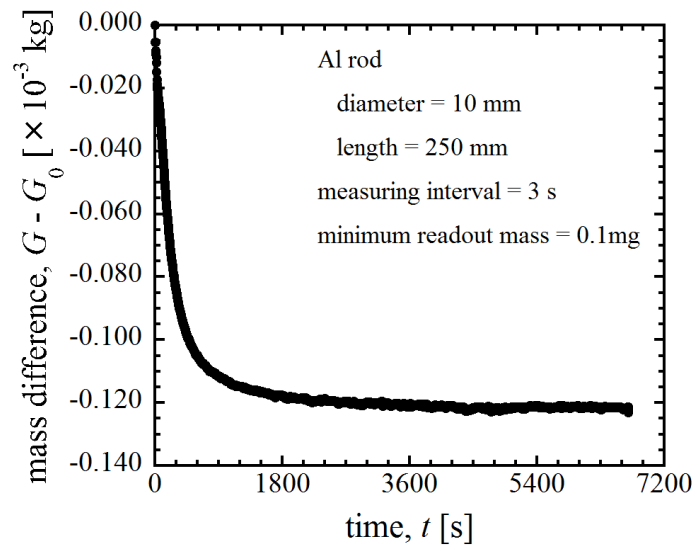


Figure 5.7 Time course change in the apparent mass of the weighing bar using the 1000 ml graduated cylinder.

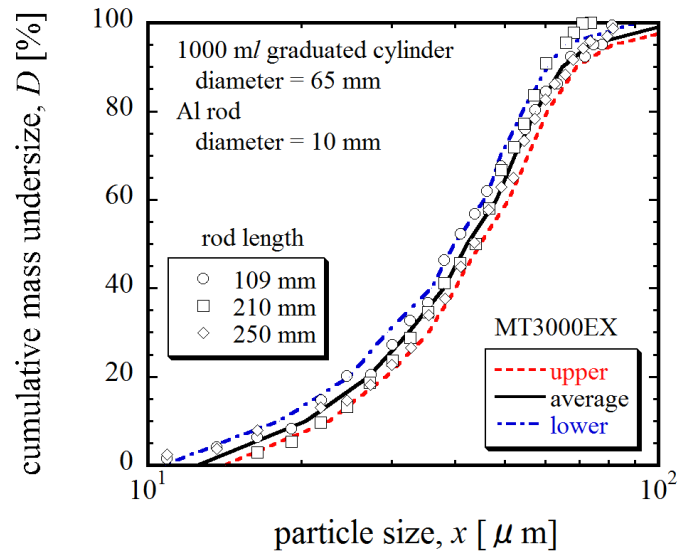


Figure 5.8 Influence of rod length on PSD (vessel diameter = 65 mm).

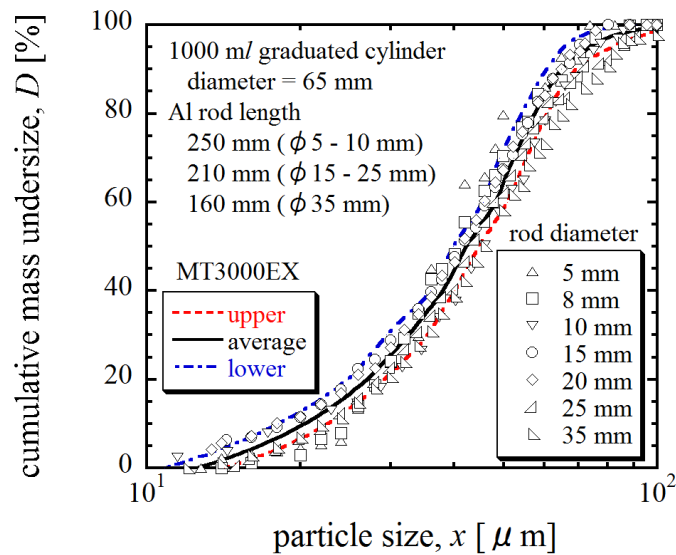


Figure 5.9 Influence of rod diameter on PSD (vessel diameter = 65 mm).

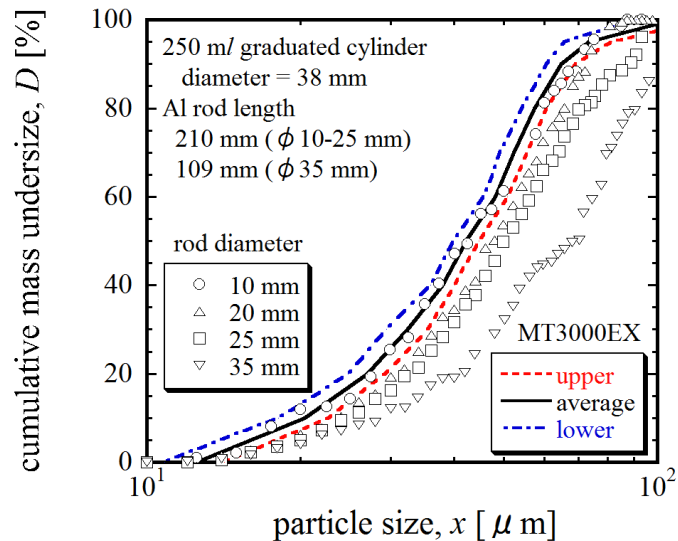


Figure 5.10 Influence of rod diameter on PSD (vessel diameter = 38 mm).

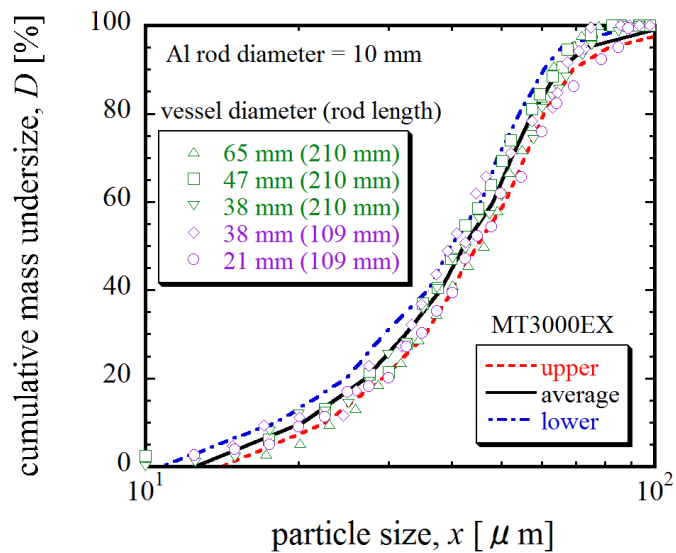


Figure 5.11 Influence of vessel size on PSD.

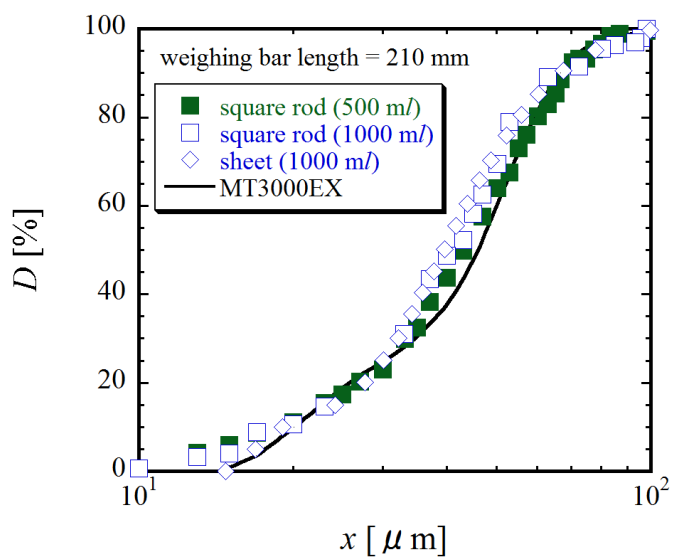


Figure 5.12 Influence of weighing bar shape on PSD.

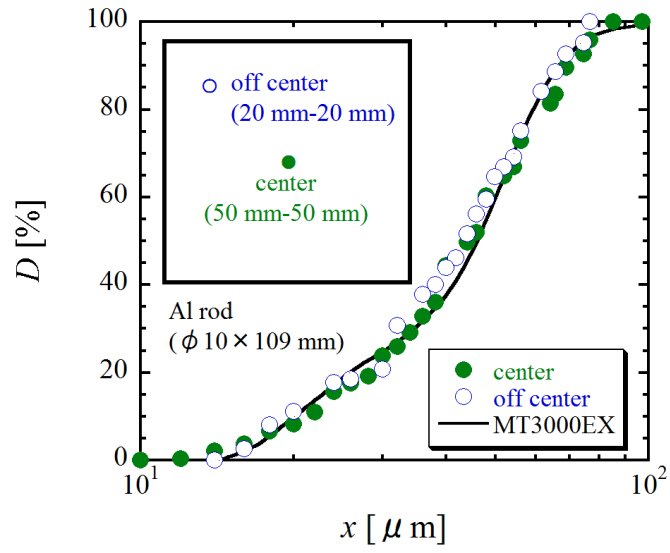


Figure 5.13 PSDs measured in the square vessel.

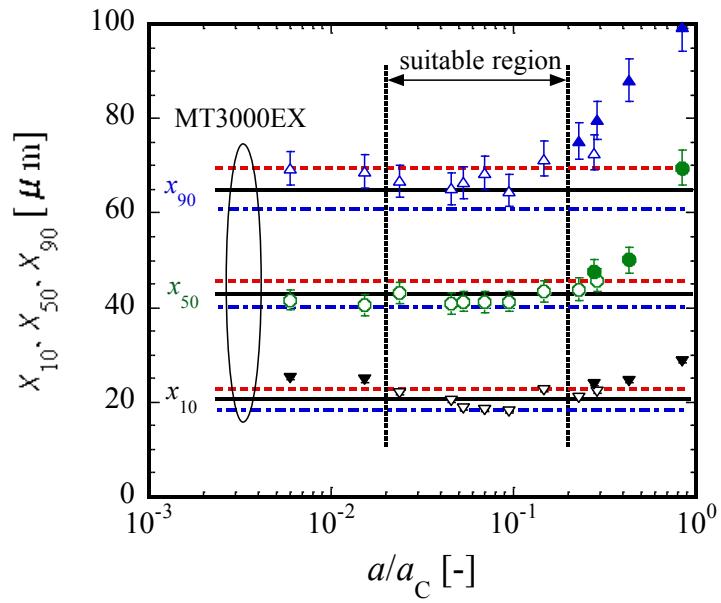


Figure 5.14 Particle sizes as a function of sectional area ratio.

Table 5.1 Sizes of weighing bar and vessel

weighing bar		vessel (graduated cylinder)		
rod diameter, d	rod length, h	inner diameter, D	height, H	(volume)
φ 5 mm	250 mm	φ 21 mm	220 mm	(50 ml)
φ 8 mm	250 mm	φ 38 mm	305 mm	(250 ml)
φ 10 mm	109 mm	φ 47 mm	360 mm	(500 ml)
φ 10 mm	210 mm	φ 65 mm	420 mm	(1000 ml)
φ 10 mm	250 mm			
φ 15 mm	210 mm			
φ 20 mm	210 mm			
φ 25 mm	210 mm			
φ 35 mm	160 mm			
φ 35 mm	109 mm			

Table 5.2 Particle size, standard deviation and variation coefficient

D [%]	MT3000EX			BWM		
	x_{av} [μ m]	σ [μ m]	σ / x_{av} [-]	x_{av} [μ m]	σ [μ m]	σ / x_{av} [-]
10	21.02	2.00	0.095	19.73	0.31	0.016
20	27.71	1.84	0.066	28.02	2.44	0.087
30	33.59	1.95	0.058	33.28	2.71	0.082
40	38.54	1.97	0.051	38.06	2.81	0.074
50	42.67	2.62	0.061	42.15	2.22	0.053
60	48.23	3.04	0.063	47.20	3.04	0.064
70	52.41	3.71	0.071	52.56	3.83	0.073
80	57.41	3.74	0.065	57.82	3.50	0.061
90	64.96	4.86	0.075	68.89	3.54	0.051

Chapter 6

Size Distribution Measurement of Floating Particles in the Allen Region by the Buoyancy Weighing-Bar Method

6.1 Introduction

Information about particle size distribution (PSD) is important to remove particles in a liquid via floatation and/or sedimentation. In this section, we aim to develop an innovative method to measure the PSD using the buoyancy weighing-bar method (BWM). The BWM measures the change in suspension density due to particle migration by weighing the buoyancy against a weighing bar hung in the suspension, and subsequently calculating the PSD using the length of the weighing bar and the time-course change in the apparent mass of the weighing bar [1,2,6]. We have previously reported that the PSDs of floating particles can be measured using the BWM [5]. This method has been used to measure the PSD of paraffin beads, nylon beads, and hollow glass beads in the Stokes region. Moreover, the size of larger particles can be measured by the sieving method or laser scattering/diffraction method. However, the large particle sizes measured by the sieving or laser scattering/diffraction method may not correspond to particle sizes based on the movement in a liquid. Theoretically, the BWM should be applicable to measure the PSD in both the Stokes and Allen regions. Although size distribution measurements of large particles in the Stokes region require special skills to adjust the liquid properties, measurements in the Allen region do not.

Herein we experimentally investigate the applicability of the BWM to measure the PSD of floating particles in the Allen region ($2 < Re < 500$).

6.2 Theory

In this section, the theory about floating particle refers to Chapter 1.2.2, but the particle size x is given by the Allen formula [3]

$$x = \frac{1}{\phi} v(x) \left\{ \frac{225}{4} \frac{\mu_L \rho_L}{(\rho_L - \rho_P)^2 g^2} \right\}^{1/3} \quad (6.1)$$

where ϕ is Wadell's shape factor, g is the gravitational acceleration, and μ_L is the viscosity of the dispersion liquid containing the dispersant. Wadell's shape factor for a cylindrical particle ϕ is calculated using Eq. (6.2) [4] as

$$\phi = \frac{\text{surface area of a sphere with the same volume as the particle}}{\text{surface area of the particle}} \quad (6.2)$$

The floating velocity of the particles $v(x)$ is calculated using Eq. (1.34) in Chapter 1. From Eqs. (6.1) and (1.34), time t is an inverse function of particle size x . The PSD of the suspended particles is calculated using the particle size at each time, and then plotting the

corresponding undersize mass percentage. Although we employed the Allen formula instead of the Stokes formula, this theory and the procedure are the same as those in a previous paper [5].

6.3 Materials and Methods

The diagram of the apparatus used in the experiment is shown in **Figure 2.3** in Chapter 2. **Table 6.1** shows the particle and liquid properties. The sample particles were polystyrene beads (spherical) and nylon beads (cylindrical, FNB#800, Fuji Manufacturing Co., Ltd.). Although the shape of the nylon particles varied slightly, most particles were cylindrical with a diameter to length ratio of approximately 1.0. The particle densities of the polystyrene beads and nylon beads were 1026 kg/m^3 and 1120 kg/m^3 , respectively. Sodium chloride (reagent grade, Kanto Chemical Co., Inc.) solutions prepared with ion exchanged water were used as the liquid phase. The concentrations of sodium chloride were 10 wt% (density: 1069 kg/m^3 , viscosity: $1.07 \text{ mPa}\cdot\text{s}$) and 24 wt% (density: 1170 kg/m^3 , viscosity: $1.55 \text{ mPa}\cdot\text{s}$) for polystyrene beads and nylon beads, respectively. The initial volume concentration of the suspension C_0/ρ_P was set to 0.01, and the temperature during the experiment was maintained at 298 K. Measurements lasted 150 seconds. A laser diffraction/scattering method (Microtrac MT3000EX, Nikkiso Co., Ltd.) and a sieving method ($425\text{--}2000 \mu\text{m}$, JIS testing sieve, Tokyo Screen Co., Ltd.) were used to validate the experimental PSD.

To prepare a suspension, 1000 ml liquid and the particles to be tested were mixed in a graduated cylinder. The weighing bar was hung from an electronic precision weighing balance using a hanging wire, which did not extend due to the weight of the weighing bar. After thoroughly stirring the suspension using an agitator, the weighing bar was set with the balance, and this was recorded as $t = 0 \text{ s}$. The measuring data, which consisted of time t and the corresponding mass of the weighing bar G_B , were recorded on a personal computer. After the measurements, we calculated the PSD of the tested particles based on the above-described theory.

6.4. Results and Discussion

6.4.1. Spherical particles

Figure 6.1 shows the change in the apparent mass of the weighing bar $G_B - G_{B0}$ with time when polystyrene particles were used. The apparent mass of the weighing bar linearly decreased for approximately 100 s, at which point the polystyrene particles floated above the upper end of the weighing bar, and the apparent mass of the weighing bar became constant $G_{B\infty}$. From Eqs. (1.21) and (1.27) in Chapter 1,

$$G_{B\infty} - G_{B0} = \frac{V_B C_0}{\rho_P} (\rho_P - \rho_L) \quad (6.3)$$

The volume of the weighing bar V_B , initial volume concentration C_0/ρ_P , particle density ρ_P and liquid density ρ_L were $1.96 \times 10^{-5} \text{ m}^3$, 0.01, 1026 kg/m^3 , 1069 kg/m^3 , respectively. The value of the apparent mass difference $G_{B\infty} - G_{B0}$ calculated by Eq. (6.3) was $-8.4 \times 10^{-6} \text{ kg}$, which is identical to the apparent mass difference of measured data. The change in the apparent mass was due to the change in the buoyant mass against the weighing bar along with the floating particles. Thus, we confirmed that the floating PSD of spherical particles in the Allen region can be measured using the BWM.

Figure 6.2 shows the PSDs in the Allen region obtained from the floating experiments using polystyrene particles as well as those measured by a laser diffraction/scattering method and a sieving method. Theoretically, Wadell's shape factor of the polystyrene particles was 1.0 because the particles were spherical. All three methods gave similar PSDs. The particle sizes calculated by Eq. (6.1) were included in the Allen region. Hence, our results confirm that the BWM can measure the PSD of floating spherical particles in the Allen region.

6.4.2. Cylindrical particles

Figure 6.3 shows the change in the apparent mass of the weighing bar $G_B - G_{B0}$ with time when nylon particles were used. The apparent mass of the weighing bar linearly decreased for approximately 30 s, at which point all the nylon particles floated above the upper end of the weighing bar, and the apparent mass of the weighing bar became constant. The volume of the weighing bar V_B , initial volume concentration C_0/ρ_P , particle density ρ_P , and liquid density ρ_L were $1.96 \times 10^{-5} \text{ m}^3$, 0.01, 1120 kg/m^3 , 1170 kg/m^3 , respectively. The apparent mass difference $G_{B\infty} - G_{B0}$ calculated by Eq. (6.3) was $-9.8 \times 10^{-6} \text{ kg}$. The measured value of the apparent mass difference was $-9.4 \times 10^{-6} \text{ kg}$, which is almost the same as the calculated value. Thus, we confirmed that the floating PSD of cylindrical particles can be measured using the BWM.

Figure 6.4 shows the PSDs of the nylon particles in the Allen region measured using the BWM, laser diffraction/scattering method, and sieving method. Wadell's shape factor of the nylon particles was theoretically 0.873 because the ratio of the diameter to the length was 1.0. The sizes of the nylon particles calculated by Eq. (6.1) were in the Allen region. We also measured the PSDs for nylon particles by a laser diffraction/scattering method and a sieving method. Regardless of the method, the measured PSDs were similar.

6.5 Conclusions

Using the BWM, we measured the PSDs of floating solid particles in liquid phases where the density was adjusted by the concentration of sodium chloride. The results led to the following conclusions:

1. Although particles in the Allen region migrate, the floating PSDs of solid particles can be measured by the BWM.

2. The precision of the PSD by the BWM is comparable to that obtained by a laser diffraction/ scattering method or a sieving method.

Nomenclature

C	solid concentration of suspension, kg/m^3
$D(x)$	undersize mass percentage of particle size x , %
g	gravitational acceleration, m/s^2
G_B	apparent mass of weighing bar, kg
G_R	$V_B\rho_B - W_R$, kg
Re	Reynolds number ($= \frac{xv(x)\rho_L}{\mu_L}$), –
$R(x)$	oversize mass percentage of particle size x , %
t	time, s
$v(x)$	floating velocity of particle size x , m/s
V_B	volume of weighing bar, m^3
x	particle size, m
ϕ	Wadell's shape factor, –
μ_L	liquid viscosity, $\text{Pa} \cdot \text{s}$
ρ_L	liquid density, kg/m^3
ρ_P	particle density, kg/m^3
Subscripts	
0	initial $t = 0$
∞	infinity $t = \infty$

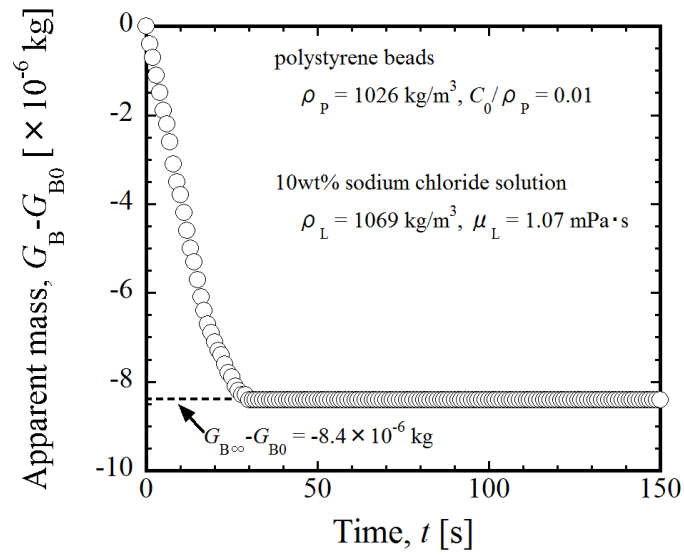


Figure 6.1 Apparent mass of the weighing bar as a function of time (spherical particle).

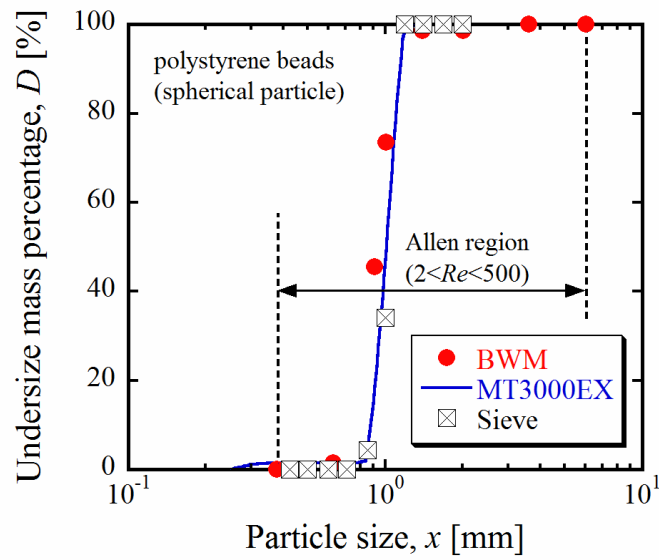


Figure 6.2 Particle size distributions of spherical particle.

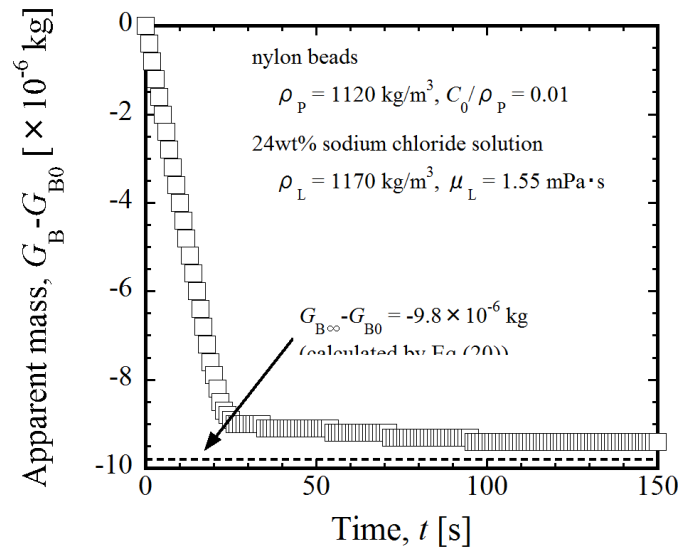


Figure 6.3 Apparent mass of the weighing bar as a function of time (cylindrical particle).

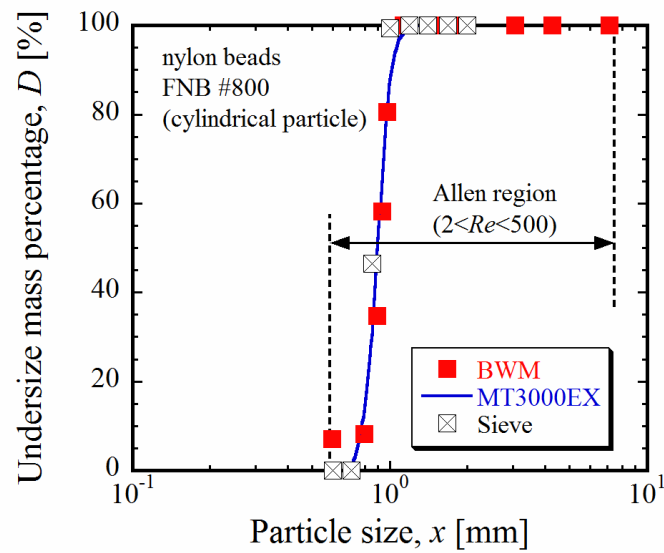


Figure 6.4 Particle size distributions of cylindrical particle.

Table 6.1 Particle and liquid properties

Particle (shape)	Particle density	Liquid	Density and viscosity
polystyrene beads (sphere)	1026 kg/m ³	10% NaCl	1069 kg/m ³ , 1.07mPa·s
nylon beads (cylinder)	1120 kg/m ³	24% NaCl	1170 kg/m ³ , 1.55 mPa·s

Chapter 7

Conclusions

The PSD of settling and floating particles can be determined by the BWM. This method is simple in operation, low-cost of equipment and can produce the high accuracy result in PSD measurement. The results led to the following conclusions.

7.1 Settling particles

- (1) The PSD of large particle up to 63 μm can be measured in water using the BWM.
- (2) There is the graphical analogy of PSD among Andreasen pipette, sedimentation balance, fluidization curve and buoyancy weighing bar methods
- (3) BWM can measure the PSD of a needle-shaped particle for one-component or two-component particles, and the result data obtained comparable to that measured by Andreasen pipette and settling balance methods.
- (4) For measuring the PSD of the JIS Test Powder 2, No.4 (White fused alumina), the suitable initial concentration is 10 kg/m^3 or less. The PSDs measured by the BWM was close to those measured by the Andreasen pipette method, but not close to those measured by the laser diffraction/scattering method.
- (5) BWM can measure the PSD of glass beads GBL 30 (JIS Test Powders 2) and gave the close result to those measured by Andreasen pipette, Coulter counter and laser diffraction/scattering methods.
- (6) When a bar composed of aluminum, copper, acryl resin and SUS 304 were used to measure the PSD of non-spherical silica sand Class 3, JIS Test Powders 1, the material of the weighing bar did not influence the PSD. The PSDs measured by the BWM gave the similar result to those measured by the sedimentation balance, Andreasen pipette and laser diffraction/scattering methods.
- (7) When a bar composed of aluminum, copper and SUS 304 were used to measure the PSD of non-spherical calcium carbonate (heavy) Class 16, JIS Test Powders 1, the material of the weighing bar did not influence the PSD. The PSDs measured by the BWM gave the similar result to those measured by sedimentation balance, Andreasen pipette, microscope and laser diffraction/scattering methods.
- (8) BWM can measure the PSD of magnesite (China) and soft-burned magnesia (China). The PSD measured by the BWM agreed well to those measured by laser diffraction/scattering method.
- (9) BWM can measure the PSD of JIS Test Powders 1, class 8 (KANTO loam). The PSD measured by the BWM agreed well to those measured by sedimentation balance, Andreasen pipette and laser diffraction/scattering methods.
- (10) BWM can measure the PSD of JIS Test Powders 1, fly ash class 5. The PSD measured

by the BWM agreed well to those measured by sedimentation balance and laser diffraction/scattering methods.

- (11) BWM can measure the PSD of JIS Test Powders 1, talc class 4 used the ion exchanged water and ethanol as dispersion liquid. The PSD measured by the BWM agreed well to those measured by sedimentation balance and Andreasen pipette methods, but not close to those measured by laser diffraction/scattering method.
- (12) The PSDs of JIS Test Powders 1, class 3, class 10 and class 11 can be measured by the BWM within two hours, and the Rosin-Rammler distribution can be estimated.
- (13) The PSD of JIS Test Powders 1, class 17 cannot be estimated because the cumulative mass oversize is up to about 0.1 within two hours.
- (14) The PSD of suspended solids in spring water obtained at a construction site can be measured by the BWM and its Rosin-Rammler distribution.
- (15) The velocity mean size of all particles (\bar{x}_0) and the velocity mean size of particles from x_{\min} to x_i (\underline{x}_i) by the BWM are determined by

$$\bar{x}_0 = \left(\sum_{i=1}^n \frac{\Delta G_i x_i^2}{G_\infty} \right)^{\frac{1}{2}} \quad \left(\sum_{i=1}^n \Delta G_i = G_\infty \right)$$

$$\underline{x}_i = \left(\sum_{i=1}^i \frac{\Delta G_i x_i^2}{G_\infty} \right)^{\frac{1}{2}} \quad \left(\sum_{i=1}^i \Delta G_i = G_\infty - G_i \right)$$

where ΔG_i is the buoyancy difference mass of particles x_i .

- (16) The velocity mean sizes of particles (\underline{x}_i) can be recognized graphically by the BWM. The maximum particle size can be defined by t_{\max} .
- (17) The PSD and mean particle size of multi-component particles can be measured by the BWM as the BWM and laser diffraction/scattering method yield similar results.
- (18) The PSD and mean particle size for a ternary spherical particle mixture of glass beads (GBL 60, GBL 40 and GBL 30) can be measured by the BWM because the BWM measured and calculated results are similar.

7.2 Floating particles

- (1) The PSDs of hollow glass beads K37 (Sumitomo 3M) can be measured by the BWM and the result obtained is comparable to those determined by microscopy and laser diffraction/scattering methods.
- (2) The influence of the weighing bar length on the PSD could not be confirmed for the hollow glass beads K37.
- (3) When the graduated cylinder was used as the vessel, the PSDs of hollow glass beads K37 could be measured by using the square rod or sheet as the weighing bar.
- (4) When the rod with the 10 mm diameter was used as the weighing bar, the PSDs of hollow glass beads K37 could be measured by using the square vessel. The location of

the weighing bar does not influence the PSDs.

- (5) The PSDs can be measured by the BWM when the sectional area ratio is 0.02-0.2.
- (6) The PSDs of the hollow glass beads K1 (Sumitomo 3M) can be measured using the BWM and the precision of the PSD is comparable to that obtained by the laser diffraction/scattering and microscope methods.
- (7) The PSDs of the hollow glass beads S60HS (Sumitomo 3M) can be measured using the BWM and the precision of the PSD is comparable to those obtained by the laser diffraction/scattering method and the microscope method.
- (8) When the long type weighing bar (250 mm) was used, small particle of the hollow glass beads S60HS could not measure in 2 h.
- (9) The PSDs of hollow glass beads GBL 100 (JIS Test Powders 2) can be measured in sodium polytungstate solution and close to those measured by the laser diffraction/scattering and microscope methods.
- (10) Although particles in the Allen region migrate, the floating PSDs of solid particles can be measured by the BWM.
- (11) The precision of the PSD is comparable to that obtained by a laser diffraction/scattering method or a sieving method.

References

<Chapter 1>

- [1] E. Obata, H. Takahashi, M. Akiyoshi, K. Ando and H. Watanabe, Measurement of particle size distribution by superficial velocity and pressure drops across liquid–fluidized beds, *Kagaku Kougaku Ronbunshu*, **14**, 103–106 (1988).
- [2] E. Obata, H. Takahashi, M. Akiyoshi and K. Ando, The measurement of the size distribution of irregular particles by liquid–solid fluidization in a high Reynolds number, *Journal of the Society of Powder Technology*, **27**, 301–307 (1990)
- [3] E. Obata, H. Watanabe, K. Mukaida, M. Akiyoshi and K. Ando, Measurement of particle size distribution by numerical values of fluidization curve, *Kagaku Kougaku Ronbunshu*, **12**, 619–621 (1986).
- [4] E. Obata and H. Watanabe, Measurement of particle sizes by fluidization, *Encyclopedia of Fluid Mechanics*, vol. 4, Gulf Publishing, Houston, pp. 221–236 (1986).
- [5] E. Obata, H. Watanabe and N. Endo, Measurement of size and size distribution of particles by fluidization, *Journal of Chemical Engineering of Japan*, **15**, 23–28 (1982).
- [6] E. Obata and K. Ando, Particle size measurements by fluidization: From laminar flow region to the turbulent flow region, *Encyclopedia of Fluid Mechanics*, Supplement 2, Gulf Publishing, Houston, pp. 169–189 (1993).
- [7] E. Obata, M. Maruyama, Y. Ohira, M. Akiyoshi and K. Ando, The simultaneous measurement of crystal sizes and mass in a fluidized crystallizer, *Journal of the Society of Powder Technology*, **33**, 456–461 (1996).
- [8] E. Obata, Y. Ohira and M. Ohta, New measurement of particle size distribution by buoyancy weighing–bar method, *Powder Technology*, **196**, 163–168 (2009).
- [9] H. Minoshima, K. Matsushima and K. Shinohara, Experimental study on size distribution of granules prepared by spray drying: the case of a dispersed slurry containing binder, *Kagaku Kogaku Ronbunshu*, **31**, 102–107 (2005).
- [10] J. P. Bardet and J. Young, Grain–size analysis by buoyancy method, *Geotechnical Testing Journal*, **20**, 481–485 (1997).
- [11] K. Fukui, H. Yoshida, M. Shiba and Y. Tokunaga, Investigation about data reduction and sedimentation distance of sedimentation balance method, *Journal of Chemical Engineering of Japan*, **33**, 393–399 (2000).
- [12] M. Arakawa, G. Shimomura, A. Imamura, N. Yazawa, T. Yokoyama and N. Kaya, A New apparatus for measuring particle size distribution based on centrifugal sedimentation, *Journal of the Society of Materials Science of Japan*, **33**, 1141–1145 (1984).
- [13] M. Kuriyama, H. Tokanai and E. Harada, Maximum stable drop size of pseudoplastic dispersed–phase in agitation dispersion, *Kagaku Kogaku Ronbunshu*, **26**, 745–748 (2000).
- [14] N. G. Stanly–Wood, E. Obata, H. Takahashi and K. Ando, Liquid fluidisation curves,

Powder Technology, **60**, 61–70 (1990).

- [15] S. Odén, The size distribution of particles in soils and the experimental methods of obtaining them, *Soil Science*, **19**, 1–35 (1925).
- [16] Society of Chemical Engineering of Japan, *Chemical Engineering Handbook*, 5th edition, Maruzen, Tokyo, Japan, pp. 224–231 (1988).
- [17] T. Allen, *Particle Size Measurement*, Fourth edition, Chapman and Hall, London, pp. 345–355 (1990).
- [18] T. Motoi, Y. Ohira and E. Obata, Measurement of the floating particle size distribution by buoyancy weighing–bar method, *Powder Technology*, **201**, 283–288 (2010).
- [19] Y. Ohira, H. Takahashi, M. Takahashi and K. Ando, Wall heat transfer in a double-tube coal-slurry bubble column, *Kagaku Kogaku Ronbunshu*, **30**, 360–367 (2004).

<Chapter 2>

- [1] E. Obata and H. Watanabe, Measurement of particle sizes by fluidization, *Encyclopedia of Fluid Mechanics*, vol. 4, Gulf Publishing, Houston, pp. 221–236 (1986).
- [2] E. Obata, H. Watanabe and N. Endo, Measurement of size and size distribution of particles by fluidization, *Journal of Chemical Engineering of Japan*, **15**, 23–28 (1982).
- [3] E. Obata and K. Ando, Particle size measurements by fluidization: From laminar flow region to the turbulent flow region, *Encyclopedia of Fluid Mechanics*, Supplement 2, Gulf Publishing, Houston, pp. 169–189 (1993).
- [4] E. Obata, Y. Ohira and M. Ohta, New measurement of particle size distribution by buoyancy weighing–bar method, *Powder Technology*, **196**, 163–168 (2009).
- [5] N. G. Stanly–Wood, E. Obata, H. Takahashi and K. Ando, Liquid fluidisation Curves, *Powder Technology*, **60**, 61–70 (1990).
- [6] R. Tambun, Y. Ohira and E. Obata, Graphical analogy of particle size distribution among Andreasen pipette, settling balance, fluidization–curve and buoyancy weighing–bar methods, *Proceeding of the 13th Asia Pacific Confederation of Chemical Engineering Congress*, Taipei, Taiwan, CD–ROM (2010).
- [7] T. Allen, *Particle Size Measurement*, Fourth edition, Chapman and Hall, London, UK, pp. 313–355 (1990).
- [8] T. Motoi, Y. Ohira and E. Obata, Measurement of the floating particle size distribution by buoyancy weighing–bar method, *Powder Technology*, **201**, 283–288 (2010).

<Chapter 3>

- [1] A. H. M. Andreasen, The grinding of materials. Theoretical and experimental researches on particle–size distribution incident to the disintegration process, *Kolloid Beihefte*, **27**, 349–358 (1928).
- [2] E. Obata, Y. Ohira and M. Ohta, New measurement of particle size distribution by

- buoyancy weighing–bar method, *Powder Technology*, **196**, 163–168 (2009).
- [3] G. J. Bouyoucos, The hydrometer as a new method for the mechanical analysis of soils, *Soil Science*, **23**, 343–354 (1927).
 - [4] H. Minoshima, K. Matsushima and K. Shinohara, Experimental study on size distribution of granules prepared by spray drying: The case of a dispersed slurry containing binder, *Kagaku Kogaku Ronbunshu*, **31**, 102–107 (2005).
 - [5] J. K. Donoghue and W. Bostock, Technique for particle–size analysis by centrifugal sedimentation, *Trans. Inst. Chem. Eng.*, **33**, 72–75 (1955).
 - [6] Japan Standard Association, JIS A1202 Testing methods for density of soil particles, 1–8, (2009).
 - [7] Japan Standard Association, JIS A1226 Testing methods for ignition loss of soils, 1–6 (2009).
 - [8] Japan Standard Association, JIS K0102 Testing methods for industrial wastewater, 1–66 (2008).
 - [9] Japan Standard Association, JIS K8803-01 Methods for viscosity measurement of liquid, 1–40 (2011).
 - [10] Japan Standard Association, JIS Z8807 Measuring methods for specific gravity of solid, 1–12 (1976).
 - [11] Japan Standard Association, JIS Z8901 Test powders and test particles, 1–23 (2006).
 - [12] K. Furukawa, Y. Ohira, E. Obata and Y. Yoshida, Measurements of mineral particle size distributions by a buoyancy weighing method, *Journal of MMIJ*, **126**, 577–582 (2010).
 - [13] S. Odén, The size distribution of particles in soils and the experimental methods of obtaining them, *Soil Science*, **19**, 1–35 (1925).
 - [14] T. Allen, Particle size measurement, Fourth edition, Chapman and Hall, London, 163–164 (1990).
 - [15] W. H. Coulter, Means for counting particles suspended in a fluid, US patent No. 2656508 (1953).
 - [16] W. Stober and A. Fink, Controlled growth of monodisperse silica in the micron size range, *J. Colloid Interface Sci.*, **26**, 62–69 (1968).
 - [17] Y. Ohira, K. Furukawa, R. Tambun, M. Shimadzu and E. Obata, Buoyancy weighing–bar method: A particle size distribution measurement using new settling method, *Journal Sedimentological Society of Japan*, **69**, 17–26 (2010).

<Chapter 4>

- [1] E. Obata and H. Watanabe, Measurement of particle sizes by fluidization, *Encyclopedia of Fluid Mechanics*, vol. 4., pp. 221–236, Gulf Publishing, Houston, U.S.A. (1986).
- [2] E. Obata and K. Ando, Particle size measurements by fluidization: from laminar flow region to the turbulent flow region, *Encyclopedia of fluid mechanics*, Supplement 2, pp. 169–189, Gulf Publishing, Houston, U.S.A. (1993).

- [3] E. Obata, H. Watanabe and N. Endo, Measurement of size and size distribution of particles by fluidization, *J. Chem. Eng. Japan*, **15**, 23–28 (1982).
- [4] E. Obata, Y. Ohira and M. Ohta, New measurement of particle size distribution by buoyancy weighing-bar method, *Powder Technology*, **196**, 163–168 (2009).
- [5] H. Satone, K. Nishiuma, K. Iimura, M. Suzuki, T. Mori and J. Tsubaki, Particle size measurement by hydrostatic pressure measurement method – effect of initial concentration, *J. Soc. Powder Technology, Japan*, **48**, 456–463 (2011).
- [6] J. F. Richardson and W. N. Zaki, Sedimentation and fluidisation, Part I, *Trans. Inst. Chem. Eng.*, **32**, 35–53 (1954).
- [7] J. Rincon, J. Guardiola, A. Romero and G. Ramos, Predicting the minimum fluidization velocity of multicomponent systems, *J. Chem. Eng. Japan*, **27**, 177–181 (1994).
- [8] N. G. Stanly–Wood, E. Obata, H. Takahashi and K. Ando, Liquid fluidisation curves, *Powder Technology*, **60**, 61–70 (1990).
- [9] R. H. Perry, D. W. Green. and J. O. Maloney, Fluid and particle mechanics, *Perry's Chemical Engineers' Handbook*, 6th ed., pp. 5–54, McGraw–Hill Book Company, Tokyo (1984).
- [10] R. Tambun, Y. Ohira. and E. Obata, Graphical analogy of particle size distribution among Andreasen pipette, settling balance, fluidization–curve and buoyancy weighing-bar methods, *Proceeding of the 13th Asia Pacific Confederation of Chemical Engineering Congress*, CD–ROM, Taipei, Taiwan (2010).
- [11] T. Allen, Particle size measurement, 4th ed., pp. 249–281, Chapman and Hall, London, UK (1990).
- [12] Y. Ohira, K. Furukawa, R. Tambun, M. Shimadzu and E. Obata, Buoyancy weighing-bar method: A particle size distribution measurement using new settling method, *Journal of the Sedimentological Society of Japan*, **69**, 17-26 (2010)

<Chapter 5>

- [1] E. Obata, Y. Ohira and M. Ohta, New measurement of particle size distribution by a buoyancy weighing–bar method, *Powder Technology*, **196**, 163–168 (2009).
- [2] H. Becker, H. Rechmann and P. Tillmann, Contribution to the determination of grain sizes by sedimentation analysis for equivalent diameters in the range from 0.1 to 10 μ , *Kolloid Z*, **169**, 34–41 (1960).
- [3] J. F. Richardson and W. N. Zaki, Sedimentation and fluidisation: Part I, *Trans. Inst. Chem. Engrs.*, **32**, 35–52 (1954).
- [4] M. Arakawa and T. Kobayashi, Experimental studies on sedimentation balance, *Funtai Kogaku Kenkyukaishi*, **1**, 80–86 (1964).
- [5] Particle Engineering Society, Particle size measurement technique, *Nikkan Kogyo Shimbun*, Tokyo, pp.202–205 (1975).
- [6] R. Tambun, T. Motoi, M. Shimadzu, Y. Ohira and E. Obata, Size distribution

- measurement of floating particles in the Allen region by a buoyancy weighing–bar method, *Advanced Powder Technology*, **22**, 548–552 (2011).
- [7] T. Allen, *Particle Size Measurement*, Fourth edition, Chapman and Hall, London, pp. 128–140 (1990).
 - [8] T. Motoi, Y. Ohira and E. Obata, Measurement of floating particle size distributions by a buoyancy weighing–bar method, *Powder Technology*, **201**, 283–288 (2010).
 - [9] Y. Ohira, K. Nakano, R. Tambun, M. Shimadzu, M. Ohta and E. Obata, Size distribution measurement of floating spherical particles by the buoyancy weighing–bar method, *Kagaku Kogaku Ronbunshu*, **37**, 310–316 (2011).
 - [10] Y. Ohyama, *Kagaku kogaku II*, Iwanami Zensho, Tokyo, p.40 (1963).

<Chapter 6>

- [1] E. Obata, Y. Ohira and M. Ohta, New measurement of particle size distribution by a buoyancy weighing–bar method, *Powder Technology*, **196**, 163–168 (2009).
- [2] K. Furukawa, Y. Ohira, E. Obata and Y. Yoshida, Measurements of mineral particle size distributions by a buoyancy weighing method, *Journal of MMIJ*, **126**, 577–582 (2010).
- [3] SPTJ, *Powder Technology Handbook*, pp. 329–332. Nikkan Kogyo Shimbun, Tokyo (1986).
- [4] T. Allen, *Particle size measurement*, Fourth edition, pp. 128–140. Chapman and Hall, London (1990).
- [5] T. Motoi, Y. Ohira and E. Obata, Measurement of floating particle size distributions by a buoyancy weighing–bar method, *Powder Technology*, **201**, 283–288 (2010).
- [6] Y. Ohira, K. Furukawa, R. Tambun, M. Shimadzu and E. Obata, Buoyancy weighing–bar method: A particle size distribution measurement using new settling method, *Journal of the Sedimentological Society of Japan*, **69**, 17–26 (2010).

Acknowledgements

I would like to acknowledge and extend my heartfelt gratitude to the following persons who have made the completion of my doctoral study:

1. My advisor Prof. Eiji Obata and co-advisor Asc. Prof Yuichi Ohira for their guidance, understanding, patience and support during my study at Muroran Institute of Technology.
2. All my friends in Reaction Laboratory, Muroran Institute of Technology for their understanding and assistance.
3. All the civitas academia of Muroran Institute of Technology for helpful and kindness during my study at Muroran Institute of Technology.
4. All of those who supported me in any respect during the completion of the study that I could not mention personally one by one.
5. My wife Yanti Hutapea, my daughter Ruth Stephanie Tambun and my son Raymond Yehezkiel Tambun for their forbearance and understanding.

Finally, I would like to thank God and His son Jesus Christ, who made all things possible.